NASA TN D-1778

90 p.

TECHNICAL NOTE

D-1778

ESTIMATES OF ATTENUATION AND REFLECTION OF TELEMETERING SIGNALS BY IONIZED FLOW FIELDS SURROUNDING TYPICAL REENTRY BODIES

By Anthony J. Russo, Jr.

Langley Research Center
Langley Station, Hampton, Va.

NATIONAL AERONAUTICS AND SPACE ADMINISTRATION
WASHINGTON
August 1963

[redacted]

NATIONAL AERONAUTICS AND SPACE ADMINISTRATION

TECHNICAL NOTE D-1778

ESTIMATES OF ATTENUATION AND REFLECTION OF TELEMETERING SIGNALS BY IONIZED FLOW FIELDS SURROUNDING TYPICAL REENTRY BODIES

By Anthony J. Russo, Jr.

SUMMARY

Estimates of the degree of signal loss due to attenuation and reflection by the inviscid equilibrium plasma sheath were made for spherically blunted cones with half-angles of 30°, 9°, and 0° at Mach numbers as high as 25, 20, and 19.25, respectively. The computations were made for transmitting frequencies of 30 mc, 240 mc, and 10,000 mc and over the altitude range from 60,430 feet to 230,000 feet. Calculations, utilizing the simplest application of electromagnetic theory, were made by using normalized body shape parameters, and methods for applying the resulting tabulated data to specific vehicle reentry problems are discussed.

The possible significance of viscous interaction and nonequilibrium effects on the applicability of the results to a given problem is discussed briefly.

Charts of the electromagnetic properties of equilibrium air for temperatures from 3,000° K to 7,000° K are presented from which attenuation and reflection estimates can be made when the density and temperature distributions are known. Included also are charts which may serve as a guide in the selection of telemetering frequencies for particular environmental conditions.

INTRODUCTION

The plasma sheath surrounding a hypersonic reentry vehicle does much to impede the transmission of radio signals traveling to and from the vehicle (ref. 1). The physics of the interaction of the plasma and the electromagnetic wave in the region of the vehicle is generally understood. However, the ability to predict quantitatively these effects for an actual flight transmission problem is not yet demonstrated because of the lack of actual flight data of this nature and because of the great number of simplifying assumptions which must be made in order to readily obtain numerical answers. Such flight confirmation is, of course, very much desired. Experimental flight data of a passive nature exist, however, in that a significant number of reentering vehicles lose radio contact somewhere along their trajectories and these blackout points are quite often

known. Regretably, however, in these blackouts that part of the signal loss due to attenuation and reflection is not known since other factors, such as antenna breakdown, pattern shift, antenna impedance mismatch, or simply overheating of the transmitting equipment, also contribute to the total signal loss. It is very likely that attenuation and reflection are the primary reasons for the signal loss and at times may be solely responsible for the loss. These uncertainties point up the need for a controlled experiment in which the contribution to signal loss of each factor can be determined. An experiment in which attenuation and reflection could be measured independently of all other factors would be most valuable since it would provide a check on the reliability of the theoretical methods for estimating the signal loss.

In the present analysis only the action of the ionized flow field on the electromagnetic wave (that is, attenuation and reflection) is considered and the simplest theoretical approach is employed. The object of this analysis is to predict theoretically (within the limits imposed by the assumptions) the degree of signal loss for a number of environmental conditions which are similar to those commonly experienced by suborbital reentry vehicles. The calculations are of a general nature in that they may be applied to bodies of arbitrary size (accuracy increasing with size) and they cover a range of environmental conditions which allow interpolations to be made for a number of trajectories which fall within the bounds considered. Also, estimates may be made for bodies whose shapes are similar to the ones considered here by noting the change of signal loss with change in body shape, all other factors being equal.

Theoretical estimates have been made in the literature for isolated conditions and the general variations of the more important parameters discussed. However, calculations are not presently available to enable specific estimates to be made for entire trajectories.

In order to estimate the effect of the plasma sheath on the attenuation and reflection of signals, it is first necessary to have an accurate description of the flow conditions surrounding the vehicle. The solutions to the equations of the flow about blunt-nose bodies are quite difficult to obtain and this problem has for some time stimulated effort by theoretical aerodynamicists. Much progress has been made, however, in producing approximate descriptions of hypersonic real-gas inviscid-flow fields but additional effort should be directed toward obtaining flow solutions in the low Reynolds number regime where the inviscid approach loses its validity.

Inviscid equilibrium flow is used in the present analysis because these solutions were available and will make the results applicable to a general range of body sizes. Classically thin boundary-layer effects pertinent to a particular body might be included in such an analysis at the cost of additional complexity of the method but this was not done.

The simple plane-wave electromagnetic theory used in this analysis has been shown to be in fairly close agreement with experimental data obtained in tests with a chemically produced homogeneous plasma (ref. 1). These tests, however, were unlike an actual flight in that (1) the plasma stream contained no large temperature or density gradients, and (2) the plasma was of the high-density

(and, correspondingly, high electron collision frequency) variety; whereas, for a hypervelocity reentry vehicle (1) the flow field contains, for the most part, very high temperature and density gradients, and (2) the plasma is a low-density (low electron collision frequency) type. At the present time, the available low-density ground testing facilities cannot produce rarefied plasmas which fully simulate real conditions. Thus, the only means for obtaining such data for comparison with theory is a flight experiment.

SYMBOLS

C_p	pressure coefficient
c	speed of light in a vacuum, 3×10^{10} cm/sec
D	diameter, cm
d	dissociation distance, cm
d_e	effective plane slab thickness, cm
f_p	plasma frequency, cps
f	signal frequency, cps
l	mean-free path, cm
m	mass of electron
M	Mach number
N_e	electron concentration, cm^{-3}
n_i	number density of ith species
p	pressure
Q_i	electron collision cross section of ith species
R	power reflection coefficient
R_{12}	power reflection coefficient for uniform semi-infinite plasma
r	radius, cm
S	entropy
$(SL)_A$	signal loss due to attenuation, db

$(SL)_R$	signal loss due to reflection, db
$(SL)_T$	total signal loss
T	temperature, ^oK
t	time, sec
u_1	flight velocity, ft/sec
x	axial distance from body nose, cm
y	distance from body surface along normal
α	attenuation coefficient (homogeneous media), nepers/cm
β	phase constant (homogeneous media), cm^{-1}
ϵ	dielectric constant
k	Boltzmann constant
θ	cone half-angle, deg
δ_{BL}	boundary-layer thickness
δ_{12}	relative phase difference
γ	propagation factor
Δ	shock detachment distance, cm
ν	electron collision frequency, sec^{-1}
Ψ	stream function
σ	electrical conductivity
μ	permeability
ω	radial signal frequency, radians/sec
ω_p	radial plasma frequency, radians/sec
ρ	density
λ	wavelength, cm

Subscripts:

B	plasma conditions at body surface for inviscid flow
max	maximum
NS	normal shock
n	nose
S	behind shock
1	ambient
0	free space or standard conditions

Primed symbols indicate reference values as taken from flow-field solutions.

FLOW FIELDS

Both attenuation and reflection losses are functions of the temperature and density of the surrounding ionized gas and thus an accurate prediction of these flow-field properties is necessary.

One major difficulty in obtaining flow-field solutions has been the inability to readily obtain accurate descriptions of the subsonic flow in the forward stagnation region. This region is important because the part of the flow field in the aft regions of a blunt body which influences signal loss is made up of particles of air which have been processed through the near-normal portion of the bow shock (fig. 1). The path traversed by one such particle of air is illustrated in the figure by the streamline ψ.

The equations of motion for the flow in the stagnation region are of the elliptic type. Conventional numerical methods for the solution of elliptic equations are unstable and often give erroneous results. Gravalos (ref. 2) has developed an iterative scheme which seems to provide satisfactory results for the subsonic and transonic regions. The equations for the supersonic flow on the afterbody are of the hyperbolic type and are easily solved by the real-gas characteristics method. The subsonic and transonic results are used as input data for the method of characteristics which gives solutions for the afterbody region. Thus, the properties at any point in the aft flow field are only as good as the solutions to the flow equations in the stagnation region. The solutions of Gravalos for conditions listed in figure 2 were used in this analysis and were made available to the NASA by the Missile and Space Vehicle Department of the General Electric Company from computations of H. W. Ridyard and S. FitzGibbon. Flow-field solutions based on the Gravalos method are also found in references 3 and 4. Figure 2 indicates the various body configurations and flight conditions which were included in the analysis.

The flow-field solutions were calculated by using the assumptions of inviscid flow and thermochemical equilibrium at every point in the flow field.

In order to make predictions of signal loss for a specific body shape which can be generally applied to any trajectory falling within the reentry corridor, it is necessary to carry out flow-field calculations for many combinations of velocity and altitude. Since the calculation of flow fields is a time-consuming and expensive procedure, the present analysis is made by taking solutions for a range of Mach numbers, but limited number of altitudes, and adjusting the solutions to a range of altitudes by the method of appendix A. Although such a method is not completely rigorous, the range of applicability is greatly broadened and it is believed that the results are only slightly compromised.

Attenuation

When an electromagnetic wave is imposed upon a medium containing free electrons, each electron may be considered to act as a miniature antenna and to absorb energy from the wave. Since the electron is accelerated by the electric field, the energy of the wave may be thought of as being converted into energy of the electrons. This conversion of energy results in a decrease of signal strength and may cause reflective and refractive effects. See reference 5 for a general discussion of absorption mechanisms.

A tractable expression for the attenuation coefficient can be obtained from Maxwell's equations and the equation of motion for an electron. Plane-wave solutions to Maxwell's equations, for homogeneous media, in their simplest form were employed in obtaining an expression for the attenuation coefficient. The simplest theory was used since analyses involving more mathematical rigor are extremely laborious and many times present insolvable expressions, and in view of other related uncertainties (nonequilibrium effects, viscous interactions, and electron-heavy particle collision cross sections, for example) such rigor is not clearly warranted.

The development of the plane-wave expression for the attenuation coefficient is shown in appendix B. The attenuation coefficient is

$$\alpha = \omega\left[\frac{\epsilon\mu}{2}\left(\sqrt{1 + \frac{\sigma^2}{\epsilon^2\omega^2}} - 1\right)\right]^{1/2} \tag{1}$$

For a slightly ionized homogeneous gas, the dielectric constant ϵ and the conductivity σ may be written as follows (ref. 6):

$$\epsilon = \epsilon_0\left(1 - \frac{\omega_p^2}{\nu^2 + \omega^2}\right) \tag{2}$$

$$\sigma = \epsilon_0 \nu \left(\frac{\omega_p^2}{\nu^2 + \omega^2} \right) \tag{3}$$

Substitution of equations (2) and (3) into equation (1) results in

$$\alpha = \frac{\omega}{c_0} \frac{1}{\sqrt{2}} \left[\left(\frac{\omega_p^2}{\nu^2 + \omega^2} - 1 \right) + \sqrt{\left(1 - \frac{\omega_p^2}{\nu^2 + \omega^2} \right)^2 + \left(\frac{\omega_p^2 \nu}{\omega(\nu^2 + \omega^2)} \right)^2} \right]^{1/2} \tag{4}$$

where α is in nepers per centimeter and where ω_p and ν are defined by equations (14) and (15), respectively. A great deal of insight may be gained by studying graphical representations of equation (4). (See, for example, figs. 3 and 4.) In figure 3 is shown the effect of changing the signal frequency ω for a constant plasma frequency ω_p and in figure 4 is illustrated the effect of a varying plasma frequency for a given signal frequency. It is readily seen from figure 3 that for very high frequencies and for very low frequencies the attenuation will drop off markedly. It is not feasible to take full advantage of these indications, however, since, in order to obtain low attenuation during severe reentry conditions, the signal frequency used quite often would have to be higher than is practical at present or so low that antenna size and atmospheric noise become problems.

Reflection

When electromagnetic waves are incident upon a boundary between media in which the phase velocity is appreciably different, such as the discontinuity in going from the antenna surface out into the ionized flow field, the incident wave is divided into reflected and transmitted trains. The larger the change in phase velocity across the boundary of the two media, the larger will be the fraction of incident energy R returned in the reflected wave train.

A reflection study may be greatly simplified by considering only normally incident waves. An analysis of this type is employed here and should suffice for obtaining first-order estimates of the reflected energy.

In studying the reflection of electromagnetic waves it is again necessary to prescribe the properties of the medium (flow field in the immediate vicinity of the antenna). Reflection calculations for any general property variation may not be carried out conveniently (refs. 7, 8, and 9) due to the great complexity of the problem. An approximate method is presented herein whereby an effective medium based on the known property variations may be set up which lends itself to a simplified analysis that can be rapidly performed.

Let us consider the plane sheet model (fig. 5) which is treated in reference 10. Let medium 1 be free space on both sides of medium 2 which is the effective homogeneous plasma slab. Figure 6 illustrates the model by which an effective homogeneous plasma slab is substituted in the present method for the actual problem of varying plasma properties. The development of the reflection

coefficient for a homogeneous slab of finite thickness is given in reference 10 and is

$$R = \frac{R_{12}\left[\left(1 - e^{-2\alpha d_e}\right)^2 + 4e^{-2\alpha d_e}\sin^2\beta d_e\right]}{\left(1 - R_{12}e^{-2\alpha d_e}\right)^2 + 4R_{12}e^{-2\alpha d_e}\sin^2\left(\delta_{12} + \beta d_e\right)} \tag{5}$$

where R_{12} is the power reflection coefficient (ratio of reflected to incident power) at normal incidence for the plane interface dividing two semi-infinite media or, simply, the value of R for d_e approaching infinity. The reflection coefficient R_{12} at an interface is zero when the intrinsic impedances of the adjoining media are equal. In general, for the present purposes, an ionized gas having a temperature of approximately 3,000° K or lower may be considered to have electromagnetic properties which are essentially those of free space. The reflection coefficient R_{12} is a simple function of the attenuation coefficient and the phase constants (of free space and the conducting medium) as given in reference 10 and may be written as

$$R_{12} = \frac{\left(\beta_0 - \beta\right)^2 + \alpha^2}{\left(\beta_0 + \beta\right)^2 + \alpha^2} \tag{6}$$

The relative phase difference δ_{12} is obtained from the following relation (ref. 10):

$$\delta_{12} = \tan^{-1}\left(\frac{-2\beta_0\alpha}{\beta_0^2 - \beta^2 - \alpha^2}\right) \tag{7}$$

The phase constant is derived simultaneously with the attenuation coefficient (appendix B) and is given by the relation

$$\beta = \omega\left[\frac{\mu\epsilon}{2}\left(\sqrt{1 + \frac{\sigma^2}{\epsilon^2\omega^2}} + 1\right)\right]^{1/2} \tag{8}$$

Then substituting equations (2) and (3) into equation (8) gives

$$\beta = \frac{\omega}{c_0\sqrt{2}}\left\{\left(1 - \frac{\omega_p^2}{\nu^2 + \omega^2}\right) + \sqrt{\left(1 - \frac{\omega_p^2}{\nu^2 + \omega^2}\right)^2 + \left[\frac{\omega_p^2\nu}{\omega\left(\nu^2 + \omega^2\right)}\right]^2}\right\}^{1/2} \tag{9}$$

Graphical illustrations of equation (9) are presented in figures 7 and 8. The phase constant may be expressed, also, in terms of the attenuation coefficient as

$$\beta = \frac{\mu_0 \sigma \omega}{2\alpha} \tag{10}$$

or

$$\beta = \frac{\omega}{2\alpha c_0^2}\left(\frac{\nu\omega_p^2}{\nu^2 + \omega^2}\right) \tag{11}$$

The effect on R of increasing the slab thickness d_e is shown in figure 9 where the reflection coefficient of water is seen to vary quite markedly with thickness, reaching maximums at approximately

$$d_e = \frac{\lambda}{4}, \frac{3\lambda}{4}, \frac{5\lambda}{4} \ldots (2n - 1)\frac{\lambda}{4}$$

and oscillating about R_{12}. Of course, the reflection-coefficient variation for a high-entropy plasma sheath is somewhat different from that of water. However, it is interesting to compare the two for an illustration of the effect of increased conductivity. Therefore, the reflection-coefficient variation for a typical high-entropy plasma sheath is also shown in figure 9, where it can be seen that R closely approaches unity at the first maximum and for this reason the value of R shows little oscillation. Thus, for $d_e > \lambda/4$, generally $R \approx R_{12}$ for high entropy plasmas. Hence, use of semi-infinite reflection theory should suffice for a plasma sheath whose effective thickness is greater than $\lambda/4$ and whose properties (α,β) are sufficiently severe (dissipative) to make the oscillation of R with d_e virtually negligible.

Note that the wavelength λ referred to here is the wavelength within the effective medium itself and may differ by several times the value of the free-space wavelength λ_0. The magnitude of the wavelength in a homogeneous isotropic medium is given by

$$\lambda = \frac{2\pi}{\beta} = \frac{2\pi c}{\omega} \tag{12}$$

and that of the wavelength in free space by

$$\lambda_0 = \frac{2\pi}{\beta_0} = \frac{2\pi c_0}{\omega} \tag{13}$$

Since the wavelength is inversely proportional to the phase constant (eq. (12)), an idea of the wavelength variations with temperature and density may be gained from figures 10, 11, and 12.

The foregoing equations are applicable until the radius of curvature of the body surface is small with respect to the incident wavelength. When this condition occurs, the reflectivity will, in general, be reduced from that given by these equations (ref. 10).

ELECTROMAGNETIC WAVE PROPAGATION PROPERTIES OF AIR

In a gas at chemical equilibrium, which is assumed throughout this paper, the temperature and constituents within the plasma are constant with time and the mole fraction of these constituents can be found by the methods of quantum statistical thermodynamics (ref. 11), which determine the partition of the energy states of a particle species into rotational, vibrational, translational, dissociation, and ionization energies. Results of calculations of this type are recorded in table form in reference 12.

The electron collision frequency ν and the plasma frequency ω_p must be known in order to calculate attenuation and reflection (eqs. (4) and (9)) and are both functions of temperature and density for equilibrium air. The plasma frequency is a simple function of the electron concentration - that is,

$$\omega_p = 2\pi f_p = 2\pi(8970)\sqrt{N_e} \tag{14}$$

Some good discussions, along with some guides to the literature, on plasma oscillations are given in references 13, 14, and 15.

The numerical values of N_e used in this analysis were taken from charts provided in reference 16 where N_e is shown as a function of temperature and density for equilibrium air. These charts, along with charts provided in reference 17, illustrate the rapid increase in ionization at temperatures in the neighborhood of 3,000° K. Also, from these charts, it can be seen that the rate of increase of N_e with respect to temperature begins to decrease at the higher temperatures where the constituents are becoming singly ionized.

From the kinetic theory of gases the electron collision frequency is expressed as

$$\nu = \frac{4}{3}\sqrt{\frac{8kT}{\pi m}} \sum n_i Q_i \tag{15}$$

The values of collision cross section Q_i available at the present time are in some disagreement and, therefore, any collision frequency calculations are only order-of-magnitude estimates. Collision frequency data used in this analysis are from reference 6. These data were selected because, for the most part, they result in conservative (in that they are higher) attenuation calculations. More precise collision frequency calculations must await the refinement of experimental determination of the collision cross sections.

By using the aforementioned data along with equations (9), (4), and (6), the more pertinent electromagnetic parameters β, α, and R_{12} were calculated and are presented in figures 10 to 33.

Figures 13, 14, and 15 show the variation of the attenuation coefficient with temperature. The best overall picture of the behavior of α is illustrated by figure 15 where the effect of plasma resonance $(\omega/\omega_p = 1)$ is seen to result in a very sharply increasing attenuation coefficient for the lower densities $(\rho/\rho_0 = 10^{-3}, 10^{-4}, \text{and } 10^{-5})$. When plasma resonance is brought about at lower signal frequencies, the increases begin at proportionally lower temperatures. The fact that sharp increases in attenuation coefficient take place at low densities may be explained by first inspecting figure 34 and noting that very low values of ν/ω_p correspond to the lower densities (higher altitudes). Now, in figure 4 in the direction of increasing temperature (decreasing ω/ω_p), for very small values of ν/ω_p, it is seen that a very sharp increase in attenuation is encountered at the plasma resonance condition $(\omega/\omega_p = 1)$. Consequently, the abrupt increase in α evidenced in figure 15 is to be expected.

Figures 10, 11, and 12 illustrate the variations of the phase constant β with temperature. The phase constant decreases very sharply at plasma resonance, corresponding to the sharp increase in attenuation coefficient, and again this sharp change occurs at the lower densities. This abrupt behavior of the phase constant may be explained in a manner similar to the foregoing explanation of the abrupt increase in attenuation coefficient. Examination of figure 8 shows that for low values of ν/ω_p, which correspond to low densities, abrupt decreases in phase constant occur as the temperature is increased $(\omega/\omega_p$ is decreased) through the region of plasma resonance.

Referring again to equation (12) it is seen that the sudden decrease in phase constant will sharply increase the wavelength of the electromagnetic wave within the plasma. The low densities corresponding to the abruptly changing values of α and β occur at the altitudes of most interest for reentry vehicles. From figures 13, 14, and 15 it can be further seen that the attenuation coefficient begins to level off at the much higher temperatures, which indicates that the gas is beginning to approach a state in which all the constituents are becoming singly ionized.

Figures 16, 17, and 18 picture the dependence of the attenuation coefficient on density. It is seen that, for a constant temperature and signal frequency, α will reach a maximum at some particular density value. Since density decreases exponentially with increasing altitude, the density scale may be thought of as a linear altitude scale. These figures help to illustrate why the signal-loss profile plotted as a function of altitude for a reentry vehicle is quite often very sharp. If the temperature history of a point on the vehicle should be such that it peaks at an altitude corresponding to the density where α is a maximum at a given temperature, then the attenuation profile will be doubly sharpened. Figure 35 shows the normal-shock (approximately stagnation) temperature for constant velocities over the altitude range.

It is seen from figures 16, 17, and 18 that the effect of increasing the signal frequency for a given temperature is to move the point of maximum α in the direction of higher density or lower altitude.

Figures 19 to 24 illustrate, a little more vividly, the fact brought out by figure 3 - that is, lower attenuation for high and low frequencies than for the intermediate frequencies.

Variations of the semi-infinite reflection coefficient for ionized equilibrium air R_{12} may be studied in figures 25 to 33. The coefficient R_{12} is seen to be affected pronouncedly by the density as shown in figures 25, 26, and 27. As was true for the attenuation coefficient, the effect of increasing signal frequency is to shift the maximum value of R_{12} for a given temperature in the direction of higher density. The value of R_{12} generally decreases with an increase in frequency for the temperature range considered. For the lower densities, however, the decrease of R_{12} becomes much more pronounced when the frequencies are increased above a certain point.

VISCOUS FLOW EFFECTS

In order to completely describe a flow field, it is necessary to consider the viscous effects near the body surface. For this purpose the Navier-Stokes momentum equations are usually written in approximate form and solved. For example, when the ratio of inertia forces to viscous forces (Reynolds number) is very high, the Navier-Stokes equations are greatly simplified since almost all of the viscous terms can be deleted. The equations are thus amenable to analysis.

For a hypervelocity, high Reynolds number flow about a body, the entire flow field may be assumed to be inviscid with the exception of a very thin layer of viscous flow at the wall. Then, these two regions of flow may be computed separately since the influence of one region on the other is relatively small (classical boundary-layer approach).

For a low Reynolds number flow, however, the viscous terms and the inertia terms in the Navier-Stokes equations are of nearly equal magnitude. Thus, neither of the terms can be deleted and the equations are rendered insolvable.

Adams and Probstein (ref. 18) have formulated an expression which gives, to a first approximation, the ratio of the boundary-layer thickness to the shock detachment distance at the stagnation point:

$$\frac{\delta_{BL}}{\Delta} \approx \left(\frac{l_1}{r_n}\right)^{1/2} M_1^{1/2} \left(\rho_{NS}/\rho_1\right) \tag{16}$$

Equation (16) is illustrated in figure 36. When δ_{BL}/Δ becomes appreciable (for example, $\delta_{BL}/\Delta \geqq 0.1$), the error involved in calculating the flow field under the inviscid assumption begins to become significant so that in order to have a

high degree of confidence in an inviscid flow-field calculation δ_{BL}/Δ should be much less than unity. Figure 36 may be used to estimate the degree of confidence with which the usual assumptions can be applied in calculating the flow field. At present, the usual practice in approximating low Reynolds number flow fields is to make calculations by using classical methods and then to apply first-order corrections for the low-density viscous effects based on arbitrary considerations.

NONEQUILIBRIUM FLOW

For many flight conditions, in particular those at high altitudes, the flow about a hypervelocity vehicle may be considerably removed from the chemical and thermodynamic equilibrium state.

In air plasma, which contains monatomic and diatomic species, neutral and charged, several processes can cause departure from equilibrium: vibrational energy lag, dissociation lag, ionization lag, and recombination lag. These processes must be treated separately and for each constituent of the plasma; thus, the problem becomes one of great complexity because of the large number of reaction times to be considered. The resulting thermal effects, in general, are proportional to the ratio of reaction time to flow time and to the energy involved in the reaction. Vibrational effects, in some instances, can be neglected since their contribution toward removal of the gas from equilibrium is quite often negligibly small. In general, it may be said that the major result of nonequilibrium process on the shock-layer flow is one of change of the thermodynamic properties of the gas, and only in certain instances will the dynamical behavior depart significantly from that of an equilibrium flow.

All data presented in this analysis pertain to air in chemical equilibrium. This assumption is thought to be quite valid for a substantial range of conditions. A number of exceptions, however, may occur such as the one related in reference 19 where Bortner has shown the effect of the rate constants on the electron concentration to be very pronounced (that is, an order of magnitude change in the oxygen dissociation rate constant can cause increases in the electron concentration of over 10^2). Nonequilibrium effects should be more pronounced at the higher altitudes since two-body reaction rates are proportional to the square of the density. In reference 16 some effects of nonequilibrium flow on the trail properties are discussed and in reference 20 such effects are computed for both shock-wave compressions and flow expansions.

Quite generally, it is believed that the first effects of nonequilibrium flow (that is, as altitude is increased) are those resulting from a recombination lag (frozen flow) beginning in the wake of a vehicle. As the altitude is increased, for a constant velocity, the region of recombination lag will move upstream. For even higher altitudes, the region of frozen flow may engulf the entire vehicle (ref. 20), that is, flow becomes frozen in the region of the stagnation point. This effect may be of major importance to the ionization properties in the shock layer. As the altitude is increased further (beyond the point where frozen-flow effects have become large), the effect of dissociation lag

begins to become large. The distance required for the dissociation to approach equilibrium will increase with increasing altitude.

As an example of one phase of nonequilibrium flow, some dissociation-lag data are presented and briefly discussed. It is not to be inferred that dissociation lag is more important than the consideration of ionization lag and recombination lag, but this effect is selected as an example for discussion purposes only since an investigation of all phases of nonequilibrium flow in its fullest extent is not the purpose of this report. These data, calculated by Teare (shown in ref. 16), aid in determining the flight conditions at which dissociation lag, characteristic of compression flow, begins to show prominence. Teare has calculated the distance d behind a normal shock at which the gas temperature has relaxed down to a value 35 percent above that predicted by equilibrium considerations. It was further concluded that a distance of the order of 10d is required for the temperature to drop to within 10 percent of equilibrium temperature. Figure 37 taken from reference 16 illustrates the nomenclature used in making these estimates.

The dissociation distance d becomes larger with increasing altitude while the shock detachment distance Δ at the stagnation point becomes smaller as based on the following approximate relation:

$$\frac{\Delta}{r_n} \approx \frac{1}{\rho_{NS}/\rho_1} \tag{17}$$

An interesting parameter by which to judge the degree of nonequilibrium effect due to dissociation lag is the ratio of the dissociation distance to the shock detachment distance d/Δ which may be written as

$$\frac{d}{\Delta} \approx \frac{d}{r_n} \frac{\rho_{NS}}{\rho_1} \tag{18}$$

When $d/\Delta \geqq 1$, the flow over the nose is of a nonequilibrium nature. A quasi-equilibrium state may be defined by $0 < d/\Delta < 1$ and the equilibrium state might be assumed for $d/\Delta \approx 0$. Figure 38 illustrates the variation of the parameter $r_n \frac{d}{\Delta}$ with altitude. Once the flow attains velocities typical of the hypersonic regime little effect is seen due to increasing velocity, the major factor influencing the onset of dissociation lag being the altitude for a given r_n. The literature on nonequilibrium flow is extensive (refs. 16 and 19 to 24) with more knowledge being gained as time passes. The present discussion is merely a cursory one for the purpose of calling attention to the problem.

METHOD OF ANALYSIS

Having discussed briefly some of the problems involved in estimating the nature of a hypersonic flow field and its effect on electromagnetic wave

propagation, the steps to be taken in obtaining a quantitative estimate of signal loss are next outlined.

Figure 39 illustrates, qualitatively, the property distributions along a line normal to the vehicle wall and extending from the wall to the shock. If these property distributions are known, the α distribution can be obtained by using equation (4) or the values can be taken directly from figures 13, 14, and 15 for those particular signal frequencies. Graphical integration of the distribution of α along a normal provides the total attenuation loss

$$\frac{(SL)_A}{D_n} = 8.686 \int_{Body}^{Shock} \alpha d\left(\frac{y}{D_n}\right) \tag{19}$$

in db/cm since all spatial coordinates in the available inviscid flow-field solutions have been nondimensionalized with respect to the nose diameter. To obtain the absolute attenuation in decibels simply insert the desired nose radius into the identity

$$(SL)_A \equiv \left[\frac{(SL)_A}{D_n}\right] D_n \tag{20}$$

The applicability of the equation to attenuation estimates becomes more valid with increased nose diameter since for small diameters the wavelengths may be very large with respect to the spatial variation of conductivity (refs. 7, 8, 10, and 25). A criterion for the applicability of these results as a function of the effective depth of the plasma sheath is presented and discussed in the section entitled "Results" and in appendix B.

The loss in decibels due to reflection $(SL)_R$ may be approximated by equation (5) along with the following relation:

$$(SL)_R = 10 \log \frac{1}{1 - R} \tag{21}$$

The total signal loss is the sum of the attenuation and reflection losses - that is,

$$(SL)_T = (SL)_A + (SL)_R \tag{22}$$

As mentioned previously, for generality and simplicity the effect of the boundary layer is not considered herein. The inviscid portion of the shock layer has thus been accounted for in such a manner as to make the results applicable to a particular shape regardless of its size, although with the least accuracy for the smaller bodies (smaller Reynolds number).

The dashed lines in figure 39 indicate some qualitative modifications to the inviscid distribution due to the viscous boundary layer. For the blunt-body

cases considered herein, a laminar boundary layer either decreases or has no effect on the attenuation and reflection. The effect of very thin laminar boundary layers can be entirely neglected, generally. A laminar boundary layer of significant thickness may alleviate the signal-loss problem somewhat. This alleviation is due to an increased fraction of the energy in the shock layer being transferred to the body with a consequent lowering of the high temperature in the high entropy layer adjacent to the body. Such an increase in the ratio of boundary-layer thickness to shock-layer thickness occurs as altitude is increased. A highly dissipative boundary layer on the other hand (higher Mach number flow) may increase attenuation and reflection somewhat, although this point is not clearly resolved. The term "highly dissipative boundary layer" refers herein to a boundary layer in which the static enthalpy increases above the maximum static enthalpy in the inviscid flow field. This condition is usually associated with sharp-nose vehicles and probably will not be encountered with blunt-nose vehicles, except for aft positions on the body.

In any event, if the boundary layer is classically thin, its attenuation effect can be calculated independently and can simply be added to the attenuation caused by the inviscid portion of the flow field. The reflection effects can be calculated anew to include the boundary-layer results.

RESULTS

Attenuation and reflection computations have been made for all the flow-field solutions at conditions listed in figure 2, but with the altitude range expanded. Only the inviscid portion of the flow field was considered and the resulting data are presented in table I.

The parametric results are only discussed in general here since the number of the computations is so large that discussion of each is deemed impractical. The parameters to be discussed are: the total attenuation normalized to nose diameter $(SL)_A/D_n$, the nondimensional effective plasma-sheath thickness d_e/D_n, the signal loss due to reflection $(SL)_R$, the wavelength within the plasma at the inviscid body wall and/or at the edge of a classically thin boundary layer λ_B, and the ratio of wavelength to nondimensional plasma-sheath thickness $\frac{\lambda_B D_n}{d_e}$.

Figures 40, 41, and 42 show, respectively, a variation of attenuation, effective plasma thickness, and reflection loss with axial distance along the body center line. It is seen that the lowest signal losses occur at the rear. It is interesting to note that the attenuation loss (fig. 40) appears to peak in the vicinity of the shoulder (that is, tangency of hemisphere to cone) although it might be expected to be a maximum farther toward the stagnation region. This result may be understood more clearly by writing the simple expression for the attenuation loss

$$(SL)_A = 8.686\alpha_B d_e \tag{23}$$

and differentiating with respect to axial distance x to give

$$\frac{d(SL)_A}{dx} = 8.686\left[\alpha_B \frac{d(d_e)}{dx} + d_e \frac{d(\alpha_B)}{dx}\right] \tag{24}$$

Because the flow is expanding and cooling,

$$\frac{d(\alpha_B)}{dx} \lessapprox 0$$

Thus, the significant part of equation (24) for the present argument is the variation of $d(d_e)/dx$, and as long as

$$0 < \alpha_B \frac{d(d_e)}{dx} > \left| d_e \frac{d(\alpha_B)}{dx} \right|$$

the attenuation will keep increasing with x. As soon as

$$\alpha_B \frac{d(d_e)}{dx} \lessapprox \left| d_e \frac{d(\alpha_B)}{dx} \right|$$

the attenuation will peak and begin to decrease with x. A typical variation of d_e with x is shown in figure 41.

Figures 43 and 44 show, respectively, the variation of the attenuation and reflection losses with altitude for a constant Mach number for signal frequencies of 30, 240, and 10,000 mc. It should be remembered that these are only examples of the variation, not necessarily typical variations. See table I for particular conditions of interest.

Values of $(SL)_A/D_n$ are presented in table I. It must be remembered that the value of the nose diameter being considered has to be multiplied by the tabulated value, as shown in equation (20), in order to obtain attenuation. An approximate attenuation history may then be constructed for any of the configurations given for any subcircular trajectory by interpolating directly between the Mach numbers presented. Application of such results is, of course, only valid in the range of altitudes and velocities where viscous and nonequilibrium effects are small, as discussed previously.

The tabulated values of $(SL)_R$ illustrate the signal loss due to reflection for all the bodies and flight conditions considered. These calculations were based on equation (5) with (d_e/D_n), evaluated for four numerical values of D_n, as the slab thickness. These four nose diameters were chosen to encompass a range including: (1) a sheath thickness always less than one-quarter wavelength and (2) three sheath thicknesses which are, for a number of frequency and body-shape combinations, in the neighborhood of, or slightly greater than, one-quarter

wavelength. It is seen that, for the smaller sheath thickness (for D_n = 5.08 cm), the estimated reflection loss is always less than that associated with the larger sheath thicknesses (D_n = 30.48, 25.40, and 20.32 cm), as can be explained by examination of figure 9. At the point where the data for the larger diameters coincide, the plasma sheath is approximately equal to or larger than one-quarter wavelength and acts in a manner similar to one of infinite thickness. As for attenuation, a rough history of the reflection loss for a particular trajectory may be obtained by interpolating directly between the Mach numbers given. The history of the total signal loss over the trajectory may then be obtained by summing the attenuation and reflection losses.

The nondimensional effective plasma-sheath thickness d_e/D_n is given along with the attenuation in table I. These data may be useful in making reflection calculations other than those considered herein. Because of the large variety of configurations presented here, the data may serve as a guide (by careful interpolation and extrapolation) to the selection of effective thicknesses for blunted configurations for which flow-field solutions are not available. Furthermore, since the thermodynamic properties at the body are often estimable without complete flow-field solutions (that is, from pressure coefficient and normal-shock entropy), an attenuation coefficient may be estimated based on the body properties and effective slab thickness, and may suffice for the calculation of attenuation (eq. (23)) and reflection.

The wavelength λ within the plasma is frequently seen to be a minimum at an intermediate altitude, depending upon frequency, and will approach its free-space value λ_0 as the density becomes very small, as at increasing altitude. These data may prove useful in the selection of antenna characteristics.

The ratio of wavelength to nondimensional sheath thickness $\lambda D_n/d_e$ should give some insight as to possible limits of applicability of such solutions, which assume homogeneity of plasma, to a flow field which is highly nonhomogeneous. (See appendix B.) If conditions are such that $\lambda/d_e \leqq 1$, then the homogeneous solution approach should be very accurate. This condition may not be achieved in many practical problems even for large bodies (large D_n) except when higher than standard telemetry frequencies are used. It is believed that the accuracy diminishes proportionally as λ/d_e increases greatly beyond unity ($\lambda/d_e \gg 1$), but it is difficult to say at this time just how inaccurate plane-wave, homogeneous solutions are when λ/d_e becomes very large.

CONCLUDING REMARKS

Estimates of signal loss in transmitting through the plasma sheath for a variety of hypersonic reentry situations have been made and presented in tabular form. It is seen from inspection of the data that very high signal loss is to be expected in many reentry situations. It is also seen, however, that the loss may be minimized by proper selection of frequency and location of the antenna at a rearward point on the body. Use of small bodies is also indicated on the basis of the equilibrium-flow considerations used in the analysis.

These data should be applied to specific problems with reservations in view of the assumptions which were used in making the calculations. Even though many qualifications apply to the results, it is believed that these results should be useful in estimating the qualitative variations of signal loss with respect to parameters such as Mach number, altitude, cone half-angle, and signal frequency.

Langley Research Center,
National Aeronautics and Space Administration,
Langley Station, Hampton, Va., March 7, 1963.

APPENDIX A

EXTRAPOLATION OF A GIVEN FLOW-FIELD SOLUTION TO DIFFERENT ALTITUDES

Consider the flow properties along a line normal to the afterbody (assumed direction of electromagnetic wave propagation). For a constant free-stream Mach number the inviscid, equilibrium properties along this normal are estimated for new ambient conditions (that is, range of altitudes) from the known property distribution along this normal at a particular ambient condition and by imposing the following conditions:

(1) Shock shape and shock-layer thickness do not change with variation in altitude.

(2) The normalized pressure coefficient at the body surface does not change with altitude.

(3) Variation of properties across the shock layer remains similar with changing altitude.

The flow can then be approximated by calculating the properties behind the shock (using condition (1)) and the properties at the body surface (using condition (2)), and by applying the similarity assumption (using condition (3)) between these two points.

The properties immediately behind the shock may be calculated by the usual Rankine-Hugoniot relations for the given shock angle and ambient flow conditions, including the real-gas effects when the shock is strong (ref. 26). The properties at the body (or immediately outside a thin boundary layer) may be found by employing the Mollier chart for equilibrium air (ref. 27) with the surface pressure and entropy. The pressure coefficient expressed in the normalized form is

$$\frac{C_p}{C_{p,max}} = \frac{p - p_1}{p_{NS} - p_1} \tag{A1}$$

and is considered constant at a particular body point for M = Constant and varying altitude (condition (2)). The normal-shock pressure p_{NS} may be calculated or is readily available in chart form (ref. 26) and the ambient pressure p_1 is taken from the ARDC model atmosphere (ref. 28). Thus, the local pressure p is easily calculated from equation (A1). The entropy at the body is simply the normal-shock entropy since the body streamline passes through the normal shock and the flow thereafter is isentropic. Inasmuch as two state properties (p, S_{NS}) at the body have been calculated, any other state properties, such as temperature and density, may be determined from the Mollier chart. By denoting the properties given by the flow-field solution as "base" properties and indicating them with primes, it is now possible to write expressions for the properties at the new altitude as functions of the "base" properties and the newly calculated body and shock properties.

First consider the temperature variation of the "base" solution (fig. 45)

$$T' = T'(y/d_e) \tag{A2}$$

In close proximity to the body it is reasonable that

$$\frac{T}{T'} \approx \frac{T_B}{T_B'} \tag{A3}$$

where the subscript B denotes conditions at the body (or edge of a classically thin boundary layer). By similar reasoning, at points close to the shock

$$\frac{T}{T'} \approx \frac{T_S}{T_S'} \tag{A4}$$

where the subscript S indicates properties immediately behind the shock. By use of assumption (3) T and T' can be related at points within the shock layer. If the origin $y/\Delta = 0$ is taken at the wall, it can be assumed that the effect of T_B/T_B' on T/T' is a linear one and decreases with increasing y/Δ as $T_B/T_B'(1 - y/\Delta)$. Likewise, in progressing toward the shock, it can be assumed that the effect of T_S/T_S' is a linear one also and increases with increasing y/Δ as $(y/\Delta)T_S/T_S'$. Now sum these two effects algebraically to obtain the expression

$$\frac{T}{T'} = \left(1 - \frac{y}{\Delta}\right)\frac{T_B}{T_B'} + \frac{y}{\Delta}\left(\frac{T_S}{T_S'}\right) \tag{A5}$$

Equation (A5) may be rearranged and written as

$$T = T'\left[\frac{T_B}{T_B'} + \frac{y}{\Delta}\left(\frac{T_S}{T_S'} - \frac{T_B}{T_B'}\right)\right] \tag{A6}$$

In the same manner as that used to obtain equation (A6), the following expression may be determined for the density:

$$\rho = \rho'\left[\frac{\rho_B}{\rho_B'} + \frac{y}{\Delta}\left(\frac{\rho_S}{\rho_S'} - \frac{\rho_B}{\rho_B'}\right)\right] \tag{A7}$$

Examples of the use of equations (A6) and (A7) are shown in figures 46 and 47, respectively.

Although this method is admittedly crude, it is an expedient means by which to extend a given flow-field solution over an altitude range and should result in

fairly close engineering estimates. Accuracy will depend upon the degree of applicability of the assumptions.

APPENDIX B

ATTENUATION AND PHASE-SHIFT COEFFICIENTS IN ONE-DIMENSIONAL NONHOMOGENEOUS CONDUCTING MEDIA

A suitable form of the wave equation is obtained by consideration of the Maxwell equations:

$$\nabla \times \overline{E} = -\frac{\partial \overline{B}}{\partial t} \tag{B1}$$

$$\nabla \times \overline{H} = \overline{J} + \frac{\partial \overline{D}}{\partial t} \tag{B2}$$

where $\overline{E}$ and $\overline{H}$ are electric and magnetic vectors, respectively. If the curl of equation (B1) is taken, equation (B2) is differentiated with respect to time, and use is made of the constitutive relation

$$\left.\begin{aligned} \overline{J} &= \sigma\overline{E} \\ \overline{D} &= \epsilon\overline{E} \\ \overline{B} &= \mu\overline{H} \end{aligned}\right\} \tag{B3}$$

then a general form of the wave equation is seen to be

$$\nabla \times \nabla \times \overline{E} = -\mu\sigma\frac{\partial \overline{E}}{\partial t} - \mu\epsilon\frac{\partial^2 \overline{E}}{\partial t^2} \tag{B4}$$

Now, consider a wave form which is one-dimensional, harmonic in time, and plane polarized. Such a wave can be represented by the wave function

$$E = E_0 \exp\left[i(\gamma y - \omega t)\right] \tag{B5}$$

The validity of equation (B5) is restricted to cases in which properties of the medium vary slightly over dimensions comparable to a wavelength.

Substitution of equation (B5) into equation (B4) results in

$$\mu\epsilon\omega^2 - \gamma^2 + i(\sigma\mu\omega) = 0 \tag{B6}$$

which becomes

$$\alpha^2 - \beta^2 + \mu\epsilon\omega^2 + i(\sigma\mu\omega - 2\alpha\beta) = 0 \tag{B7}$$

when the propagation factor is represented in complex form, $\gamma = \beta + i\alpha$.

Equating the real and imaginary parts of equation (B7) to zero gives a system of two simultaneous equations from which α and β can be determined, as follows:

$$\alpha = \omega\left[\frac{\mu\epsilon}{2}\left(\sqrt{1 + \frac{\sigma^2}{\epsilon^2\omega^2}} - 1\right)\right]^{1/2} \tag{B8}$$

$$\beta = \omega\left[\frac{\mu\epsilon}{2}\left(\sqrt{1 + \frac{\sigma^2}{\epsilon^2\omega^2}} + 1\right)\right]^{1/2} \tag{B9}$$

Inasmuch as equations (B8) and (B9) are valid only when properties of the medium vary slowly over a distance of 1 wavelength, a rough criterion can be set up which may be used in applying the calculations in this paper to a specific problem. Consider some linear distance L over which the plasma properties vary considerably. Then, the assumption used in selection of the wave function (B5) indicates that

$$\frac{\lambda}{L} \ll 1 \tag{B10}$$

must hold in order to assure accuracy. If this condition is not obtained, then the accuracy obtained in calculating α and β would be thought to diminish as the value of λ/L departs from a very small value and grows large. The value of λ may be considered to be the wavelength in the plasma adjacent to the body wall λ_B, and for a characteristic length L it is convenient to consider the effective plasma thickness d_e. Values of $\left(\lambda_B/d_e\right)D_n$ are given in table I. It is easy to see that for larger bodies (large D_n) the condition (B10) can be more nearly fulfilled.

REFERENCES

1. Huber, Paul W., and Gooderum, Paul B. (With appendix A by Theo E. Sims and Duncan E. McIver, Jr., and appendix B by Joseph Burlock and William L. Grantham): Experiments With Plasmas Produced by Potassium-Seeded Cyanogen Oxygen Flames for Study of Radio Transmission at Simulated Reentry Vehicle Plasma Conditions. NASA TN D-627, 1961.

2. Gravalos, F. G., Edelfelt, I. H., and Emmons, H. W.: The Supersonic Flow About a Blunt Body of Revolution for Gases at Chemical Equilibrium. Tech. Inf. Series No. R58SD245 (Contract AF 04(645)24), Missile and Ord. Syst. Dept., Gen. Elec. Co., June 16, 1958.

3. Ridyard, H. W.: Comparison of the Ionized Shock Layer About Two- and Three-Dimensional Blunt Shapes at Hypersonic Speeds. Planetary and Space Sci., vol. 6, June 1961, pp. 10-23.

4. FitzGibbon, Sheila A.: Real Gas Supersonic Flow Field Solutions in the Shock Layer Around a 9° Sphere-Cone at Mach = 20.4, 21.4 and 21.2. Aerod. Data Memo No. 1:48, Missile and Space Vehicle Dept., Gen. Elec. Co., May 1961.

5. Ratcliffe, J. A.: The Magneto-Ionic Theory and Its Applications to the Ionosphere. Cambridge Univ. Press, 1959.

6. Langberg, E., Baldwin, K., and Yos, J.: Radiation and Propagation of Telemetry Signals During Hypersonic Reentry. IRE Proceedings of the 1958 National Symposium on Telemetering, Section 3.2, Sept. 22-24, 1958, pp. 1-8.

7. Mitra, S. K.: The Upper Atmosphere. Second ed., The Asiatic Society (Calcutta, India), 1952. (Available from Hafner Pub. Co., New York.)

8. Schelkunoff, S. A.: Remarks Concerning Wave Propagation in Stratified Media. Communications on Pure and Appl. Math., vol. IV, no. 1, June 1951, pp. 117-128.

9. Hines, C. O.: Reflection of Waves From Varying Media. Quarterly Appl. Math., vol. XI, no. 1, Apr. 1953, pp. 9-31.

10. Stratton, Julius Adams: Electromagnetic Theory. McGraw-Hill Book Co., Inc., 1941.

11. Logan, J. G., Jr.: The Calculation of the Thermodynamic Properties of Air at High Temperatures. Rep. No. AD-1052-A-1 (AFOSR-TN-56-344, AD-95220), Cornell Aero. Lab., Inc., May 1956.

12. Logan, J. G., Jr., and Treanor, C. E.: Tables of Thermodynamic Properties of Air From 3,000° K to 10,000° K at Intervals of 100° K. Rep. No. BE-1007-A-3, Cornell Aero. Lab., Inc., Jan. 1957.

13. Delcroix, J. L.: Introduction to the Theory of Ionized Gases. Interscience Publ., Inc. (New York), 1960.

14. Spitzer, Lyman, Jr.: Physics of Fully Ionized Gases. Interscience Publ., Inc. (New York), 1956.

15. Ter Haar, D.: Introduction to the Physics of Many-Body Systems. Interscience Publ., Inc. (New York), 1958.

16. Feldman, Saul: Trails of Axi-Symmetric Hypersonic Blunt Bodies Flying Through the Atmosphere. Res. Rep. 82 (Contract No. DA-19-020-ORD-4765), Avco-Everett Res. Lab., Dec. 1959.

17. Bachynski, M. P., Johnston, T. W., and Shkarofsky, I. P.: Electromagnetic Properties of High-Temperature Air. Proc. IRE, vol. 48, no. 3, Mar. 1960, pp. 347-356.

18. Adams, Mac C., and Probstein, Ronald F.: On the Validity of Continuum Theory for Satellite and Hypersonic Flight Problems at High Altitudes. Jet Propulsion, vol. 28, no. 2, Feb. 1958, pp. 86-89.

19. Bortner, M. H.: The Effect of Errors in Rate Constants on Non-Equilibrium Shock Layer Electron Density Calculations. Planetary and Space Sci., vol. 6, June 1961, pp. 74-78.

20. Vaglio-Laurin, R., and Bloom, M. H.: Chemical Effects in External Hypersonic Flows. [Preprint] 1976-61, American Rocket Soc., Aug. 1961.

21. Sedney, Raymond: Some Aspects of Nonequilibrium Flows. Jour. Aerospace Sci., vol. 28, no. 3, Mar. 1961, pp. 189-196, 208.

22. Bloom, Martin H., and Steiger, Martin H.: Inviscid Flow With Nonequilibrium Molecular Dissociation for Pressure Distributions Encountered in Hypersonic Flight. Jour. Aerospace Sci., vol. 27, no. 11, Nov. 1960, pp. 821-835, 840.

23. Wray, Kurt L.: Chemical Kinetics of High Temperature Air. Hypersonic Flow Research, Frederick R. Riddell, ed., Academic Press (New York), 1962, pp. 181-204.

24. Wurster, Walter H., and Marrone, Paul V.: Study of Infrared Emission in Heated Air. Rep. No. QM-1373-A-4 (Contract DA-11-022-ORD-3130), Cornell Aero. Lab., Inc., July 1961.

25. Shklovsky, I. S. (Richard B. Rodman and Carlos M. Varsavsky, trans.): Cosmic Radio Waves. Harvard Univ. Press (Cambridge, Mass.), 1960.

26. Huber, Paul W.: Tables and Graphs of Normal-Shock Parameters at Hypersonic Mach Numbers and Selected Altitudes. NACA TN 4352, 1958.

27. Moeckel, W. E., and Weston, Kenneth C.: Composition and Thermodynamic Properties of Air in Chemical Equilibrium. NACA TN 4265, 1958.

28. Minzner, R. A., Champion, K. S. W., and Pond, H. L.: The ARDC Model Atmosphere, 1959. Air Force Surveys in Geophysics No. 115 (AFCRC-TR-59-267), Air Force Cambridge Res. Center, Aug. 1959.

TABLE I.- ESTIMATES OF ATTENUATION, REFLECTION, AND EFFECTIVE PLASMA THICKNESS

AS FUNCTIONS OF BODY GEOMETRY AND REENTRY PARAMETERS

θ, deg	M	x/D_n	f, cps	Altitude, ft	$(SL)_A/D_n$, db/cm	d_e/D_n	$(SL)_R$, db, for -				λ_B, cm	$\lambda_B D_n/d_e$, cm	$(R_{12})_B$
							D_n = 5.08 cm	D_n = 20.32 cm	D_n = 25.40 cm	D_n = 30.48 cm			
0	15	0.17	30×10^6	100×10^3	0.100	0.0422	3.15	7.68	8.53	9.24	22.980	544.94	0.9552
				154	.212	.0357	8.69	14.33	15.25	15.97	9.362	262.6	.9818
				174	.222	.0338	9.15	14.83	15.75	16.46	8.694	256.9	.9835
				200	.106	.0275	4.42	9.40	10.29	11.03	15.830	576.3	.9724
				230	.053	.0272	.97	3.87	4.56	5.15	43.102	1,582.9	.9494
			240×10^6	100	.286	.0420	3.15	7.59	8.34	8.88	8.190	195.0	.8794
				154	.637	.0355	8.66	13.36	13.50	13.44	3.635	102.4	.9532
				174	.685	.0337	9.12	13.90	14.10	14.10	3.770	111.9	.9602
				200	.320	.0278	4.20	9.33	10.20	10.87	10.920	393.7	.9462
				230	.100	.0284	.22	2.11	2.79	3.44	108.30	3,813.4	.9338
			$10,000 \times 10^6$	100	1.740	.0383	2.56	3.53	3.53	3.53	2.390	62.4	.5568
				154	1.555	.0298	4.53	10.47	10.53	10.54	13.990	470.0	.9118
				174	.951	.0241	1.85	10.47	11.48	11.89	330	1,372	.9385
				200	0	.0183	.019	.29	.42	.57	5.450	298.3	.0845
				230	0	.0184	0	0	0	0	3.063	166.3	.0001151
		.60	30×10^6	100×10^3	.043	.0989	.12	.92	1.21	1.49	127.93	1,293.5	.7772
				154	.204	.1728	2.78	7.14	7.96	8.63	55.67	322.2	.9133
				174	.242	.1654	3.55	8.27	9.11	9.79	53.49	323.4	.9324
				200	------	------	------	------	------	------	-------	--------	---------
				230	------	------	------	------	------	------	-------	--------	---------
			240×10^6	100	.120	.0952	.11	.87	1.14	1.41	47.90	503	.5110
				154	.588	.1905	2.40	7.04	7.66	8.03	57.90	304	.8559
				174	.576	.2000	2.53	8.26	9.10	9.63	112.7	564	.9074
				200	------	------	------	------	------	------	-------	--------	---------
				230	------	------	------	------	------	------	-------	--------	---------
			$10,000 \times 10^6$	100	0	.1207	.01	0	0	0	3.080	25.5	.0001992
				154	0	.4560	.01	0	0	0	3.057	6.7	.0001034
				174	0	.4545	.01	0	0	------	3.040	6.69	.0000556
				200	------	------	------	------	------	------	-------	--------	---------
				230	------	------	------	------	------	------	-------	--------	---------
		2.00	30×10^6	100×10^3	------	------	------	------	------	------	-------	--------	---------
				154	.142	.2124	.9415	3.793	4.463	5.044	113.9	536.5	.8572
				174	.1527	.2140	.9751	4.008	4.715	5.325	143.4	6,700	.8810
				200	------	------	------	------	------	------	-------	--------	---------
				230	------	------	------	------	------	------	-------	--------	---------
			240×10^6	100	------	------	------	------	------	------	-------	--------	---------
				154	.2763	.2115	.2720	2.410	3.147	3.822	215	1,016	.7972
				174	.206	.211	.1075	1.342	1.914	2.512	509	2,410	.8501
				200	------	------	------	------	------	------	-------	--------	---------
				230	------	------	------	------	------	------	-------	--------	---------

TABLE I.- ESTIMATES OF ATTENUATION, REFLECTION, AND EFFECTIVE PLASMA THICKNESS

AS FUNCTIONS OF BODY GEOMETRY AND REENTRY PARAMETERS - Continued

θ, deg	M	x/D_n	f, cps	Altitude, ft	$(SL)_A/D_n$, db/cm	d_e/D_n	$(SL)_R$, db, for -				λ_B, cm	$\lambda_B D_n/d_e$, cm	$(R_{12})_B$
							D_n = 5.08 cm	D_n = 20.32 cm	D_n = 25.40 cm	D_n = 30.48 cm			
0	18.1	0.50	30×10^6	100×10^3	0.319	0.0873	8.39	13.92	14.71	15.23	15.16	173.6	----------
				154	.7313	.1108	13.78	18.13	18.06	17.95	9.373	84.59	0.9837
				174	.7766	.1103	13.98	18.39	18.39	18.32	9.916	89.9	.9851
				200	.5273	.1022	10.76	16.31	16.96	17.32	19.61	191.9	.9825
				230	.2220	.1091	5.015	11.06	12.06	12.86	135.1	1,238.1	.9797
			240×10^6	100	.931	.0863	8.31	11.28	11.16	11.12	5.70	66.00	.9228
				154	2.247	.1159	13.67	15.06	15.06	15.06	6.848	59.07	.9688
				174	2.1713	.1300	14.40	16.35	16.35	16.35	13.79	106.1	.9768
				200	1.0058	.1291	10.33	16.36	16.67	16.78	74.13	574.2	.9793
				230	.2508	.1187	.5417	4.905	6.353	7.690	960.8	8,091.9	.9789
			$10,000 \times 10^6$	100	3.440	.0930	6.652	7.575	7.575	7.575	12.06	129.6	.00001333
				154	2.222	.1312	5.414	13.03	13.04	13.04	126.2	961.9	.9503
				174	.860	.6672	7.617	5.343	5.378	5.428	35.44	53.12	.7135
				200	.00186	.2162	.03727	.03984	.03055	.001042	3.333	15.42	.002785
				230	--------	-------	----------	---------	---------	---------	---------	----------	----------
		1.00	30×10^6	100×10^3	.278	.1079	6.411	11.76	12.60	13.21	22.09	204.72	.9577
				154	.8159	.1379	13.58	17.65	17.58	17.50	11.20	81.22	.9821
				174	.8869	.1383	13.92	18.10	18.09	18.05	12.43	89.90	.9842
				200	.5063	.1227	9.941	15.60	16.33	16.80	32.47	264.7	.9817
				230	.1162	.1043	1.361	6.344	7.420	8.317	376.7	3,612.0	.9753
			240×10^6	100	.8195	.1076	6.380	9.916	9.828	9.753	8.615	80.06	.8935
				154	2.134	.1386	13.35	15.23	15.23	15.23	12.15	87.64	.9700
				174	1.747	.1396	13.62	16.68	16.70	16.70	27.45	196.6	.9786
				200	.6396	.1226	6.432	14.69	15.68	16.27	170.7	1,391.9	.9800
				230	.09668	.09142	.02769	.4232	.6466	.9081	2,676.9	29,281.3	.9732
			$10,000 \times 10^6$	100	.671	.04772	.6213	4.526	5.1069	5.379	23.02	482.4	.7219
				154	.0256	.0556	.3073	.2899	3.613	4.121	10.76	193.5	.3182
				174	.00448	.08634	.2032	.1644	.002752	.2337	4.292	49.71	.03145
				200	.000101	.04526	.001712	.008035	.004793	.001183	3.136	69.29	.0004985
				230	--------	-------	----------	---------	---------	---------	---------	----------	----------
		2.00	30×10^6	100×10^3	.1924	.1166	3.848	8.636	9.491	10.18	34.261	293.8	.9360
				154	.8312	.1584	12.92	17.16	17.15	17.09	14.01	88.46	.9803
				174	.9042	.1581	13.41	17.84	17.92	17.91	16.77	106.04	.9837
				200	.4045	.1356	8.326	14.17	15.05	15.69	63.24	466.4	.9801
				230	.03423	.0654	.03998	.5511	.8122	1.1003	1,217.3	18,612.0	.9655
			240×10^6	100	.5885	.1161	3.809	7.980	8.256	8.303	14.25	122.8	.8477
				154	1.8106	.1583	12.63	15.41	15.42	15.42	24.03	151.8	.9713
				174	1.4296	.15801	12.62	16.98	17.04	17.06	57.83	366.0	.9803
				200	.4450	.1332	2.797	11.17	12.78	14.03	407.8	3,061.5	.9797
				230	.01294	.04252	.0002836	.004515	.007050	.01015	5,503.9	129,443.7	.9407
			$10,000 \times 10^6$	100	.03323	.07598	.1154	.1340	.006286	.07093	3.996	52.59	.02049
				154	.00519	.09650	.1822	.002791	.1471	.3553	4.031	41.77	.02153
				174	.00132	.09685	.05794	.01535	.08844	.06357	3.481	35.94	.005525
				200	--------	-------	----------	---------	---------	---------	---------	----------	----------
				230	--------	-------	----------	---------	---------	---------	---------	----------	----------

TABLE I.- ESTIMATES OF ATTENUATION, REFLECTION, AND EFFECTIVE PLASMA THICKNESS

AS FUNCTIONS OF BODY GEOMETRY AND REENTRY PARAMETERS - Continued

θ, deg	M	x/D_n	f, cps	Altitude, ft	$(SL)_A/D_n$, db/cm	d_e/D_n	$(SL)_R$, db, for -				λ_B, cm	$\lambda_B D_n/d_e$, cm	$(R_{12})_B$
							D_n = 5.08 cm	D_n = 20.32 cm	D_n = 25.40 cm	D_n = 30.48 cm			
0	18.1	3.50	30×10^6	100×10^3	0.1450	0.1129	2.447	6.6102	7.423	8.100	44.44	393.7	0.9186
				154	.7967	.1660	12.26	16.79	16.87	16.84	16.63	100.2	.9790
				174	.8682	.1673	12.91	17.64	17.82	17.86	21.60	129.1	.9836
				200	.355	.1445	7.11	12.97	13.88	14.58	81.8	566.0	.9777
				230	-------	-------	---------	----------	---------	---------	---------	----------	----------
			240×10^6	100	.4473	.1123	2.39	6.362	6.919	7.232	19.68	174.3	.8146
				154	1.525	.1642	11.74	15.44	15.47	15.48	37.45	228.1	.9717
				174	1.203	.1655	11.41	17.05	17.21	17.26	94.52	571.13	.9813
				200	.381	.141	1.64	8.85	10.53	11.92	538.0	3,820.0	.9766
				230	-------	-------	---------	----------	---------	---------	---------	----------	----------
			$10,000 \times 10^6$	100	.0109	.08191	.02801	.00009730	.02487	.05315	3.364	41.07	.003307
				154	.00229	.09843	.07195	.01872	.1091	.07920	3.541	35.97	.006870
				174	.00060	.09728	.02312	.01263	.03498	.01137	2.539	26.10	.002021
				200	.00357	.07911	.005700	.00004170	.006261	.01074	3.036	38.38	.00003792
				230	-------	-------	---------	----------	---------	---------	---------	----------	----------
		5.00	30×10^6	100×10^3	.1094	.11	1.41	4.76	5.50	6.12	58.2	529	.8965
				154	.7211	.1677	11.31	16.26	16.51	16.55	20.65	123.1	.9776
				174	.7819	.1694	12.19	17.31	17.65	17.78	28.69	169.4	.9835
				200	.2218	.1303	4.431	10.52	11.54	12.35	176.6	1,355.4	.9777
				230	-------	-------	---------	----------	---------	---------	---------	----------	----------
			240×10^6	100	.338	.109	1.31	4.62	5.27	5.76	27.65	254.0	.7759
				154	1.225	.1671	10.36	15.33	15.46	15.50	61.09	365.6	.9719
				174	.9867	.1680	9.655	16.80	17.19	17.34	149.6	890.2	.9819
				200	.2110	.1218	.2798	3.145	4.292	5.416	1,263.8	10,376.4	.9767
				230	-------	-------	---------	----------	---------	---------	---------	----------	----------
			$10,000 \times 10^6$	100	-------	-------	---------	----------	---------	---------	---------	----------	----------
				154	.000959	.09555	.02460	.01087	.03803	.01707	3.295	34.48	.002217
				174	.000188	.0653	.005247	.003446	.0002714	.007176	3.175	48.62	.0008109
				200	-------	-------	---------	----------	---------	---------	---------	----------	----------
				230	-------	-------	---------	----------	---------	---------	---------	----------	----------

TABLE I.- ESTIMATES OF ATTENUATION, REFLECTION, AND EFFECTIVE PLASMA THICKNESS

AS FUNCTIONS OF BODY GEOMETRY AND REENTRY PARAMETERS - Continued

θ, deg	M	x/D_n	f, cps	Altitude, ft	$(SL)_A/D_n$, db/cm	d_e/D_n	$(SL)_R$, db, for -				λ_B, cm	$\lambda_B D_n/d_e$, cm	$(R_{12})_B$
							D_n = 5.08 cm	D_n = 20.32 cm	D_n = 25.40 cm	D_n = 30.48 cm			
0	18.24	0.50	30×10^6	100×10^3	0.3704	0.1039	8.884	14.37	15.05	15.42	15.51	149.31	0.9698
				154	.9555	.1206	15.75	18.81	18.68	18.65	7.607	63.08	.9864
				174	.9252	.1343	14.67	18.30	18.20	18.15	9.907	73.77	.9847
				200	.6476	.1205	11.77	17.05	17.47	17.64	18.07	149.9	.9828
				230	.3157	.1292	7.116	13.21	14.16	14.91	105.09	813.4	.9820
			240×10^6	100	1.0753	.10222	8.772	11.08	11.01	11.01	5.793	56.67	.9208
				154	2.956	.1225	15.07	15.55	15.55	15.55	4.705	38.41	.9721
				174	2.666	.1568	14.89	16.10	16.10	16.10	12.43	79.29	.9755
				200	1.3303	.1583	11.98	16.73	16.82	16.84	63.76	402.8	.9793
				230	.3723	.1446	1.4998	8.728	10.51	12.02	741.7	5,128.3	.9813
			$10,000 \times 10^6$	100	4.646	.1238	7.127	7.357	7.357	7.357	11.13	89.90	.8162
				154	4.343	.1521	12.41	14.27	14.27	14.27	90.77	596.8	.9626
				174	1.649	.3508	6.888	10.12	10.12	10.12	109.8	313.0	.9026
				200	.00369	.3290	.0002015	.003119	.004809	.006819	3.4009	10.34	.003941
				230	--------	-------	----------	---------	---------	---------	----------	----------	---------
		1.00	30×10^6	100×10^3	.3457	.1376	7.258	12.63	13.36	13.80	22.18	161.21	.9575
				154	1.1953	.1637	16.16	18.37	18.33	18.33	8.654	52.86	.9853
				174	1.1114	.1764	14.81	17.98	17.92	17.90	12.26	69.48	.9838
				200	.7077	.1587	11.58	16.86	17.29	17.48	28.62	180.4	.9825
				230	.1909	.1312	3.550	9.857	10.94	11.81	269.5	2,054.3	.9790
			240×10^6	100	1.0359	.1372	7.209	9.775	9.692	9.675	8.582	62.55	.8924
				154	3.404	.1645	15.29	15.71	15.71	15.71	7.195	43.74	.9731
				174	2.2865	.1791	14.54	16.48	16.48	16.48	24.93	139.2	.9775
				200	.9254	.1601	9.074	16.36	16.82	17.01	144.2	900.5	.9806
				230	.18102	.1263	.1524	1.984	2.834	3.721	1,966.2	15,567.6	.9787
			$10,000 \times 10^6$	100	1.034	.06807	1.291	5.404	5.542	5.574	21.78	320.0	.7233
				154	1.563	.08937	3.081	13.59	13.80	13.83	147.8	1,654.0	.9587
				174	.00745	.1221	.3882	.09305	.5601	.4321	4.420	36.20	.03667
				200	.000290	.1012	.009590	.008568	.01133	.0003608	3.169	31.31	.0007606
				230	--------	-------	----------	---------	---------	---------	----------	----------	---------
			30×10^6	100×10^3	.2637	.1610	4.789	9.818	10.64	11.26	34.47	214.1	.9356
				154	1.270	.1906	15.74	18.06	18.03	18.03	10.59	55.56	.9843
				174	1.1335	.1987	14.34	17.86	17.84	17.83	9.563	48.13	.9835
				200	.5884	.17704	10.28	15.96	16.63	17.04	55.14	311.4	.9822
				230	.09826	.1304	.5753	4.269	5.326	6.254	818.7	6,278.1	.9750
			240×10^6	100	.8008	.1594	4.731	8.255	8.228	8.165	14.23	89.25	.8460
				154	3.0892	.1990	15.34	16.19	16.19	16.19	15.42	77.50	.9759
				174	1.917	.2078	13.98	16.94	16.95	16.95	54.14	260.6	.9798
				200	.6741	.1795	5.324	14.61	15.81	16.51	351.4	1,957.8	.9813
				230	.0743	.1184	.009296	.1469	.2281	.3263	5,290.6	44,684.5	.9696
			$10,000 \times 10^6$	100	.0610	.1296	.2647	.2012	.2327	.01644	4.0357	31.14	.02193
				154	.0269	.1161	.9769	2.7912	1.6450	.3439	7.787	67.07	.1971
				174	.00245	.1632	.1048	.01175	.08682	.02500	3.507	21.49	.006093
				200	--------	-------	----------	---------	---------	---------	----------	----------	---------
				230	--------	-------	----------	---------	---------	---------	----------	----------	---------

TABLE I.- ESTIMATES OF ATTENUATION, REFLECTION, AND EFFECTIVE PLASMA THICKNESS

AS FUNCTIONS OF BODY GEOMETRY AND REENTRY PARAMETERS - Continued

θ, deg	M	x/D_n	f, cps	Altitude, ft	$(SL)_A/D_n$, db/cm	d_e/D_n	$(SL)_R$, db, for -				λ_B, cm	$\lambda_B D_n/d_e$, cm	$(R_{12})_B$
							D_n = 5.08 cm	D_n = 20.32 cm	D_n = 25.40 cm	D_n = 30.48 cm			
0	18.24	3.50	30×10^6	100×10^3	0.1852	0.1510	2.925	7.337	8.163	8.836	46.45	307.7	0.9150
				154	1.250	.2074	15.17	17.69	17.66	17.65	12.28	59.19	.9828
				174	1.029	.2038	13.47	17.58	17.63	17.63	21.27	104.4	.9827
				200	.4503	.1779	8.527	14.48	15.33	15.94	90.36	507.9	.9807
				230	.0224	.05167	.01204	.1814	.2766	.3882	1,813.5	35,097.0	.9663
			240×10^6	100	.5699	.15012	2.869	6.787	7.115	7.211	20.21	134.6	.8055
				154	2.678	.2059	14.72	16.05	16.05	16.05	21.54	104.7	.9752
				174	1.472	.2022	12.33	16.91	16.97	16.98	87.91	434.8	.9800
				200	.4711	.1734	2.337	10.75	12.52	13.90	619.9	3,575.2	.9799
				230	.001871	.03034	.00006860	.001079	.001684	.002424	2,026.5	66,791.7	.7851
			$10,000 \times 10^6$	100	.01424	.1074	.03735	.03267	.04008	.0009310	3.345	31.14	.002985
				154	.00915	.1181	.4248	.01582	.5041	.6931	4.597	38.92	.4427
				174	.000802	.1225	.03069	.03539	.003764	.2034	3.284	26.81	.002050
				200	--------	-------	----------	---------	---------	----------	---------	---------	---------
				230	--------	-------	----------	---------	---------	----------	---------	---------	---------
		5.00	30×10^6	100×10^3	.1433	.1440	1.8719	5.6424	6.4152	7.065	57.93	402.3	.8963
				154	1.216	.2119	14.74	17.61	17.57	17.56	13.97	65.96	.9825
				174	.9306	.2053	12.76	17.39	17.55	17.58	27.67	134.8	.9825
				200	.345	.177	6.74	12.94	13.90	14.64	146.3	828.0	.9796
				230	--------	-------	----------	---------	---------	----------	---------	---------	---------
			240×10^6	100	.4411	.1428	1.7850	5.401	5.953	6.282	26.99	189.0	.7735
				154	2.3291	.21115	14.35	16.27	16.28	16.28	32.02	151.7	.9764
				174	1.212	.2043	10.79	16.89	17.06	17.11	137.1	671.0	.9806
				200	.339	.1683	.87	6.65	8.36	9.89	1,046.0	6,210.0	.9787
				230	--------	-------	----------	---------	---------	----------	---------	---------	---------
			$10,000 \times 10^6$	100	.00550	.1079	.009781	.01071	.006774	.0007187	3.165	29.33	.007219
				154	.00442	.1260	.2052	.1981	.2083	.0003743	3.861	30.64	.01580
				174	.000354	.1127	.01204	.01418	.005054	.003435	3.179	28.21	.0008466
				200	--------	-------	----------	---------	---------	----------	---------	---------	---------
				230	--------	-------	----------	---------	---------	----------	---------	---------	---------

TABLE I.- ESTIMATES OF ATTENUATION, REFLECTION, AND EFFECTIVE PLASMA THICKNESS

AS FUNCTIONS OF BODY GEOMETRY AND REENTRY PARAMETERS - Continued

θ, deg	M	x/D_n	f, cps	Altitude, ft	$(SL)_A/D_n$, db/cm	d_e/D_n	$(SL)_R$, db, for -				λ_B, cm	$\lambda_B D_n/d_e$, cm	$(R_{12})_B$
							D_n = 5.08 cm	D_n = 20.32 cm	D_n = 25.40 cm	D_n = 30.48 cm			
0	19.25	0.50	30×10^6	100×10^3	0.4535	0.0875	11.20	16.60	17.05	17.17	10.664	121.87	0.9792
				154	.9248	.1150	15.63	18.90	18.77	18.72	7.589	65.991	.9886
				174	.9450	.1175	15.43	18.95	18.85	18.81	8.426	71.711	.9868
				200	.7099	.1046	13.13	18.22	18.52	18.60	13.73	131.3	.9861
				230	.3863	.1091	9.499	15.55	16.46	17.14	69.6	637.95	.9871
			240×10^6	100	1.316	.08618	11.03	12.57	12.57	12.57	3.97	46.06	.9447
				154	2.853	.1184	15.12	15.76	15.76	15.76	5.089	42.98	.9734
				174	2.755	.1370	15.61	16.71	16.71	16.71	10.20	74.45	.9787
				200	1.539	.1396	13.75	17.63	17.67	17.68	44.95	322.0	.9829
				230	.4819	.1275	3.744	13.10	14.81	16.10	490.2	3,845.0	.9867
			$10,000 \times 10^6$	100	6.25	.1054	8.948	8.990	8.990	8.990	7.56	71.7	.8738
				154	4.13	.1908	12.03	14.47	14.47	14.47	105.02	550.4	.9643
				174	2.42	.1866	6.6410	14.23	14.24	14.24	206.9	1,108.5	.9623
				200	.00726	.3086	.07202	.1488	.02618	.01294	3.8153	12.36	.01443
				230	-------	-------	---------	---------	---------	---------	---------	---------	--------
		1.00	30×10^6	100×10^3	.4729	.1194	10.24	15.53	15.93	16.0	14.07	117.8	.9728
				154	1.1171	.1527	15.81	18.43	18.37	18.36	8.933	58.5	.9854
				174	1.1402	.1551	15.58	18.64	18.58	18.57	10.48	67.6	.9861
				200	.8211	.1378	13.35	18.32	18.58	18.66	20.44	148.32	.9864
				230	.2680	.11485	7.038	13.63	14.66	15.48	165.9	1,444.7	.9872
			240×10^6	100	1.417	.1191	10.11	11.56	11.56	11.56	5.437	45.65	.9302
				154	3.024	.1549	15.25	16.02	16.02	16.02	8.983	57.99	.9750
				174	2.376	.1591	15.36	17.14	17.14	17.14	21.22	133.4	.9807
				200	1.105	.1394	11.73	17.84	18.08	18.16	98.42	706.0	.9848
				230	.2656	.1124	.7360	6.025	7.652	9.132	1,243.6	11,063.7	.9868
			$10,000 \times 10^6$	100	2.86	.08721	6.375	8.489	8.490	8.490	18.39	210.9	.8584
				154	.8163	.06129	1.021	9.427	11.47	12.63	173.29	2,827.4	.9559
				174	.01057	.0949	.5159	1.3873	.5474	.006125	5.859	61.74	.10437
				200	.0006	.0898	.02919	.004815	.04221	.04184	3.341	37.203	.002933
				230	-------	-------	---------	---------	---------	---------	---------	---------	--------
		2.00	30×10^6	100×10^3	.3997	.13816	8.299	13.67	14.29	14.58	19.49	141.03	.9630
				154	1.1431	.1738	15.23	18.06	18.01	17.99	10.92	62.83	.9841
				174	1.169	.1744	15.16	18.52	18.49	18.48	13.67	78.40	.9858
				200	.7125	.1454	12.46	17.87	18.36	18.59	33.25	228.7	.9867
				230	.1918	.1289	4.024	11.10	12.28	13.23	394.97	3,064.2	.9886
			240×10^6	100	1.223	.1379	8.228	10.46	10.42	10.42	7.984	57.897	.9092
				154	2.579	.1733	14.84	16.25	16.25	16.25	17.12	98.77	.9763
				174	1.925	.1739	14.69	17.55	17.56	17.56	43.28	248.9	.9824
				200	.8300	.1444	8.905	17.25	17.93	18.25	200.7	1,389.9	.9858
				230	.1746	.1209	.1444	1.915	2.751	3.630	2,962.3	24,502	.9860
			$10,000 \times 10^6$	100	.6655	.0531	.6705	5.088	5.799	6.146	31.21	399.5	.7708
				154	.01452	.0929	.5405	1.825	1.052	.2014	6.236	67.125	.1230
				174	.00285	.11505	.1737	.1056	.2517	.06619	5.829	33.28	.0007328
				200	.000134	.06039	.004169	.005361	.0001207	.003055	3.164	52.39	.0007328
				230	--------	-------	---------	---------	---------	---------	---------	---------	---------

TABLE I.- ESTIMATES OF ATTENUATION, REFLECTION, AND EFFECTIVE PLASMA THICKNESS

AS FUNCTIONS OF BODY GEOMETRY AND REENTRY PARAMETERS - Continued

θ, deg	M	x/D_n	f, cps	Altitude, ft	$(SL)_A/D_n$, db/cm	d_e/D_n	$(SL)_B$, db, for -				λ_B, cm	$\lambda_B D_n/d_e$, cm	$(R_{12})_B$
							D_n = 5.08 cm	D_n = 20.32 cm	D_n = 25.40 cm	D_n = 30.48 cm			
0	19.25	3.50	30×10^6	100×10^3	0.3157	0.1418	6.411	11.71	12.50	13.03	25.601	180.5	0.9522
				154	1.1503	.1892	14.78	17.85	17.80	17.80	12.96	68.48	.9833
				174	1.167	.1889	14.84	18.49	18.49	18.48	17.36	91.91	.9858
				200	.6446	.1602	11.92	17.59	18.21	18.56	53.58	334.5	.9872
				230	.12703	.4869	1.549	7.536	8.818	9.880	759.46	1,559.8	.9858
			240×10^6	100	.9768	.1414	6.361	9.599	9.545	9.511	11.17	79.03	.8878
				154	2.272	.1897	14.44	16.43	16.43	16.43	28.09	148.1	.9773
				174	1.678	.18804	14.02	17.82	17.84	17.84	71.59	380.7	.9836
				200	.6952	.1582	6.523	16.20	17.39	18.07	364.1	2,301.3	.9867
				230	.1044	.1091	.02827	.4358	.6679	.9409	5,470.4	50,141.2	.9844
			$10,000 \times 10^6$	100	.05791	.08881	.3306	.5174	.1011	.08609	5.0	56.3	.06310
				154	.00563	.1203	.2820	.1323	.4179	.1762	4.121	34.26	.02492
				174	.001316	.1242	.07294	.08589	.2416	.02744	3.456	27.828	.005056
				200	--------	-------	---------	---------	-------	---------	----------	----------	--------
				230	--------	-------	---------	---------	-------	---------	----------	----------	--------
		5.00	30×10^6	100×10^3	.2351	.1335	4.596	9.596	10.45	11.11	32.73	245.13	.9400
				154	1.0878	.1829	14.38	17.89	17.86	17.84	14.45	79.01	.9835
				174	1.034	.1812	14.16	18.44	18.53	18.54	21.72	119.9	.9860
				200	.5373	.1583	10.93	16.88	17.65	18.16	76.95	486.1	.9872
				230	.0785	.1058	.3847	3.525	4.569	5.520	1,330.8	12,580.7	.9840
			240×10^6	100	.7303	.1330	4.5309	8.604	8.757	8.759	15.26	114.7	.8650
				154	1.914	.1820	13.93	16.75	16.76	16.76	39.65	217.8	.9789
				174	1.353	.1800	12.68	17.95	18.04	18.07	106.44	591.5	.9844
				200	.5557	.1548	4.238	14.04	15.72	16.91	549.0	3,546.2	.9868
				230	.04835	.07970	.003859	.06142	.09573	.1375	8,602.7	107,938	.9804
			$10,000 \times 10^6$	100	.0178	.09498	.08660	.005905	.1067	.1295	3.632	38.24	.009176
				154	.00287	.1137	.1402	.09259	.1982	.04134	3.729	32.91	.01181
				174	.000586	.1046	.02897	.02482	.03565	.001866	3.3017	31.56	.002321
				200	--------	-------	---------	---------	-------	---------	----------	----------	--------
				230	--------	-------	---------	---------	-------	---------	----------	----------	--------

TABLE I.- ESTIMATES OF ATTENUATION, REFLECTION, AND EFFECTIVE PLASMA THICKNESS

AS FUNCTIONS OF BODY GEOMETRY AND REENTRY PARAMETERS - Continued

θ, deg	M	x/D_n	f, cps	Altitude, ft	$(SL)_A/D_n$, db/cm	d_e/D_n	$(SL)_R$, db, for -				λ_B, cm	$\lambda_B D_n/d_e$, cm	$(R_{12})_B$
							D_n = 5.08 cm	D_n = 20.32 cm	D_n = 25.40 cm	D_n = 30.48 cm			
9	15	0.42	30×10^6	85×10^3	0.0692	0.0856	0.65	2.98	3.58	4.10	67.7	791	0.8737
				100	.0851	.0963	.95	3.77	4.43	5.01	62.3	647	.8839
				154	.1818	.0982	3.87	8.68	9.54	10.24	32.32	329	.9430
				174	.2553	.0865	6.304	11.67	12.54	13.22	21.94	254	.9645
				200	.098	.0922	.977	3.93	4.61	5.21	81.8	887	.9117
				230	-------	-------	-----	------	------	------	-------	--------	-------
			240×10^6	85	.1928	.0835	.63	2.90	3.46	3.94	24.25	290.5	.6866
				100	.2413	.0940	.92	3.66	4.26	4.75	22.8	242.6	.7138
				154	.5610	.0990	3.73	8.35	8.89	9.18	19.09	192.9	.8839
				174	.7430	.0935	6.24	11.41	11.85	12.05	21.96	235.0	.9395
				200	.1960	.1088	.24	2.35	3.12	3.85	225.0	2,070.0	.8862
				230	-------	-------	-----	------	------	------	-------	--------	-------
			$10,000 \times 10^6$	85	.318	.0775	.21	.23	.16	.18	4.287	55.3	.0480
				100	.180	.1373	.21	.15	.07	.06	3.866	28.16	.0176
				154	.0121	.1811	.06	.02	.03	.03	3.364	18.57	.0033
				174	-------	.1291	.08	.09	.01	.05	3.478	26.93	.0055
				200	-------	-------	-----	------	------	------	3.015	--------	.00001
				230	-------	-------	-----	------	------	------	-------	--------	-------
		2.00	30×10^6	85×10^3	.01973	.0445	.032	.33	.46	.60	123.5	2,776	.7822
				100	.02257	.0459	.048	.46	.64	.81	112.8	2,458	.8012
				154	.1116	.0985	1.46	4.89	5.63	6.26	58.5	594	.9098
				174	.1376	.099	2.03	5.99	6.79	7.46	57.2	578	.9293
				200	-------	-------	-----	------	------	------	-------	--------	-------
				230	-------	-------	-----	------	------	------	-------	--------	-------
			240×10^6	85	.0553	.0438	.03	.32	.45	.58	44.34	1,012	.5090
				100	.0656	.04535	.046	.450	.617	.787	42.8	944	.5566
				154	.287	.0986	.91	4.36	5.16	5.83	63.45	643.5	.8520
				174	.2653	.0994	.76	4.59	5.57	6.41	126.1	1,269	.9042
				200	-------	-------	-----	------	------	------	-------	--------	-------
				230	-------	-------	-----	------	------	------	-------	--------	-------
			$10,000 \times 10^6$	85	-------	.0368	-----	------	------	------	3.16	85.9	.000755
				100	-------	.0392	-----	------	------	------	3.10	79.1	.000285
				154	-------	.0725	-----	------	------	------	3.05	42.08	--------
				174	-------	-------	-----	------	------	------	3.035	--------	--------
				200	-------	-------	-----	------	------	------	-------	--------	--------
				230	-------	-------	-----	------	------	------	-------	--------	--------

TABLE I.- ESTIMATES OF ATTENUATION, REFLECTION, AND EFFECTIVE PLASMA THICKNESS

AS FUNCTIONS OF BODY GEOMETRY AND REENTRY PARAMETERS - Continued

θ, deg	M	x/D_n	f, cps	Altitude, ft	$(SL)_A/D_n$, db/cm	d_e/D_n	$(SL)_R$, db, for -				λ_B, cm	$\lambda_B D_n/d_e$, cm	$(R_{12})_B$
							D_n = 5.08 cm	D_n = 20.32 cm	D_n = 25.40 cm	D_n = 30.48 cm			
9	15	4.00	30×10^6	85×10^3	0.0107	0.03025	0.01	0.08	0.12	0.17	154.7	5,115	0.7354
				100	.01022	.02584	.0072	.092	.13	.18	141.0	5,455	.7594
				154	.0543	.0656	.35	2.02	2.50	2.95	85.9	1,310	.8806
				174	.063	.0669	.44	2.41	2.96	3.45	96	1,435	.9028
				200	-------	-------	-------	-----	-----	-----	-------	---------	------
				230	-------	-------	-------	-----	-----	-----	-------	---------	------
			240×10^6	85	.02985	.0297	.006	.081	.12	.16	55.75	1,877	.4327
				100	.02725	.02338	.006	.074	.11	.15	55.0	2,353	.4903
				154	.1202	.065	.10	1.08	1.49	1.90	127.9	1,968	.8211
				174	.0997	.0658	.05	.67	.97	1.30	286.8	4,360	.8764
				200	-------	-------	-------	-----	-----	-----	-------	---------	------
				230	-------	-------	-------	-----	-----	-----	-------	---------	------
			$10,000 \times 10^6$	85	0	.0259	-------	-----	-----	-----	3.07	118.5	------
				100	.01043	.384	-------	-----	-----	-----	3.043	7.93	------
				154	-------	-------	-------	-----	-----	-----	3.02	---------	------
				174	-------	-------	-------	-----	-----	-----	3.01	---------	------
				200	-------	-------	-------	-----	-----	-----	-------	---------	------
				230	-------	-------	-------	-----	-----	-----	-------	---------	------
		5.20	30×10^6	85×10^3	-------	.02044	.0027	.037	.056	.077	160.0	7,825	.7276
				100	-------	.0205	.0036	.049	.073	.100	150.1	7,330	.7461
				154	.0374	.0492	.17	1.21	1.56	1.90	95.3	1,936	.8715
				174	.0425	.0494	.20	1.44	1.84	2.22	109.0	2,207	.8959
				200	-------	-------	-------	-----	-----	-----	-------	-------	------
				230	-------	-------	-------	-----	-----	-----	-------	-------	------
			240×10^6	85	0	.0202	.003	.04	.05	.07	57.7	2,857	.4207
				100	.0222	.0203	-------	-----	-----	-----	59.0	2,907	.4701
				154	.0797	.0488	.038	.48	.69	.92	152.8	3,130	.8109
				174	.0642	.0485	.02	.24	.37	.52	345.6	7,125	.8686
				200	-------	------	------	-----	-----	-----	------	---------	------
				230	-------	-------	------	-----	-----	-----	------	---------	------
			$10,000 \times 10^6$	85	-------	.01873	------	-----	-----	-----	3.064	163.6	------
				100	-------	.0189	------	-----	-----	-----	3.04	160.8	------
				154	-------	------	------	-----	-----	-----	3.013	---------	------
				174	-------	-------	------	-----	-----	-----	3.01	---------	------
				200	-------	-------	------	-----	-----	-----	-------	---------	------
				230	-------	-------	------	-----	-----	-----	-------	---------	------

TABLE I.- ESTIMATES OF ATTENUATION, REFLECTION, AND EFFECTIVE PLASMA THICKNESS

AS FUNCTIONS OF BODY GEOMETRY AND REENTRY PARAMETERS - Continued

θ, deg	M	x/D_n	f, cps	Altitude, ft	$(SL)_A/D_n$, db/cm	d_e/D_n	$(SL)_R$, db, for -				λ_B, cm	$\lambda_B D_n/d_e$, cm	$(R_{12})_B$
							D_n = 5.08 cm	D_n = 20.32 cm	D_n = 25.40 cm	D_n = 30.48 cm			
9	15	6.50	30×10^6	85×10^3	-------	0.02096	0.0023	0.032	0.048	0.066	169.1	8,070	0.7145
				100	-------	.02116	.0034	.047	.070	.096	154.3	7,290	.7402
				154	0.0339	.044	.14	1.08	1.41	1.72	95.1	2,160	.8732
				174	.03235	.0391	.12	.98	1.29	1.59	114.8	2,938	.8925
				200	-------	-------	------	-----	-----	-----	-------	--------	------
				230	-------	-------	------	-----	-----	-----	-------	--------	------
			240×10^6	85	0	.0206	------	-----	-----	-----	60.8	2,950	.4002
				100	.0222	.02085	------	-----	-----	-----	60.8	2,917	.4613
				154	.0703	.0432	.03	.38	.56	.76	158.3	3,666	.8151
				174	.04725	.0378	------	-----	-----	-----	371.0	9,820	.8644
				200	-------	-------	------	-----	-----	-----	-------	--------	------
				230	-------	-------	------	-----	-----	-----	-------	--------	------
			$10,000 \times 10^6$	85	-------	.01865	------	-----	-----	-----	3.056	163.8	------
				100	-------	.01877	------	-----	-----	-----	3.036	161.7	------
				154	-------	-------	------	-----	-----	-----	3.014	--------	------
				174	-------	-------	------	-----	-----	-----	3.006	--------	------
				200	-------	-------	------	-----	-----	-----	-------	--------	------
				230	-------	-------	------	-----	-----	-----	-------	--------	------
		7.82	30×10^6	85×10^3	-------	.0215	.0023	.032	.048	.067	171.2	7,965	.7117
				100	-------	.01526	.0017	.025	.037	.052	156.5	10,250	.7372
				154	.0302	.04085	.11	.89	1.17	1.45	99.3	2,430	.8683
				174	.0335	.04104	.12	1.0	1.32	1.62	117.5	2,863	.8916
				200	-------	-------	------	-----	-----	-----	-------	--------	------
				230	-------	-------	------	-----	-----	-----	-------	--------	------
			240×10^6	85	.01905	.0211	------	-----	-----	-----	61.6	2,920	.3962
				100	.01585	.01512	------	-----	-----	-----	61.8	4,087	.4569
				154	.0626	.0404	------	-----	-----	-----	165.7	4,100	.8081
				174	.04865	.040	------	-----	-----	-----	385.0	9,630	.8635
				200	-------	-------	------	-----	-----	-----	-------	--------	------
				230	-------	-------	------	-----	-----	-----	-------	--------	------
			$10,000 \times 10^6$	85	-------	.0189	------	-----	-----	-----	3.055	161.6	------
				100	-------	.01425	------	-----	-----	-----	3.033	212.8	------
				154	-------	-------	------	-----	-----	-----	3.01	--------	------
				174	-------	-------	------	-----	-----	-----	3.01	--------	------
				200	-------	-------	------	-----	-----	-----	-------	--------	------
				230	-------	-------	------	-----	-----	-----	-------	--------	------

TABLE I.- ESTIMATES OF ATTENUATION, REFLECTION, AND EFFECTIVE PLASMA THICKNESS

AS FUNCTIONS OF BODY GEOMETRY AND REENTRY PARAMETERS - Continued

θ, deg	M	x/D_n	f, cps	Altitude, ft	$(SL)_A/D_n$, db/cm	d_e/D_n	$(SL)_R$, db, for -				λ_B, cm	$\lambda_B D_n/d_e$, cm	$(R_{12})_B$
							D_n = 5.08 cm	D_n = 20.32 cm	D_n = 25.40 cm	D_n = 30.48 cm			
9	20	0.1333	30×10^6	60×10^3	0.548	0.0469	15.43	20.53	20.68	20.57	4.678	99.7	0.99069
				100	.575	.0489	15.66	20.62	20.70	20.56	4.651	95.1	.99074
				154	-----	-----	-----	-----	-----	-----	-----	-----	-----
				174	.559	.0408	16.13	21.21	21.35	21.25	4.059	99.5	.99206
				200	.534	.0493	14.81	20.04	20.30	20.27	5.301	107.5	.98999
				230	.427	.0473	12.70	18.34	19.00	19.34	7.186	151.9	.98816
			240×10^6	60	1.55	.0469	15.19	15.82	15.83	15.83	1.655	35.3	.9739
				100	1.631	.0489	15.37	15.87	15.88	15.88	1.631	33.8	.97415
				154	-----	-----	-----	-----	-----	-----	-----	-----	-----
				174	1.669	.0408	15.89	16.80	16.80	16.80	1.549	37.97	.97911
				200	1.659	.0491	14.64	16.26	16.26	16.26	2.405	48.98	.9764
				230	1.194	.0488	12.73	16.77	16.84	16.85	6.929	141.99	.9794
			$10,000 \times 10^6$	60	10.25	.0468	8.17	8.17	8.17	8.17	.265	5.66	.8475
				100	11.71	.0487	8.79	8.79	8.79	8.79	.326	6.69	.868
				154	-----	-----	-----	-----	-----	-----	-----	-----	-----
				174	5.708	.0415	13.79	13.89	13.89	13.89	4.908	118.3	.9591
				200	3.332	.0524	12.23	14.81	14.81	14.81	27.05	516.2	.9670
				230	1.032	.0470	1.51	12.39	14.31	15.11	171.0	3,639	.9718
		.266	30×10^6	60×10^3	.578	.0603	14.83	19.75	19.82	19.67	5.695	94.44	.9887
				100	.628	.0609	15.48	20.13	20.08	19.91	5.307	87.1	.9895
				154	.875	.0731	17.44	20.63	20.46	20.41	4.649	63.6	.9909
				174	.843	.0746	16.94	20.41	20.24	20.17	5.044	67.6	.99039
				200	.620	.0655	14.63	19.57	19.68	19.60	6.476	98.9	.9886
				230	.419	.0529	11.69	17.38	18.13	18.60	10.04	189.8	.9872
			240×10^6	60	1.635	.0602	14.52	14.99	15.00	15.00	2.016	33.5	.9683
				100	1.787	.0608	15.07	15.34	15.34	15.34	1.893	31.15	.9707
				154	2.600	.0722	16.36	16.25	16.25	16.25	1.786	24.73	.9763
				174	2.580	.0736	16.12	16.32	16.32	16.32	2.18	29.62	.9767
				200	1.905	.0675	14.58	16.49	16.49	16.49	4.40	65.20	.9775
				230	.910	.0598	11.68	17.07	17.41	17.54	22.40	374.60	.9827
			$10,000 \times 10^6$	60	11.04	.0592	7.56	7.56	7.56	7.56	.339	5.73	.8244
				100	12.90	.0614	9.08	9.08	9.08	9.08	.559	9.11	.8765
				154	9.58	.083	13.5	13.5	13.5	13.5	6.28	75.7	.9549
				174	6.39	.0871	14.6	14.6	14.6	14.6	20	229.6	.9659
				200	2.36	.0723	7.02	15.4	15.4	15.4	98.6	1,364	.9715
				230	0	.0436	.14	1.44	1.82	2.06	6.32	145.0	.1274
		.422	30×10^6	60×10^3	.607	.0898	13.55	18.29	18.28	18.12	8.085	90.0	.9840
				100	.711	.0902	14.85	18.98	18.81	18.66	6.963	77.2	.9863
				154	.910	.0915	16.67	18.81	19.66	19.62	5.797	63.4	.9891
				174	.859	.0894	16.08	19.71	19.57	19.50	6.369	71.2	.9888
				200	.673	.0816	13.96	18.93	19.11	19.09	8.812	108.0	.9874
				230	.476	.0795	11.21	16.94	17.72	18.23	22.16	278.7	.9873
			240×10^6	60	1.72	.0895	13.19	13.52	13.52	13.52	2.87	32.1	.9555
				100	2.04	.0895	14.22	14.26	14.26	14.26	2.52	28.16	.9625
				154	2.796	.0899	15.75	15.96	15.96	15.96	2.703	30.1	.9747
				174	2.65	.0923	15.71	16.54	16.54	16.54	4.32	46.75	.9778
				200	1.753	.0957	14.42	17.27	17.27	17.27	14.4	150.5	.9813
				230	.732	.096	9.34	17.04	17.78	18.18	115.7	120.5	.9860
			$10,000 \times 10^6$	60	11.93	.0861	6.68	6.68	6.68	6.68	.584	6.78	.7852
				100	12.80	.1016	9.52	9.52	9.52	9.52	1.98	19.47	.8882
				154	6.1	.1106	14.4	14.6	14.6	14.6	32.2	300	.9651
				174	3.32	.0988	10.7	15.5	15.5	15.5	96.0	972	.9720
				200	.299	.0417	.28	3.38	4.69	5.97	197.6	4,740	.9488
				230	0	.105	-----	-----	-----	-----	3.306	31.5	.0025

TABLE I.- ESTIMATES OF ATTENUATION, REFLECTION, AND EFFECTIVE PLASMA THICKNESS

AS FUNCTIONS OF BODY GEOMETRY AND REENTRY PARAMETERS - Continued

θ, deg	M	x/D_n	f, cps	Altitude, ft	$(SL)_A/D_n$, db/cm	d_e/D_n	$(SL)_R$, db, for -				λ_B, cm	$\lambda_B D_n/d_e$, cm	$(R_{12})_B$
							D_n = 5.08 cm	D_n = 20.32 cm	D_n = 25.40 cm	D_n = 30.48 cm			
9	20	2.333	30×10^6	60×10^3	0.386	0.0935	9.67	15.17	15.81	16.12	13.26	141.8	0.9739
				100	.651	.1083	13.30	17.80	17.72	17.56	9.216	85.10	.98200
				154	1.236	.1394	17.22	19.17	19.14	19.15	6.92	49.60	.9878
				174	1.198	.1406	16.58	19.13	19.08	19.07	8.187	58.2	.9876
				200	.845	.1214	13.97	18.70	18.87	18.89	14.63	120.5	.9870
				230	.395	.0996	10.22	16.29	17.20	17.87	65.28	655.4	.9889
			240×10^6	60	1.098	.0931	9.59	11.49	11.45	11.46	4.73	50.8	.9286
				100	1.92	.1081	12.87	13.23	13.23	13.23	3.457	32	.9524
				154	3.67	.139	16.01	16.22	16.22	16.22	4.77	34.3	.9761
				174	2.867	.1413	16.12	17.16	17.16	17.16	11.28	79.8	.9808
				200	1.28	.1222	13.11	18.0	18.11	18.14	55.85	457.0	.9847
				230	.4065	.0966	3.45	12.55	14.28	15.66	465.0	4,815.0	.9886
			$10,000 \times 10^6$	60	6.55	.0807	5.65	5.65	5.65	5.65	1.535	19.02	.7272
				100	5.34	.0185	9.73	9.86	9.86	9.86	7.83	96.1	.8968
				154	1.80	.0606	4.48	15.00	15.10	15.10	104.5	1,725.0	.9691
				174	.361	.0289	.22	3.00	4.34	5.76	231.0	8,000.0	.9654
				200	≈0	.0638	-----	-----	-----	-----	3.7	58	.0108
				230	≈0	-------	-----	-----	-----	-----	3.084	---------	.0002
		4.000	30×10^6	60×10^3	.301	.0939	7.71	13.19	14.01	14.56	17.10	182.1	.9665
				100	.593	.1079	12.52	17.35	17.39	17.26	10.13	93.9	.9804
				154	1.114	.1289	16.62	19.12	19.06	19.05	7.271	56.4	.9876
				174	1.092	.1345	15.83	19.07	19.01	18.99	9.460	70.3	.9874
				200	.772	.1184	13.47	18.58	18.91	19.02	18.58	156.9	.9875
				230	.307	.09878	9.00	15.49	16.48	17.26	121.8	1,233.0	.9901
			240×10^6	60	.855	.0932	7.66	10.63	10.47	10.41	6.12	65.7	.90925
				100	1.772	.1075	12.21	12.93	12.93	12.93	3.893	36.2	.94907
				154	3.197	.129	15.85	16.37	16.37	16.37	5.83	45.2	.9769
				174	2.257	.136	15.57	17.53	17.53	17.53	18.85	139.6	.9824
				200	1.028	.118	11.79	18.09	18.39	18.50	88.8	753.0	.9861
				230	.285	.0898	1.37	8.36	10.14	11.69	917	10,210	.990
			$10,000 \times 10^6$	60	4.508	.0762	4.96	4.98	4.98	4.98	2.428	31.86	.6827
				100	3.76	.0749	9.08	10.02	10.02	10.02	13.24	176.8	.9004
				154	1.26	.0513	2.25	13.91	14.8	15.04	135.6	2,643	.9692
				174	.0108	.0451	.20	2.22	2.93	3.53	10.13	224.6	.295
				200	0	.0575	-----	-----	-----	-----	3.425	59.6	.0045
				230	------	-------	-----	-----	-----	-----	3.05	---------	.00007

TABLE I.- ESTIMATES OF ATTENUATION, REFLECTION, AND EFFECTIVE PLASMA THICKNESS

AS FUNCTIONS OF BODY GEOMETRY AND REENTRY PARAMETERS - Continued

θ, deg	M	x/D_n	f, cps	Altitude, ft	$(SL)_A/D_n$, db/cm	d_e/D_n	$(SL)_R$, db, for -				λ_B, cm	$\lambda_B D_n/d_e$, cm	$(R_{12})_B$
							D_n = 5.08 cm	D_n = 20.32 cm	D_n = 25.40 cm	D_n = 30.48 cm			
9	20	6.00	30×10^6	60×10^3	0.239	0.7276	6.95	12.40	13.28	13.95	16.67	229.1	0.9673
				100	.408	.08317	10.52	16.02	16.62	16.88	11.37	136.7	.9780
				154	.786	.0973	14.78	18.99	18.92	18.84	8.073	82.97	.9868
				174	.866	.1079	14.78	19.05	19.06	19.02	9.839	91.2	.9874
				200	.546	.08935	11.86	17.52	18.20	18.61	21.63	242.1	.9875
				230	.212	.07159	7.01	13.56	14.58	15.41	126.8	1,771.2	.9896
			240×10^6	60	.681	.0723	6.92	10.86	10.75	10.61	5.98	82.7	.9116
				100	1.225	.0828	10.43	12.51	12.48	12.48	4.42	53.3	.9435
				154	2.115	.0976	14.56	16.42	16.42	16.42	8.02	82.2	.9772
				174	1.742	.1103	14.59	17.62	17.64	17.64	21.43	194.3	.9828
				200	.695	.0892	9.15	16.92	17.72	18.16	112.5	1,261	.9863
				230	.207	.0684	.71	5.79	7.31	8.69	953	13,930	.9894
			$10,000 \times 10^6$	60	3.346	.05665	4.95	5.23	5.23	5.23	2.65	46.8	.7000
				100	2.12	.051	5.52	9.64	9.64	9.64	16.75	328.5	.8915
				154	.368	.02125	.20	2.79	4.09	5.49	179.4	8,440	.9654
				174	≈ 0	.0487	.19	1.84	2.29	2.56	6.96	142.9	.1584
				200	≈ 0	.0349	-----	-----	-----	-----	3.33	95.5	.0027
				230	≈ 0	-------	-----	-----	-----	-----	3.05	---------	-------
		7.827	30×10^6	60×10^3	.215	.05429	7.26	12.76	13.65	14.36	13.82	254.6	.9728
				100	.374	.06219	11.00	16.62	17.30	17.67	9.232	148.4	.9820
				154	.625	.07492	14.05	19.00	19.13	19.06	7.546	100.7	.9871
				174	.624	.07451	13.74	18.88	19.15	19.17	8.584	115.2	.9875
				200	.457	.06557	11.43	17.15	17.91	18.42	15.56	237.3	.9875
				230	.188	.0527	6.97	13.30	14.31	15.12	89.33	1,695.1	.9899
			240×10^6	60	.613	.04385	7.22	11.60	11.61	11.47	4.96	113	.9261
				100	1.111	.0621	10.94	13.32	13.26	13.25	3.50	56.3	.9528
				154	1.766	.074	13.86	16.22	16.22	16.22	6.075	82.1	.9761
				174	1.384	.073	13.45	17.23	17.28	17.29	13.50	185.0	.9813
				200	.637	.0638	9.42	16.56	17.35	17.83	65.10	1,020.0	.9856
				230	.178	.0481	.77	5.93	7.42	8.73	660	13,720	.9897
			$10,000 \times 10^6$	60	2.97	.0407	5.40	5.93	5.93	5.93	2.17	53.3	.7445
				100	2.33	.0382	7.09	10.11	10.11	10.11	9.47	248	.9024
				154	.364	.0158	.21	2.85	4.15	5.55	138.3	8,760	.9674
				174	.0878	.00978	.02	.28	.44	.62	222.0	22,700	.9574
				200	≈ 0	.02106	-----	-----	-----	-----	3.61	171.4	.0086
				230	≈ 0	-------	-----	-----	-----	-----	3.065	--------	.00013

TABLE I.- ESTIMATES OF ATTENUATION, REFLECTION, AND EFFECTIVE PLASMA THICKNESS

AS FUNCTIONS OF BODY GEOMETRY AND REENTRY PARAMETERS - Continued

θ, deg	M	x/D_n	f, cps	Altitude, ft	$(SL)_A/D_n$, db/cm	d_e/D_n	$(SL)_R$, db, for -				λ_B, cm	$\lambda_B D_n/d_e$, cm	$(R_{12})_B$
							D_n = 5.08 cm	D_n = 20.32 cm	D_n = 25.40 cm	D_n = 30.48 cm			
30	15	0.17	30×10^6	100×10^3	0.1054	0.04352	3.329	7.934	8.792	9.506	22.58	518.9	0.9559
				154	.2178	.03703	8.734	14.38	15.29	16.01	9.488	256.2	.9816
				174	.2058	.03651	8.270	13.89	14.80	15.53	10.116	277.1	.9808
				200	.1333	.03439	5.133	10.30	11.20	11.94	15.86	461.2	.9724
				230	.05579	.02880	1.043	4.063	4.760	5.364	43.22	1,500.7	.9498
			240×10^6	100	.300	.0434	3.321	7.830	8.564	9.074	8.05	185.5	.8813
				154	.654	.0369	8.709	13.34	13.45	13.38	3.69	100	.9527
				174	.637	.0364	8.237	13.14	13.42	13.48	4.405	121	.9540
				200	.40	.03482	4.948	10.21	11.03	11.62	11.08	318.3	.9465
				230	.1058	.0302	.2452	2.272	2.9899	3.665	11.06	3,662	.9345
			$10,000 \times 10^6$	100	1.838	.03958	2.7120	3.578	3.576	3.576	2.32	58.6	.5611
				154	1.559	.0306	4.471	10.45	10.51	10.52	14.55	475.5	.9112
				174	.781	.02417	1.086	8.385	9.867	10.67	37.7	1,560	.9265
				200	0	.02065	.0236	.3339	.4871	.6468	5.34	258.5	.07916
				230	0	.01527	.00005030	.0006948	.001003	.001309	3.062	200.5	.0001130
		.60	30×10^6	100×10^3	.0524	.0325	1.1031	4.116	4.806	5.403	34.00	1,045.9	.9345
				154	.2122	.0457	7.674	13.23	14.13	14.85	12.19	266.9	.9768
				174	.2287	.0462	8.078	13.67	14.57	15.27	11.86	256.6	.9782
				200	.1051	.0387	3.203	7.769	8.625	9.338	24.38	629.95	.9614
				230	.0198	.01912	.06751	.6515	.8856	1.1215	103.29	5,403.0	.9183
			240×10^6	100	.148	.0321	1.085	4.069	4.748	5.328	12.2	380	.8279
				154	.653	.0456	7.646	12.37	12.58	12.58	5.12	112.3	.9433
				174	.712	.04625	8.026	12.88	13.17	13.24	6.165	133.3	.9523
				200	.276	.0391	2.556	7.479	8.386	9.117	26.4	675	.9357
				230	.0269	.01874	.003475	.05378	.08304	.1181	408.4	21,800	.9021
			$10,000 \times 10^6$	100	.465	.01913	.2801	1.9200	2.248	2.436	4.925	257.4	.4429
				154	.67	.0242	.7145	6.4906	7.996	8.971	34.75	1,436	.9013
				174	.239	.0139	.08369	1.232	1.851	2.548	73.0	5,250	.9169
				200	0	.02463	.002815	.03565	.04383	.05009	3.345	135.8	.002974
				230	-------	--------	----------	----------	---------	---------	-------	---------	---------
		2.00	30×10^6	100×10^3	.0262	.01298	.6059	2.843	3.422	3.937	27.116	2,089.1	.9473
				154	.09201	.01913	4.882	9.986	10.89	11.63	11.68	610.8	.9776
				174	.1038	.0194	5.542	10.79	11.71	12.46	10.82	557.2	.9798
				200	.0520	.01585	2.058	5.982	6.778	7.450	19.46	1,227.5	.9677
				230	.00740	.00538	.02023	.2366	.3373	.4454	69.13	12,853.3	.9338
			240×10^6	100	.0738	.01281	.5947	2.810	3.385	3.897	9.69	756	.8596
				154	.2804	.0191	4.860	9.931	10.77	11.41	4.71	246.5	.9438
				174	.3236	.0194	5.483	10.72	11.56	12.19	5.13	264.4	.9537
				200	.1433	.0157	1.571	5.615	6.458	7.168	17.15	1,093	.9424
				230	.01129	.00525	.001263	.01972	.03057	.04366	231	44,000	.9188
			$10,000 \times 10^6$	100	.2775	.00773	.1647	1.3687	1.770	2.123	3.275	423.8	.51610
				154	.2525	.00743	.1312	1.720	2.480	3.282	25.08	3,375	.8992
				174	.1112	.004566	.01978	.3061	.4714	.6681	56.2	12,310	.9263
				200	0	.00715	.0008220	.01286	.01984	.02814	3.755	525.0	.01252
				230	-------	--------	----------	----------	---------	---------	-------	---------	---------

TABLE I.- ESTIMATES OF ATTENUATION, REFLECTION, AND EFFECTIVE PLASMA THICKNESS

AS FUNCTIONS OF BODY GEOMETRY AND REENTRY PARAMETERS - Continued

θ, deg	M	x/D_n	f, cps	Altitude, ft	$(SL)_A/D_n$, db/cm	d_e/D_n	$(SL)_R$, db, for -				λ_B, cm	$\lambda_B D_n/d_e$, cm	$(R_{12})_B$
							D_n = 5.08 cm	D_n = 20.32 cm	D_n = 25.40 cm	D_n = 30.48 cm			
30	20	0.50	30×10^6	100×10^3	0.371	0.03994	12.83	18.51	19.20	19.57	5.889	147.4	0.9883
				154	.624	.05370	15.84	20.60	20.59	20.44	4.828	89.9	.9906
				174	.604	.0566	15.24	20.15	20.23	20.11	5.417	95.8	.9898
				200	.457	.0502	13.07	18.64	19.21	19.46	6.998	139.5	.9882
				230	.323	.0430	10.30	16.05	16.93	17.59	11.93	277.5	.9872
			240×10^6	100	1.059	.03986	12.77	14.95	14.89	14.89	2.104	52.78	.9677
				154	1.889	.05350	15.51	16.22	16.22	16.22	1.9218	35.92	.9761
				174	1.882	.05642	14.99	16.29	16.29	16.29	2.556	45.34	.9765
				200	1.312	.05150	13.08	16.68	16.71	16.71	6.0526	117.5	.9787
				230	.570	.04484	9.230	15.84	16.65	17.18	35.90	800.6	.9839
			$10,000 \times 10^6$	100	7.13	.03839	8.861	8.857	8.857	8.857	.6962	18.13	.8699
				154	4.83	.05051	13.59	13.93	13.93	13.93	10.11	200.2	.9595
				174	2.89	.04961	10.90	14.97	14.97	14.97	32.86	662.4	.9681
				200	.835	.03384	1.062	10.12	12.61	14.17	147.7	4,365.0	.9718
				230	.00112	.02900	.02646	.3210	.4261	.5023	4.289	147.9	.03132
		1.00	30×10^6	100×10^3	.228	.0229	11.10	16.90	17.81	18.51	5.492	239.9	.9891
				154	.356	.03043	13.53	19.27	20.01	20.44	4.776	156.95	.9907
				174	.348	.03134	13.13	18.88	19.64	20.12	5.152	164.4	.9902
				200	.255	.02722	10.87	16.65	17.55	18.24	6.607	242.7	.9885
				230	.170	.02201	7.951	13.57	14.51	15.27	10.66	484.2	.9871
			240×10^6	100	.646	.02278	11.07	15.53	15.46	15.30	1.9574	85.93	.9697
				154	1.067	.03031	13.47	16.27	16.19	16.17	1.856	61.23	.9759
				174	1.079	.03120	13.07	16.40	16.35	16.32	2.289	73.37	.9767
				200	.7593	.02760	10.84	16.00	16.36	16.51	4.833	175.1	.9779
				230	.327	.02272	6.707	13.28	14.29	15.08	26.32	1,158.0	.9830
			$10,000 \times 10^6$	100	4.365	.02132	8.792	8.790	8.790	8.790	.5319	24.95	.8679
				154	2.636	.02478	11.07	13.57	13.57	13.57	7.560	305.1	.9561
				174	1.565	.02303	6.391	14.68	14.77	14.79	23.80	1,033.0	.9668
				200	.443	.01468	.3611	4.449	6.230	8.005	111.98	7,628	.9719
				230	.000931	.01257	.008612	.1316	.2001	.2791	5.1957	413.3	.07185
		2.00	30×10^6	100×10^3	.175	.01623	10.36	16.13	17.07	17.82	5.069	312.3	.9899
				154	.281	.02287	12.76	18.58	19.45	20.07	4.526	197.9	.9911
				174	.275	.02358	12.38	18.20	19.07	19.71	4.857	205.98	.9907
				200	.192	.01962	9.985	15.73	16.67	17.42	6.146	313.3	.9889
				230	.112	.01358	6.717	12.19	13.11	13.88	9.106	670.5	.9874
			240×10^6	100	.496	.0161	10.33	15.53	15.85	15.86	1.807	111.96	.9720
				154	.832	.0228	12.73	16.52	16.40	16.32	1.714	75.08	.9766
				174	.842	.0235	12.35	16.48	16.45	16.39	2.020	86.05	.9769
				200	.589	.0197	9.94	15.37	15.94	16.23	3.711	188.50	.9771
				230	.240	.0138	5.71	11.89	12.89	13.69	16.640	1,208.0	.9820
			$10,000 \times 10^6$	100	3.154	.0142	8.85	9.10	9.10	9.10	.487	34.34	.8770
				154	2.105	.0163	9.96	13.22	13.22	13.22	4.776	292.3	.9524
				174	1.118	.0134	5.02	13.85	14.28	14.41	14.996	1,117.0	.9643
				200	.393	.0102	.37	4.30	5.94	7.56	74.40	7,294.0	.9711
				230	.009	.0032	.01	.02	.03	.05	99.04	30,606.0	.8885

TABLE I.- ESTIMATES OF ATTENUATION, REFLECTION, AND EFFECTIVE PLASMA THICKNESS

AS FUNCTIONS OF BODY GEOMETRY AND REENTRY PARAMETERS - Concluded

θ, deg	M	x/D_n	f, cps	Altitude, ft	$(SL)_A/D_n$, db/cm	d_e/D_n	$(SL)_R$, db, for -				λ_B, cm	$\lambda_B D_n/d_e$, cm	$(R_{12})_B$
							D_n = 5.08 cm	D_n = 20.32 cm	D_n = 25.40 cm	D_n = 30.48 cm			
30	25	0.50	30×10^6	100×10^3	0.853	0.0635	17.90	21.14	20.96	20.90	4.075	64.2	0.9919
				154	1.154	.0664	20.19	22.05	22.02	22.03	3.196	48.2	.9937
				174	1.152	.0658	20.14	22.08	22.05	22.06	3.231	49.10	.9938
				200	.875	.0593	18.06	21.55	21.41	21.34	4.064	68.5	.9927
				230	.656	.0534	15.45	20.58	20.84	20.87	6.251	117.1	.9916
			240×10^6	100	2.428	.06352	16.77	16.46	16.46	16.46	1.451	22.84	.9774
				154	3.429	.06610	18.02	17.82	17.82	17.82	1.2168	18.41	.9835
				174	3.527	.06549	18.24	18.10	18.10	18.10	1.3411	20.48	.9845
				200	2.704	.05978	17.51	18.16	18.16	18.16	2.430	40.65	.9847
				230	1.413	.05624	15.46	19.25	19.30	19.31	12.44	221.2	.9883
			$10,000 \times 10^6$	100	17.58	.0633	9.889	9.889	9.889	9.889	.37	5.85	.8974
				154	12.22	.0688	14.86	14.86	14.86	14.86	3.72	54.1	.9673
				174	8.62	.0676	16.24	16.25	16.25	16.25	9.95	147.2	.9763
				200	3.56	.0570	14.16	17.38	17.38	17.38	51	895	.9817
				230	.623	.0328	.5624	6.851	9.466	11.92	347	10,580	.9836
		1.00	30×10^6	100	.538	.0403	15.93	21.09	21.26	21.17	4.099	101.6	.9919
				154	.729	.0412	18.37	22.45	22.28	22.14	3.131	76.0	.9938
				174	.734	.0404	18.45	22.55	22.39	22.25	3.092	765	.9940
				200	.530	.0348	16.14	21.45	21.74	21.74	3.859	110.9	.9929
				230	.403	.0323	13.60	19.34	20.09	20.54	5.677	175.8	.9916
			240×10^6	100	1.531	.04031	15.70	16.42	16.43	16.43	1.455	36.10	.9773
				154	2.148	.04116	17.73	17.83	17.83	17.83	1.1699	28.42	.9835
				174	2.222	.0403	17.86	18.14	18.14	18.14	1.2305	30.53	.9846
				200	1.655	.03488	16.02	18.04	18.03	18.03	2.013	57.71	.9843
				230	.963	.03329	13.55	18.51	18.77	18.86	8.364	251.2	.9871
			$10,000 \times 10^6$	100	11.0	.0397	9.592	9.592	9.592	9.592	.3243	8.18	.8902
				154	8.46	.04125	14.39	14.39	14.39	14.39	2.5	60.6	.9636
				174	5.96	.03945	15.87	15.87	15.87	15.87	6.63	168.1	.9741
				200	2.273	.0305	10.43	17.05	17.05	17.06	33.97	1,113	.9803
				230	.4875	.01882	.3838	4.900	6.933	8.996	250	13,280	.9838
		2.00	30×10^6	100	.515	.0385	15.74	21.01	21.26	21.21	4.090	106.2	.9919
				154	.697	.0394	18.18	22.47	22.32	22.17	3.125	79.3	.9939
				174	.687	.0380	18.14	22.54	22.42	22.27	3.108	81.8	.9940
				200	.503	.0330	15.92	21.33	21.71	21.77	3.856	116.8	.9929
				230	.342	.0277	12.87	18.67	19.51	20.10	5.749	207.5	.9915
			240×10^6	100	1.462	.03846	15.55	16.42	16.44	16.44	1.454	37.81	.9773
				154	2.052	.03925	17.64	17.83	17.83	17.83	1.168	29.76	.9835
				174	2.079	.03787	17.67	18.12	18.12	18.12	1.2385	32.70	.9846
				200	1.568	.03303	15.82	18.05	18.04	18.04	2.020	61.16	.9843
				230	.818	.02866	12.80	18.16	18.57	18.75	8.553	298.4	.9870
			$10,000 \times 10^6$	100	10.43	.03765	9.594	9.594	9.594	9.594	.3238	8.6	.8902
				154	8.0	.03894	14.39	14.40	14.40	14.40	2.488	63.9	.9637
				174	5.4	.0361	15.71	15.87	15.87	15.87	6.65	184.3	.9741
				200	1.789	.0241	8.277	17.02	17.07	17.07	34.33	1,425	.9804
				230	.2955	.01196	.1420	2.059	3.063	4.181	253.3	21,200	.9836

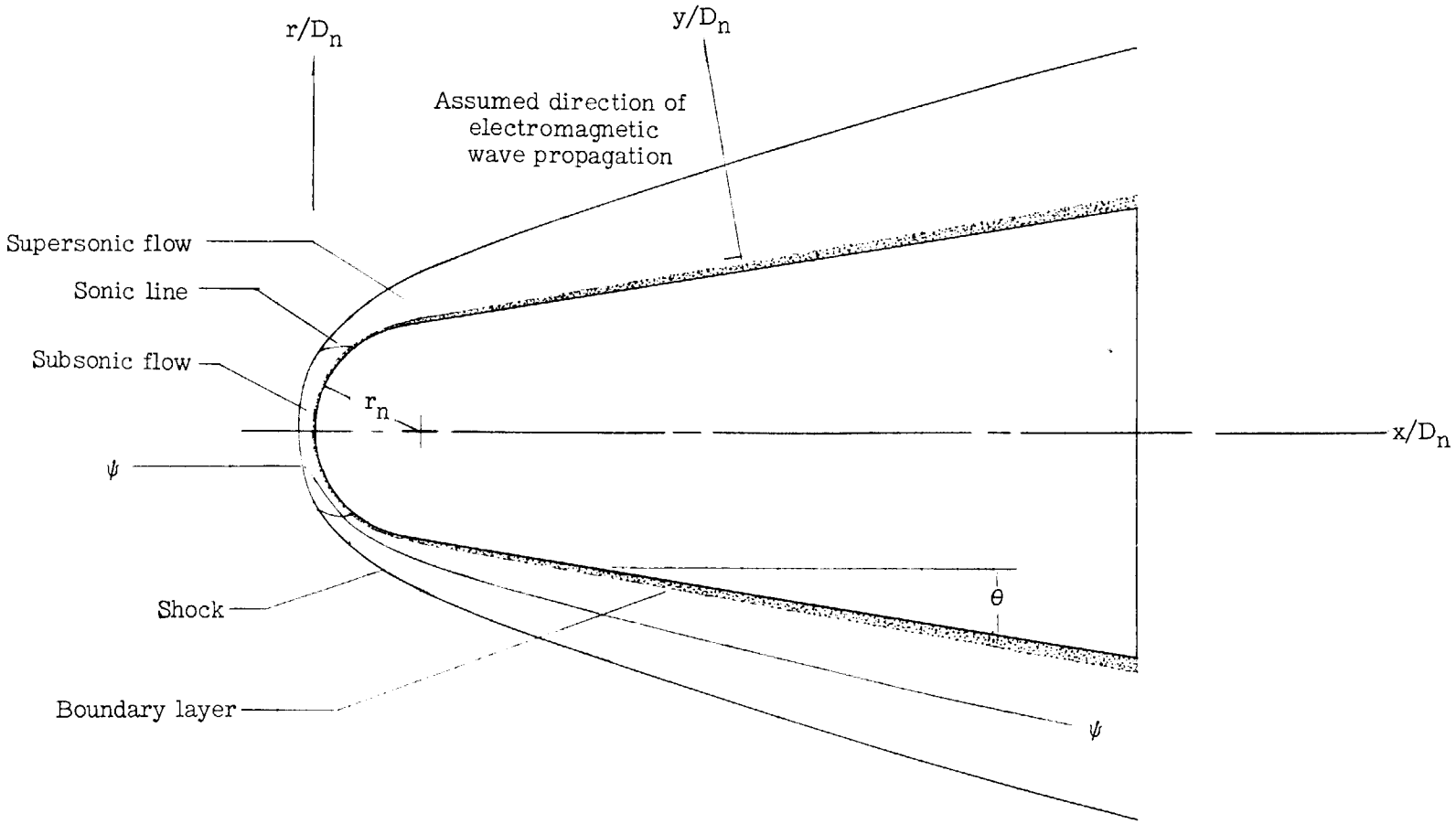

Figure 1.- Typical patterns about a hypersonic blunt body.

θ, deg	M_1	Altitude, ft
0	15.00	100,000
0	18.10	175,000
0	18.24	150,000
0	19.25	200,000
9	15.00	85,000
9	20.00	60,000
30	15.00	100,000
30	20.00	100,000
30	25.00	100,000

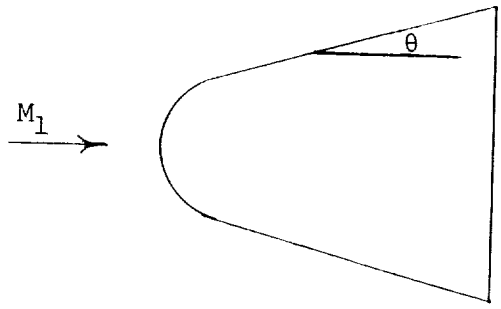

Figure 2.- Flow-field solutions obtained by real-gas characteristics method. (Ridyard and FitzGibbon computations; published by permission of the General Electric Co.)

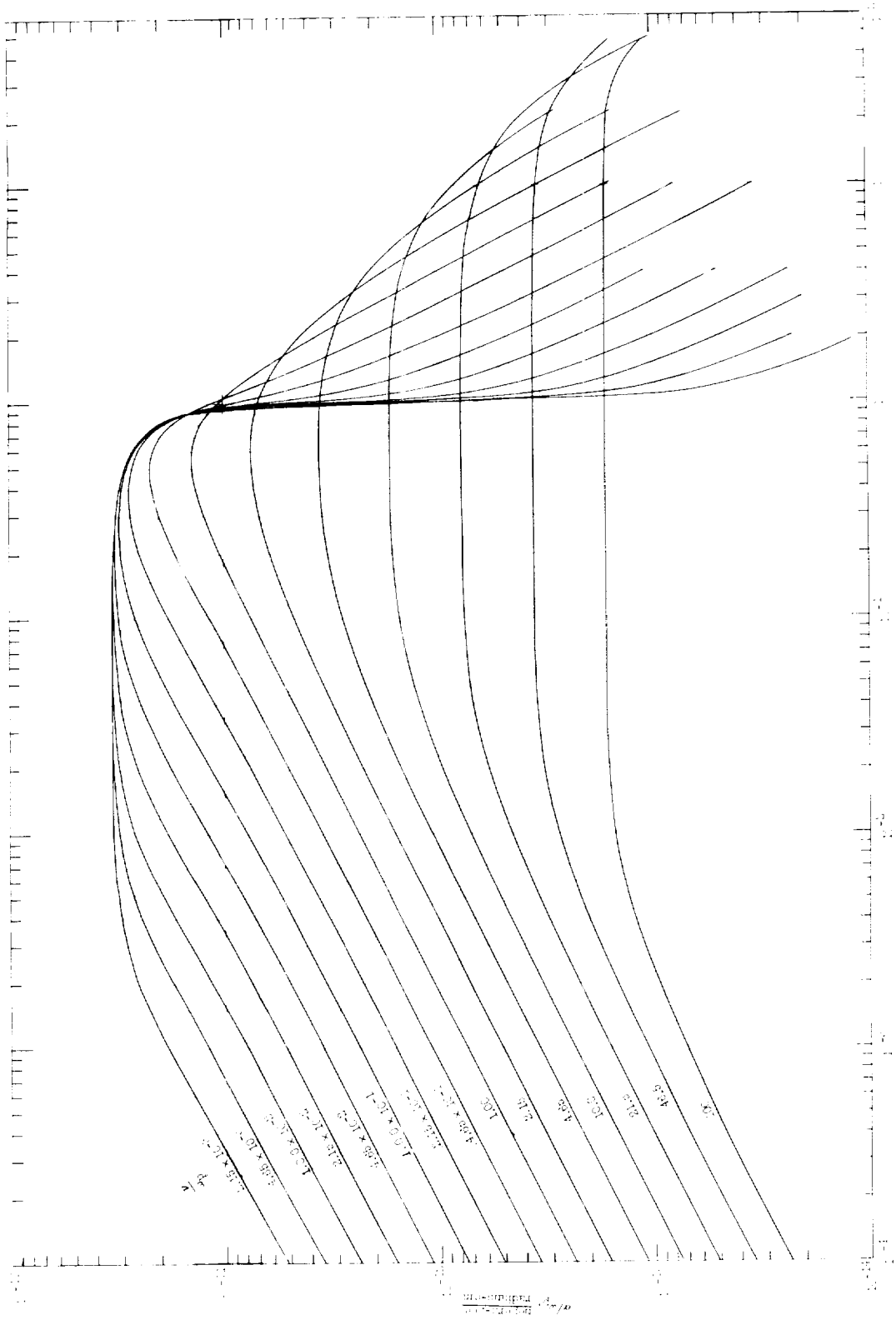

Figure 3.- Variation of plane-wave attenuation coefficient α, normalized with respect to plasma frequency ω_p, in ionized media.

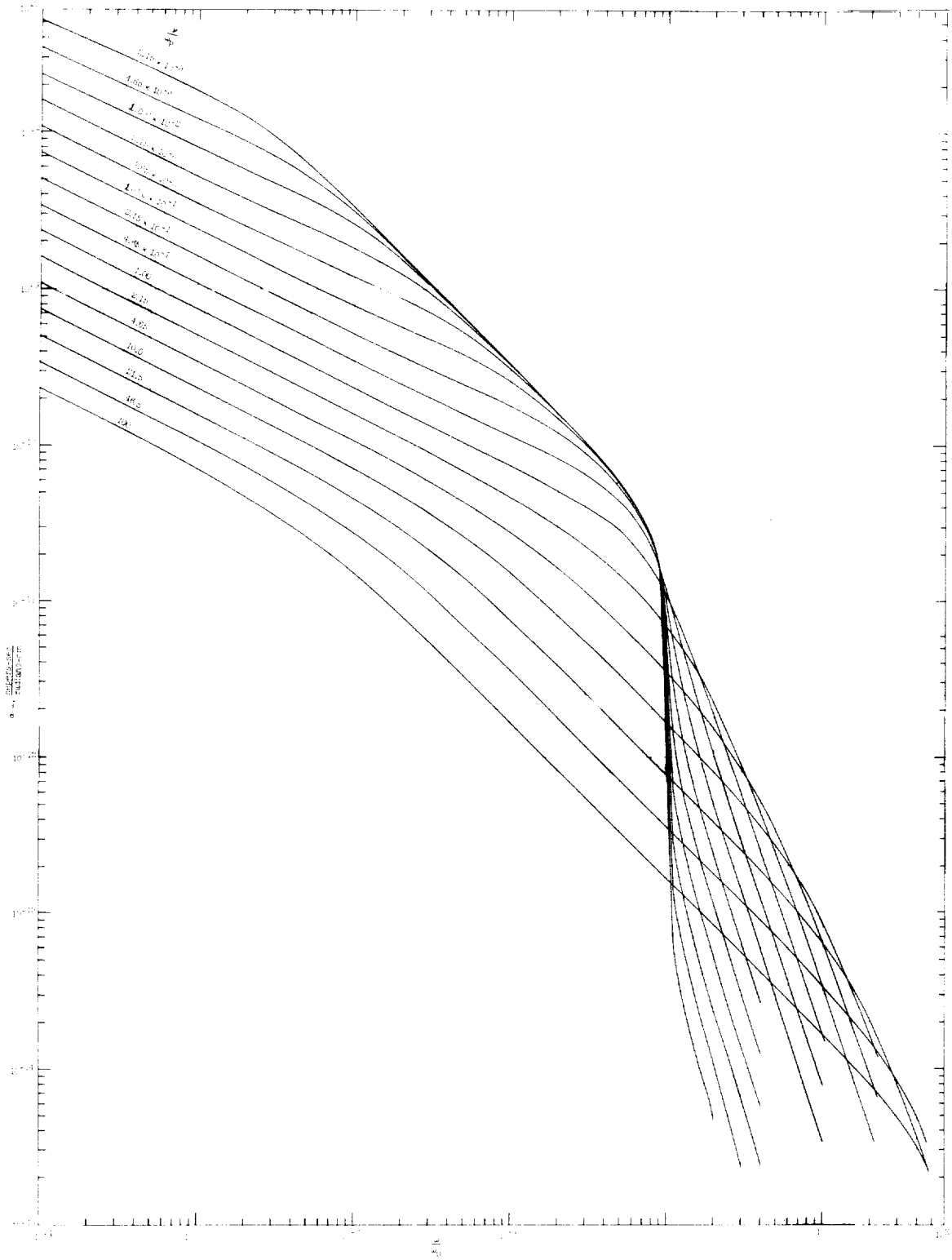

Figure 4.- Variation of plane-wave attenuation coefficient α, normalized with respect to signal frequency ω, in ionized media.

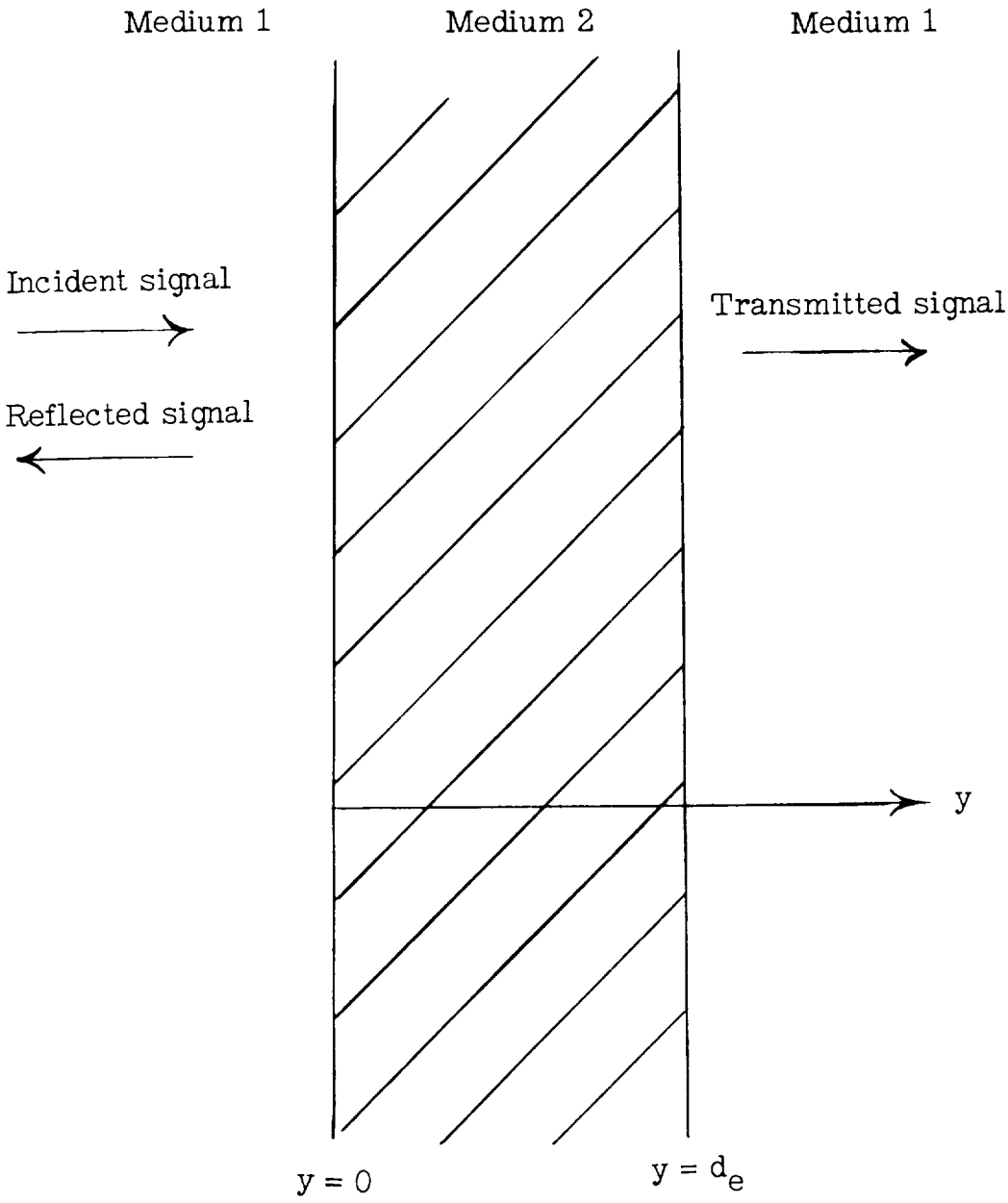

Figure 5.- Reflection and transmission of plane waves by a plane, homogeneous, electrically conducting sheet at normal incidence.

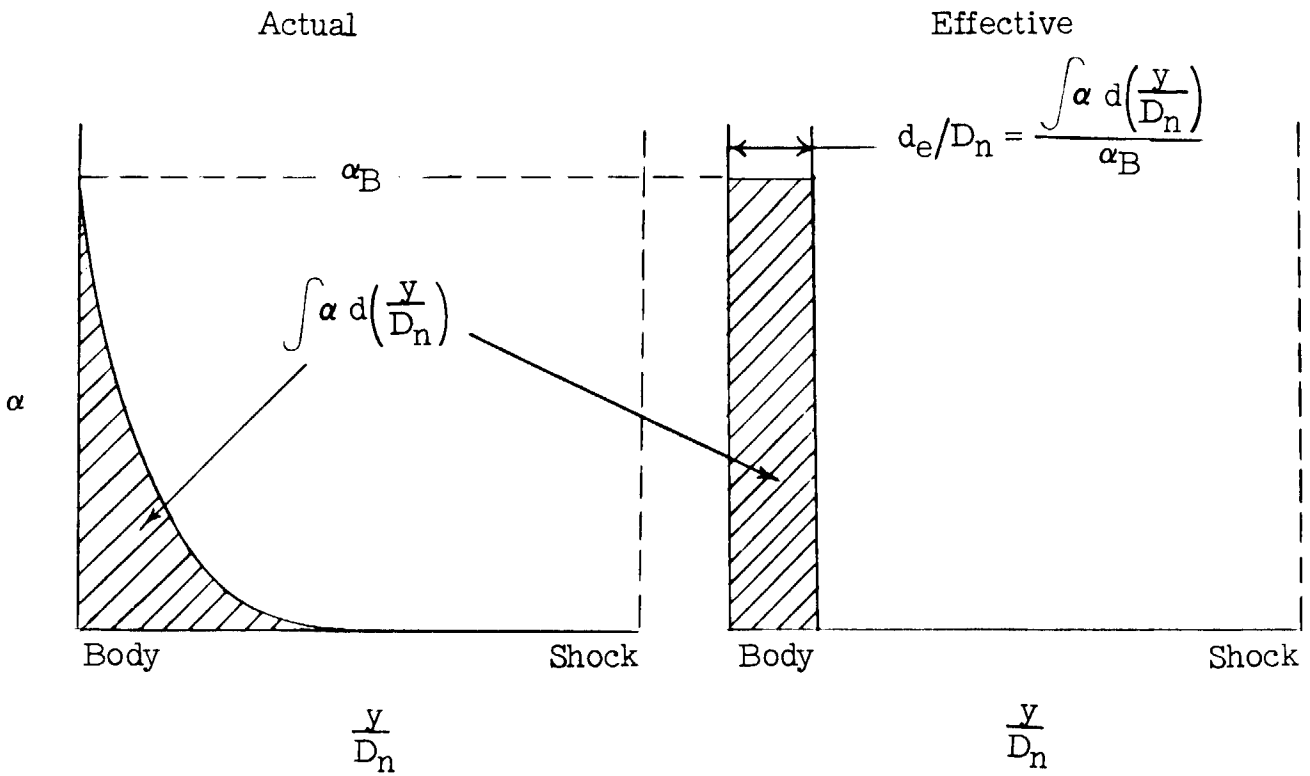

Figure 6.- Effective plasma thickness d_e for calculation of reflection losses.

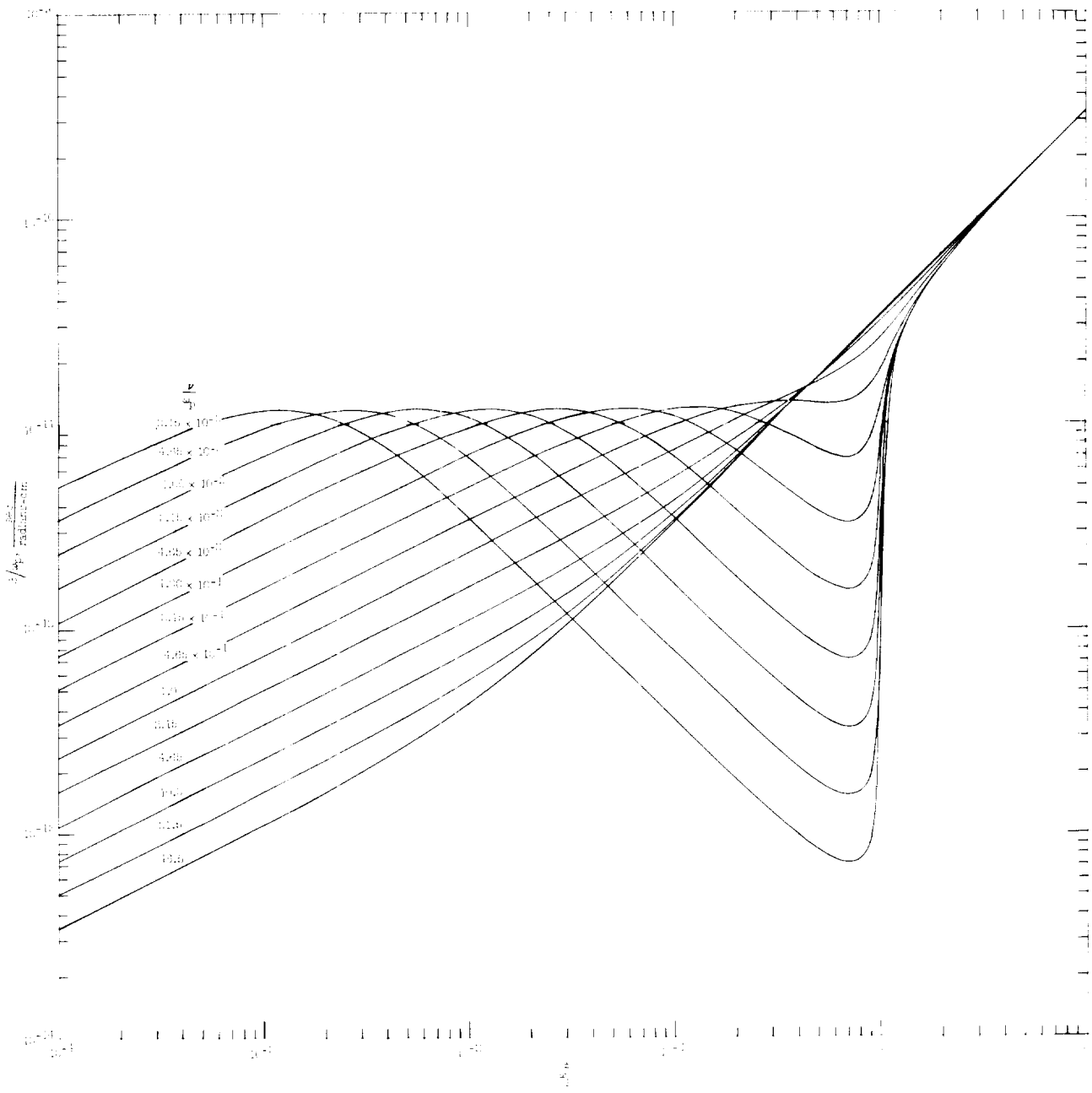

Figure 7.- Variation of plane-wave phase constant β, normalized with respect to plasma frequency ω_p, in ionized media.

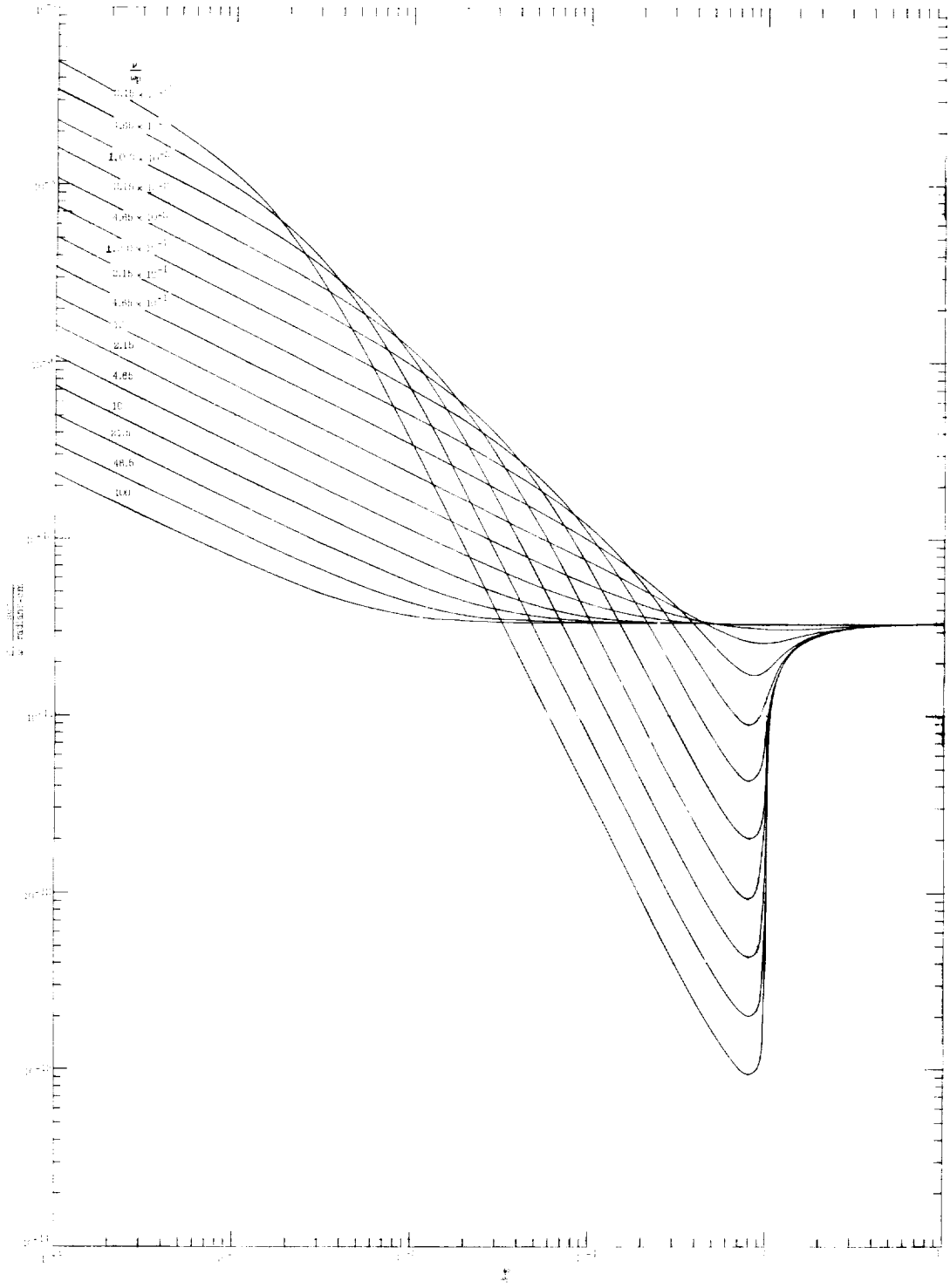

Figure 8.- Variation of plane-wave phase constant β, normalized with respect to signal frequency ω, in ionized media.

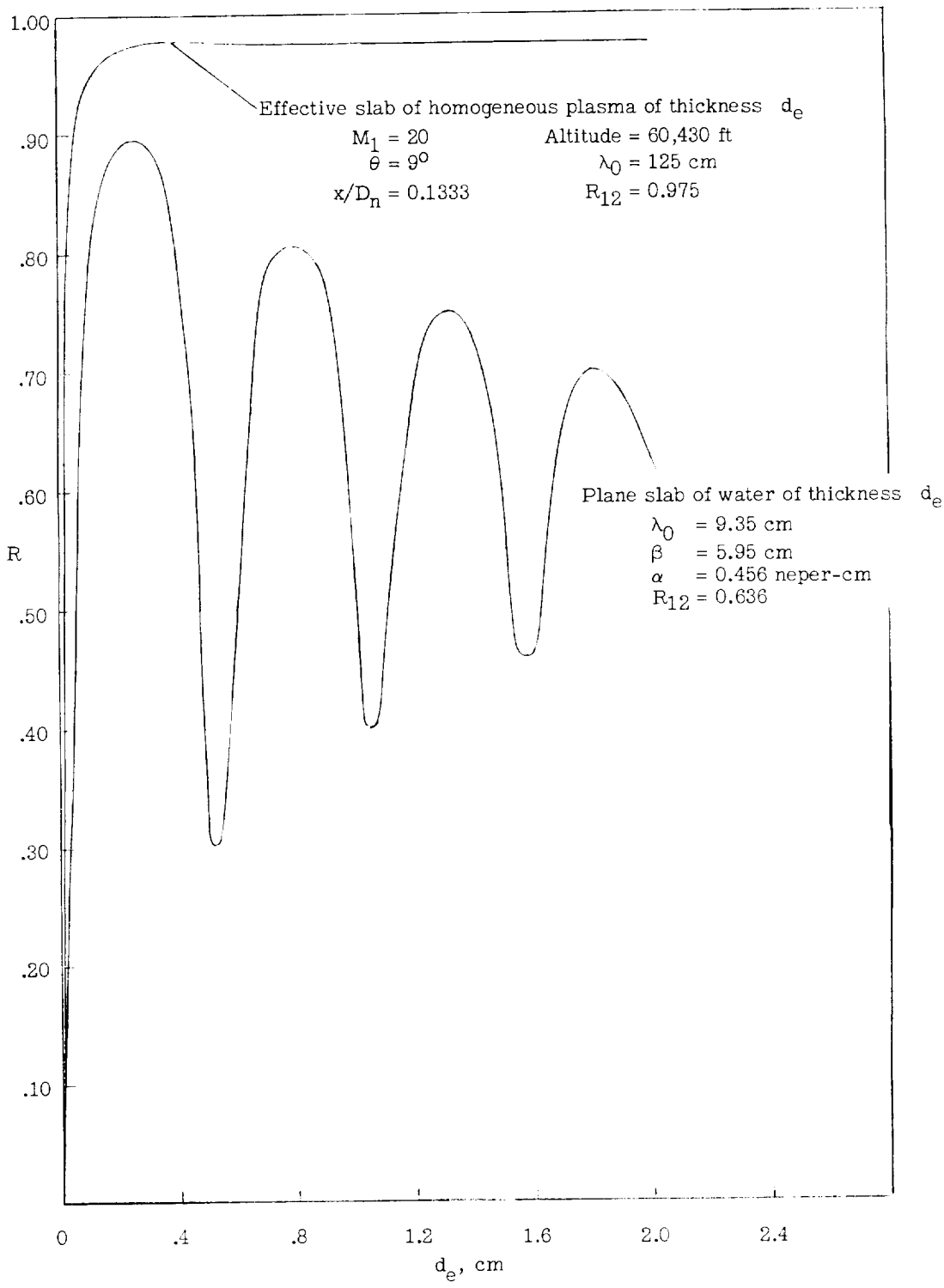

Figure 9.- Examples of reflection coefficient for a plane homogeneous slab.

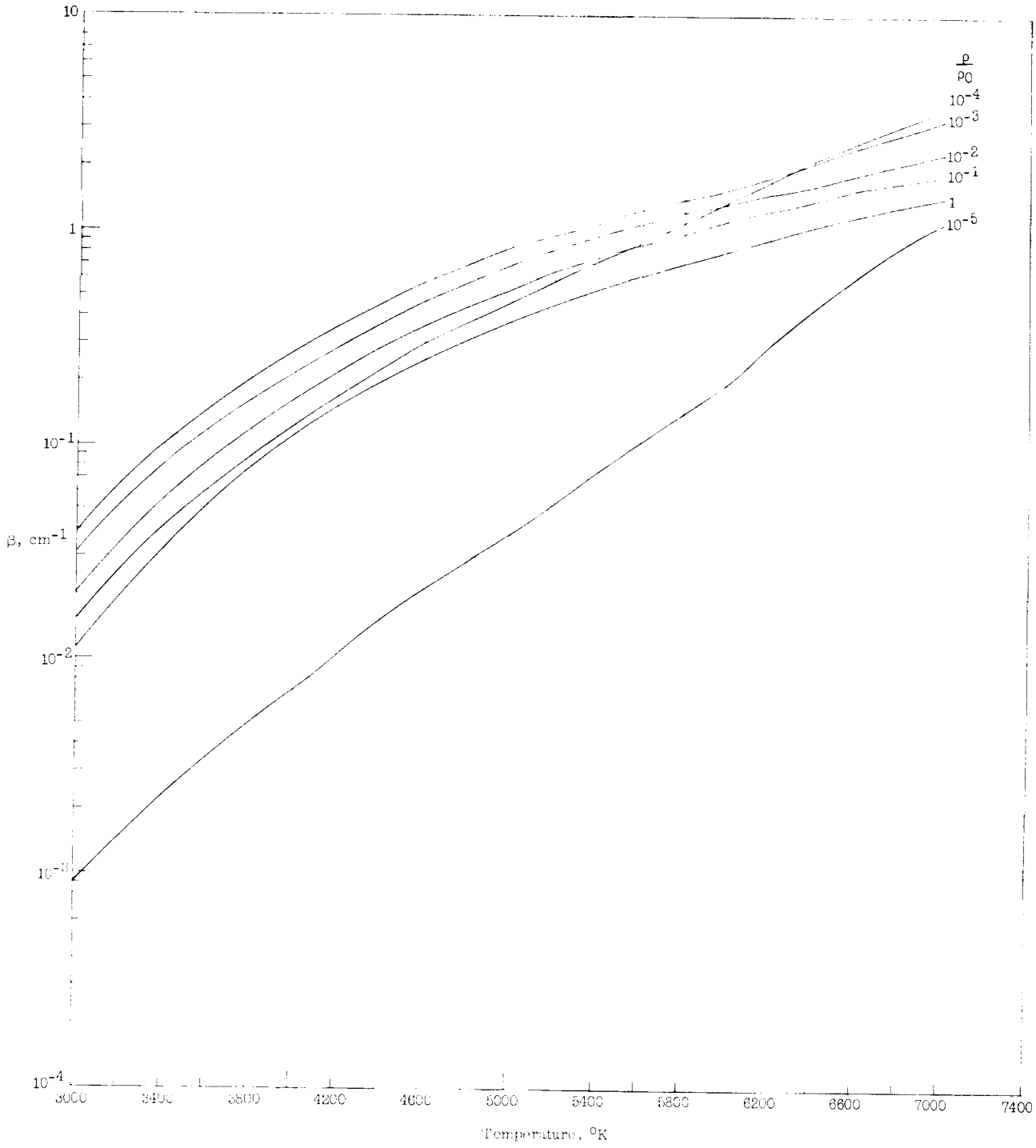

Figure 10.- Phase constant β for equilibrium air at f = 30 mc.

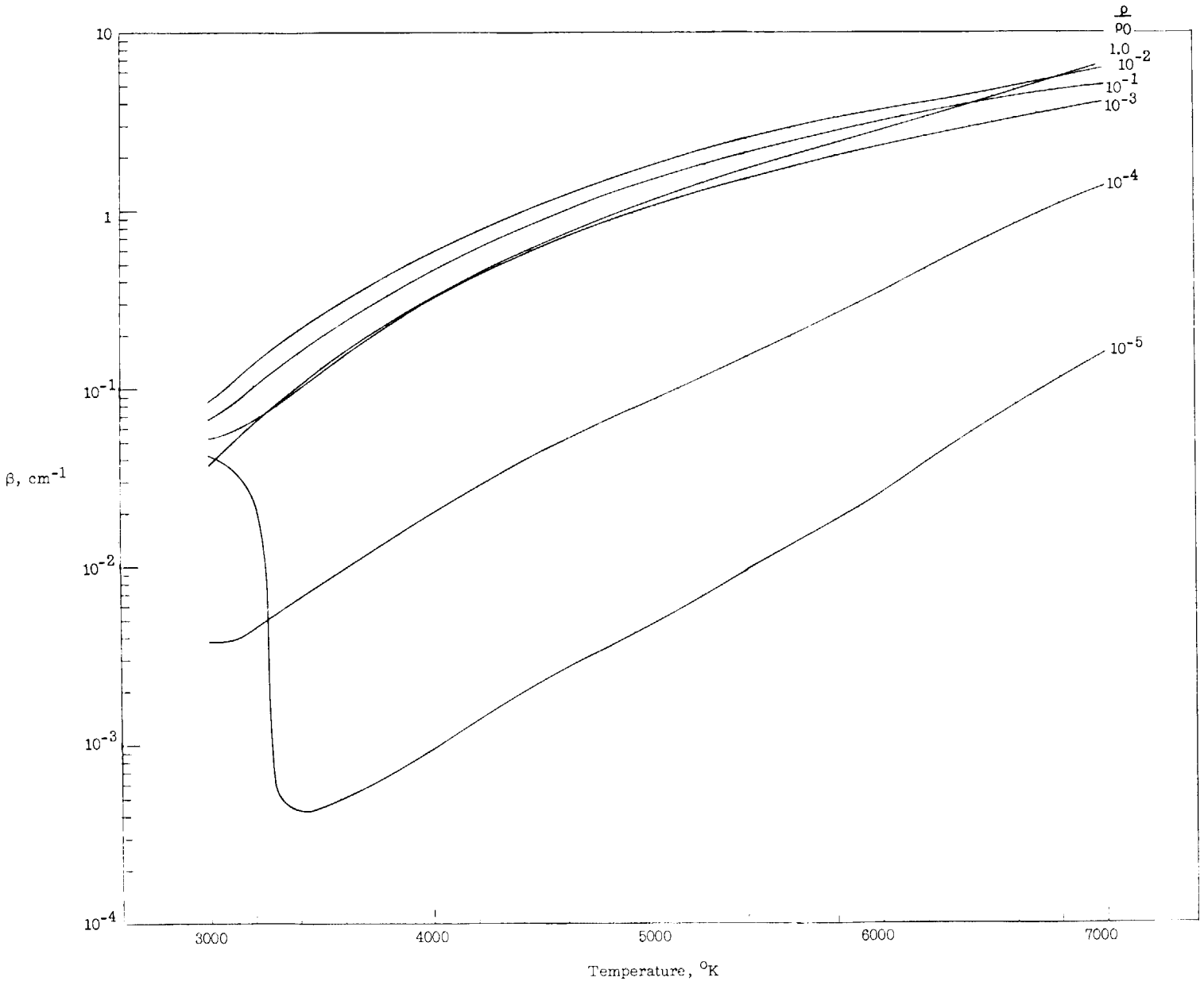

Figure 11.- Phase constant β for equilibrium air at $f = 240$ mc.

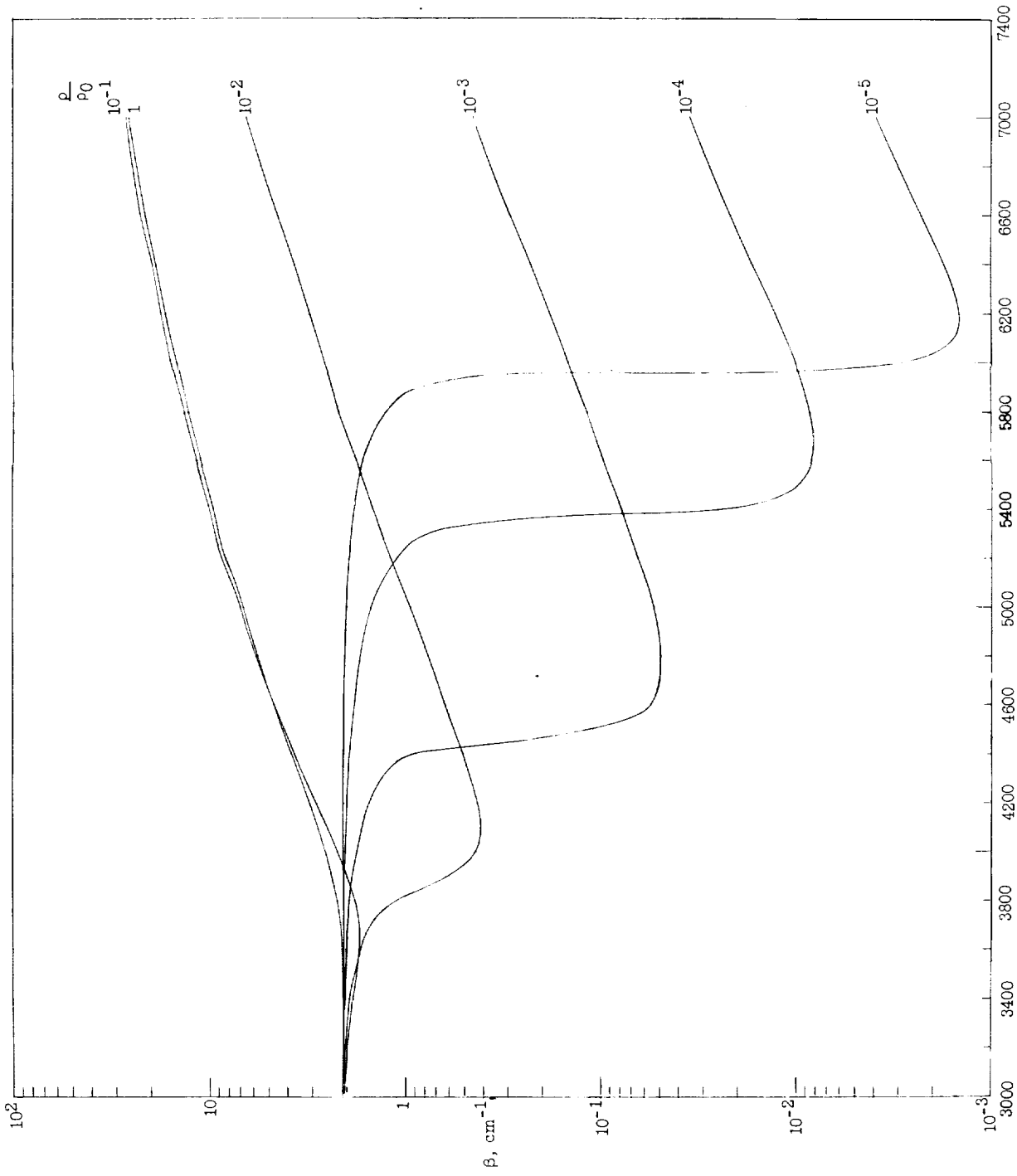

Figure 12.- Phase constant β for equilibrium air at f = 10,000 mc.

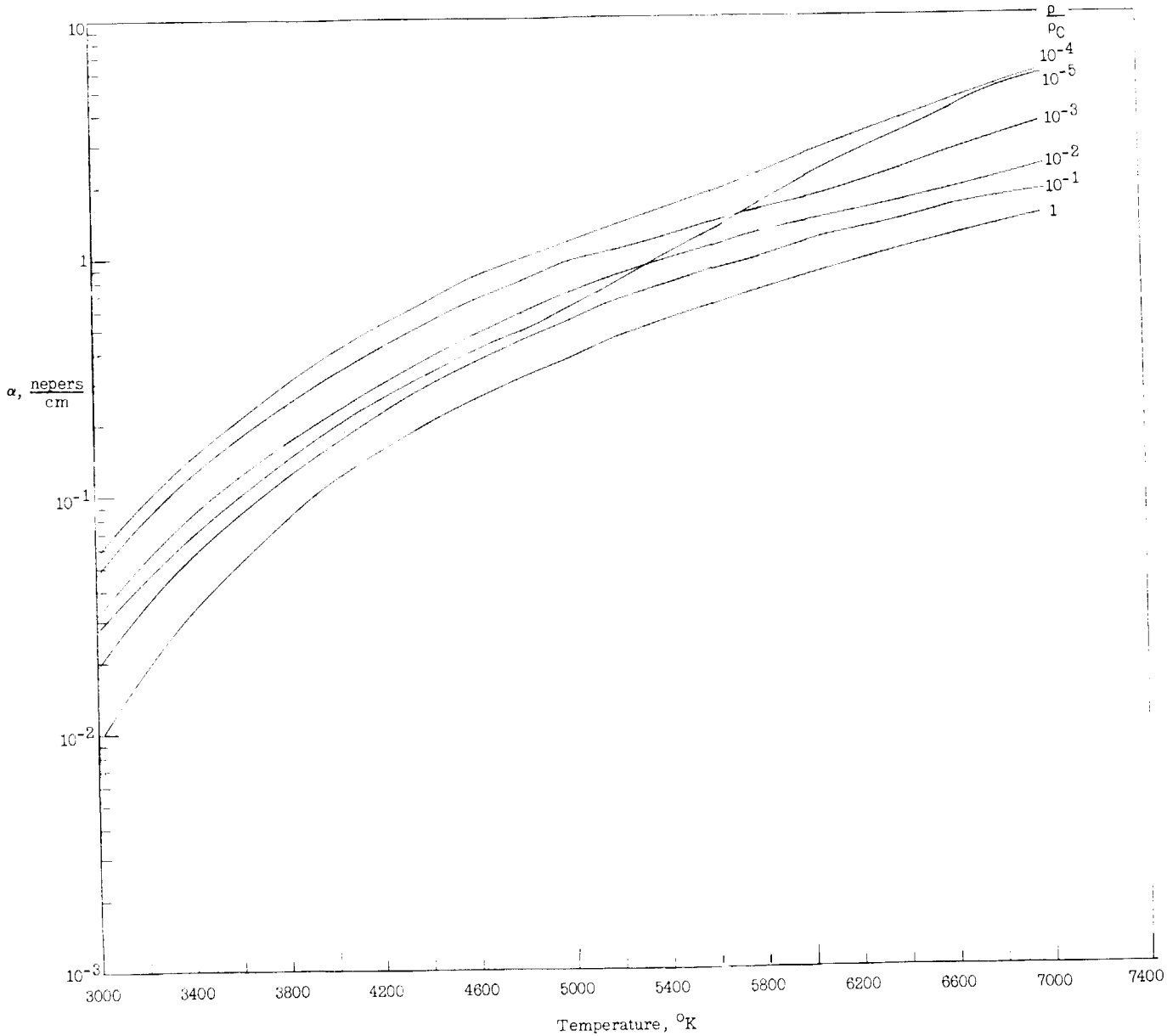

Figure 13.- Attenuation coefficient α for equilibrium air at f = 30 mc.

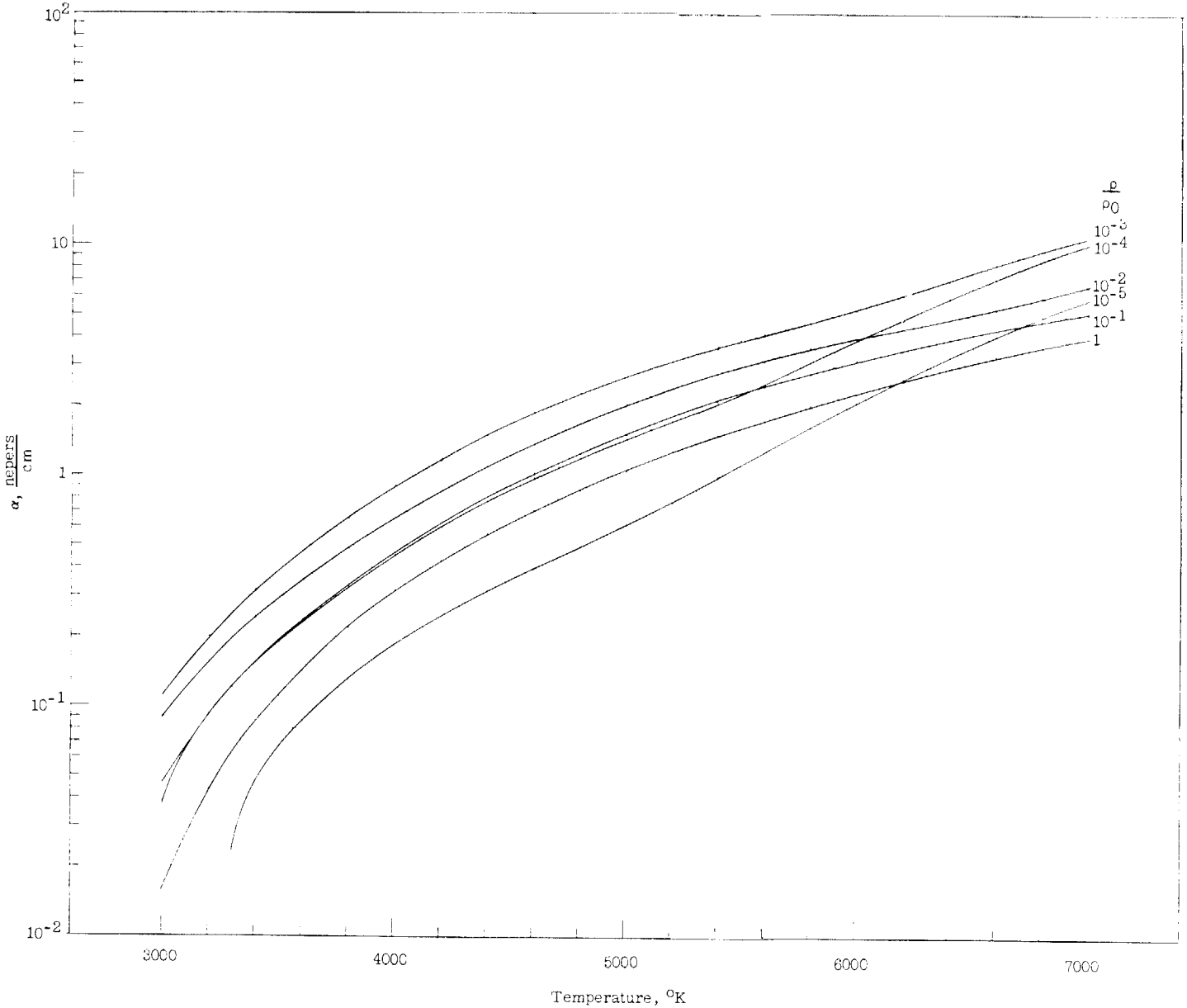

Figure 14.- Attenuation coefficient α for equilibrium air at $f = 240$ mc.

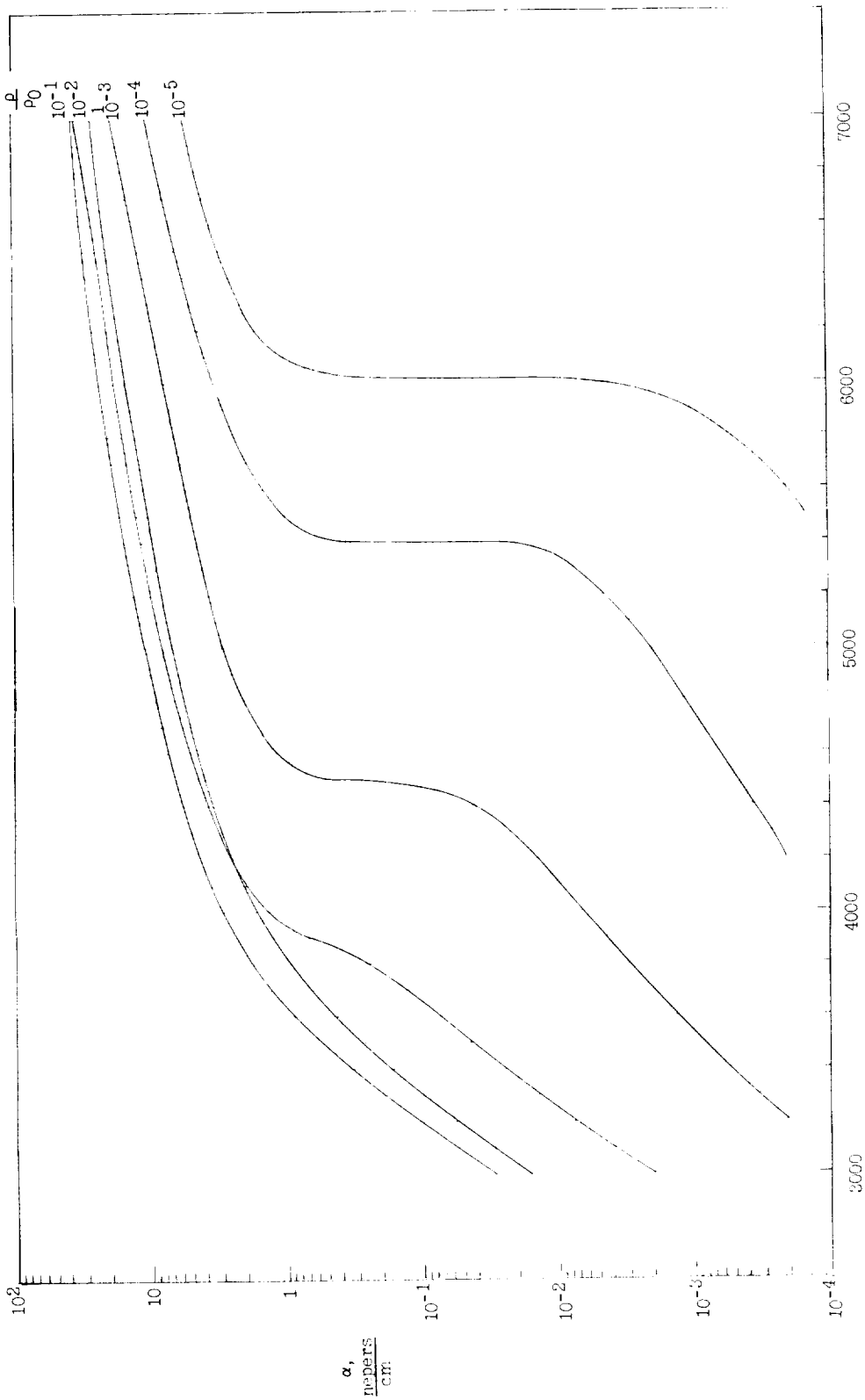

Figure 15.- Attenuation coefficient α for equilibrium air at f = 10,000 mc.

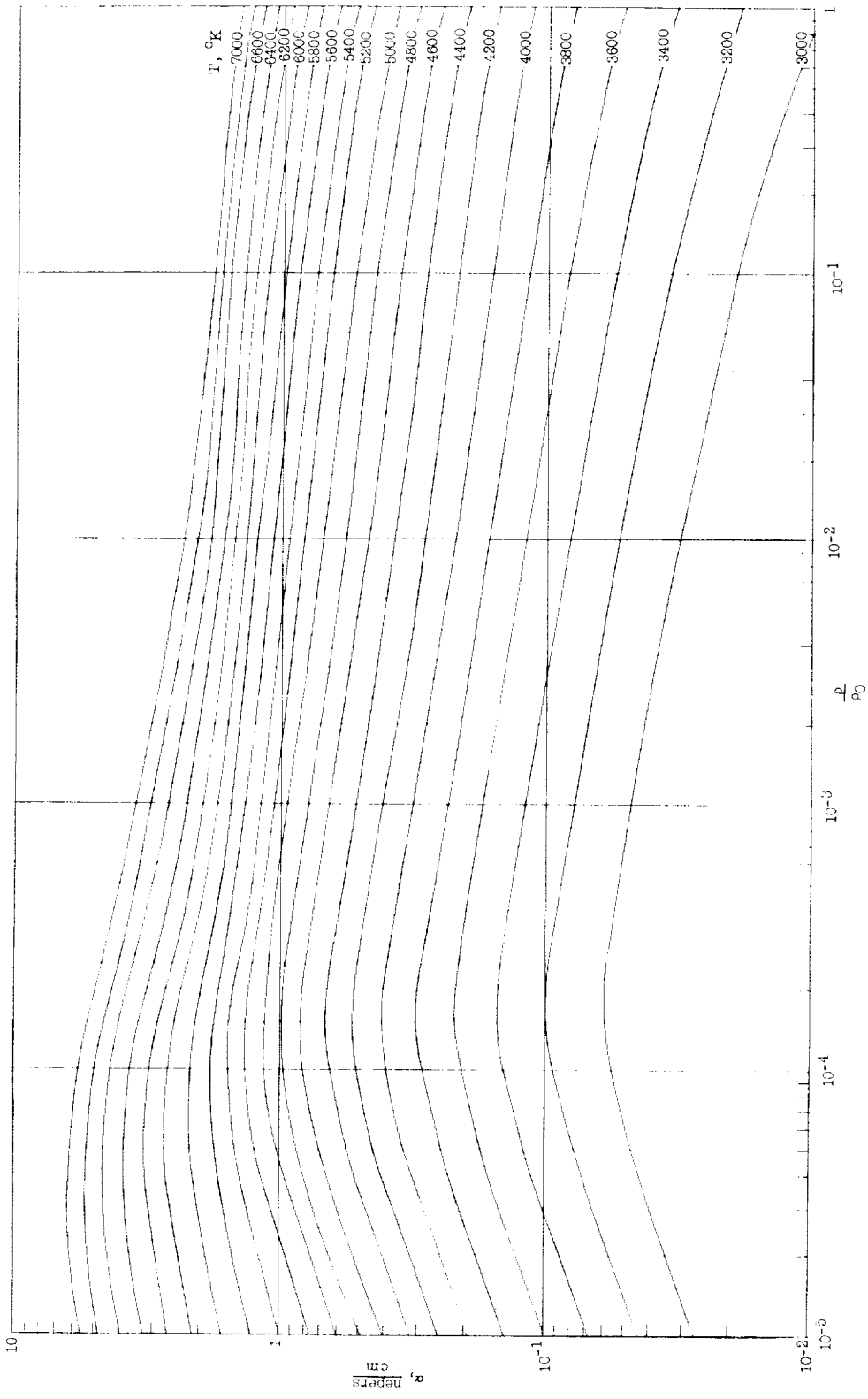

Figure 16.- Attenuation coefficient α for equilibrium air at $f = 30$ mc.

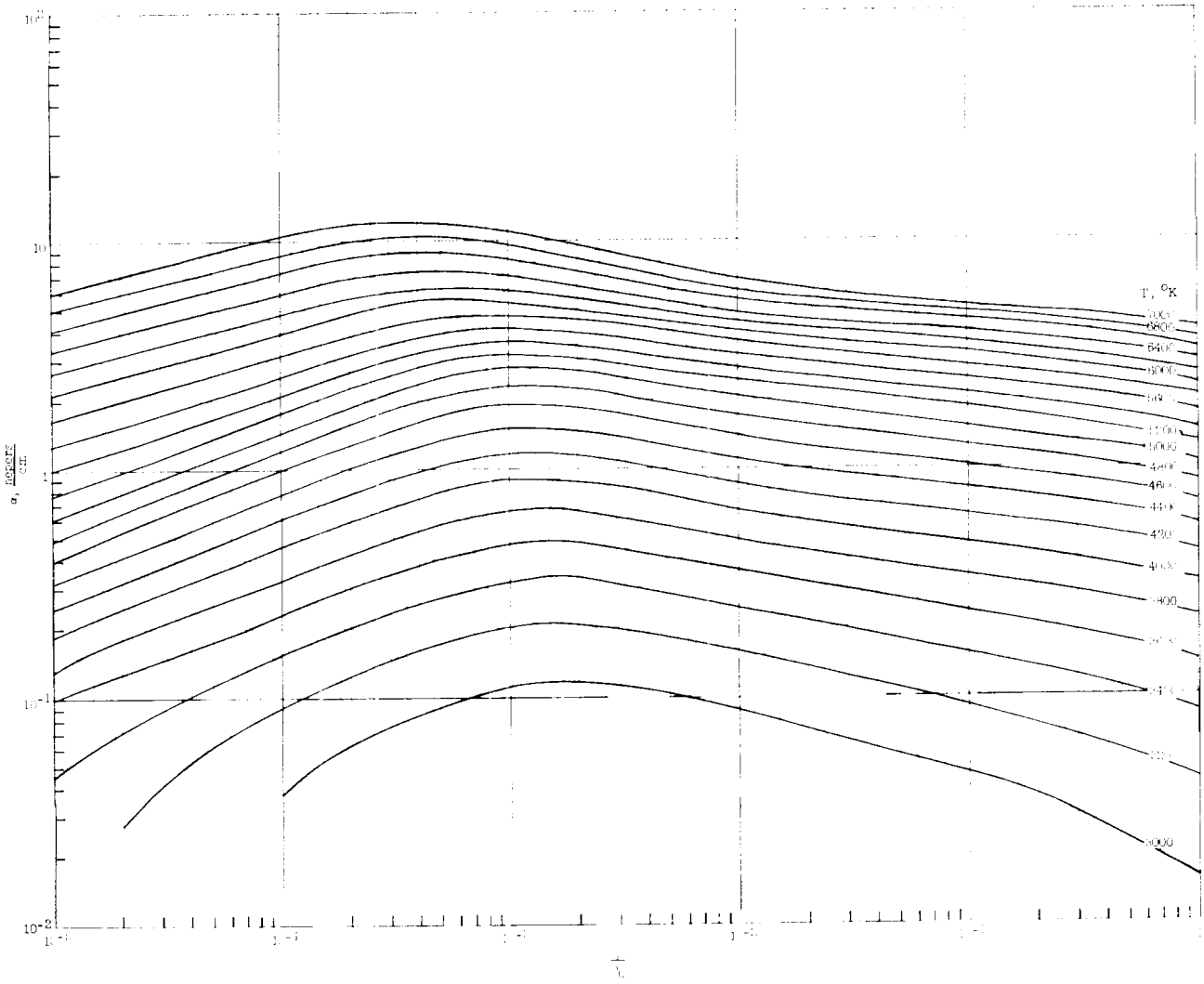

Figure 17.- Attenuation coefficient α for equilibrium air at f = 240 mc.

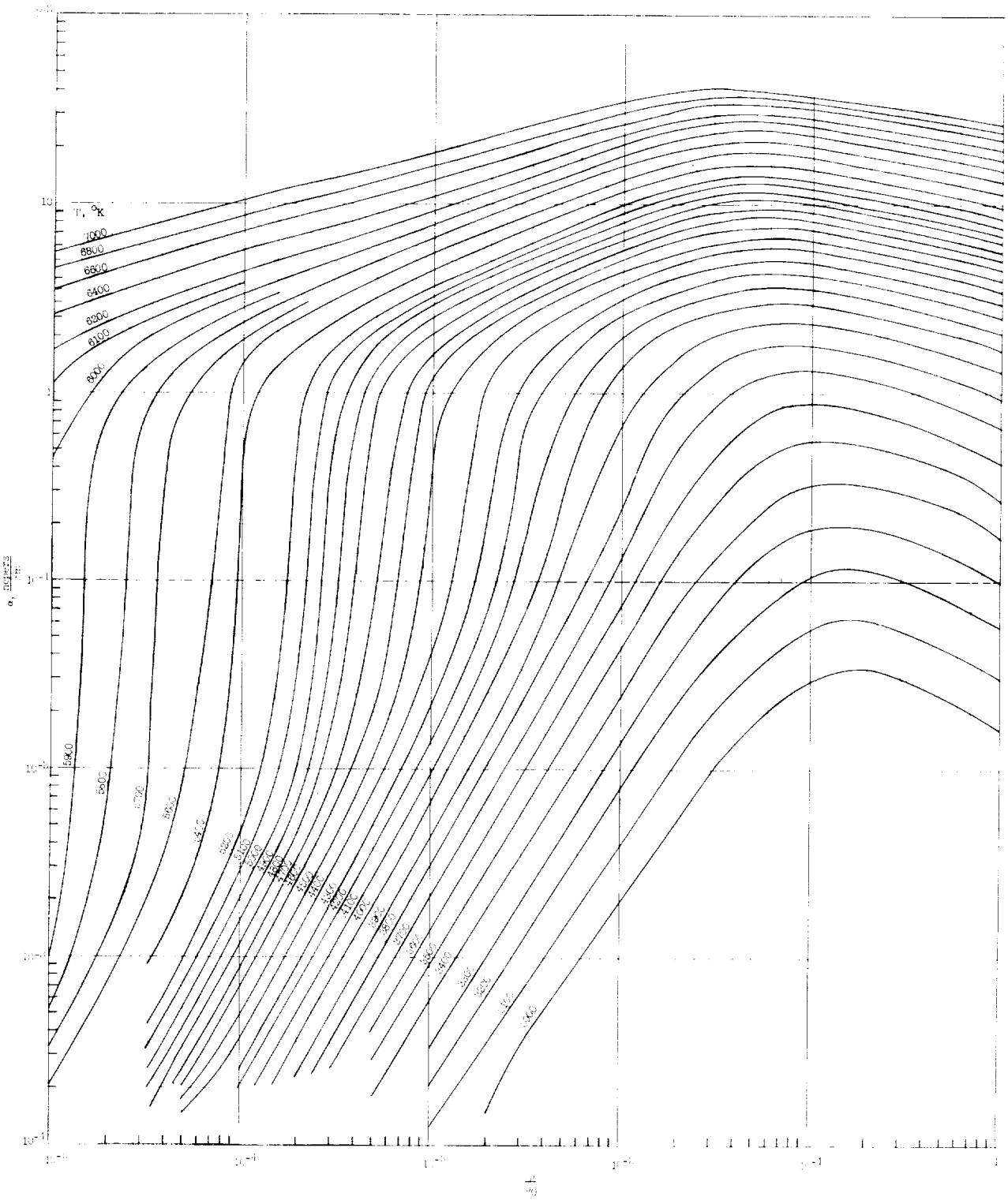

Figure 18.- Attenuation coefficient α for equilibrium air at f = 10,000 mc.

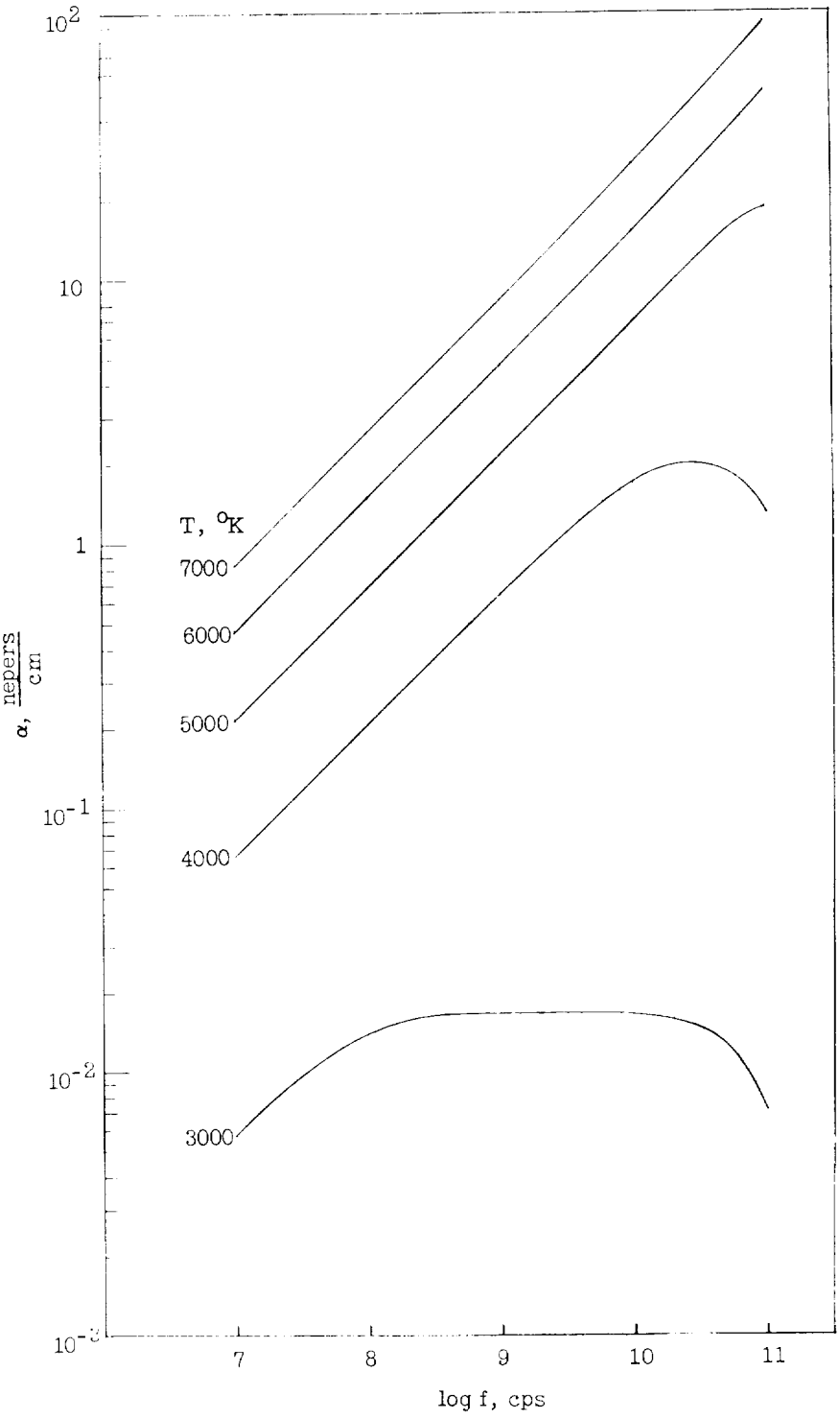

Figure 19.- Variation of attenuation coefficient α with signal frequency for equilibrium air at $\rho/\rho_0 = 1$.

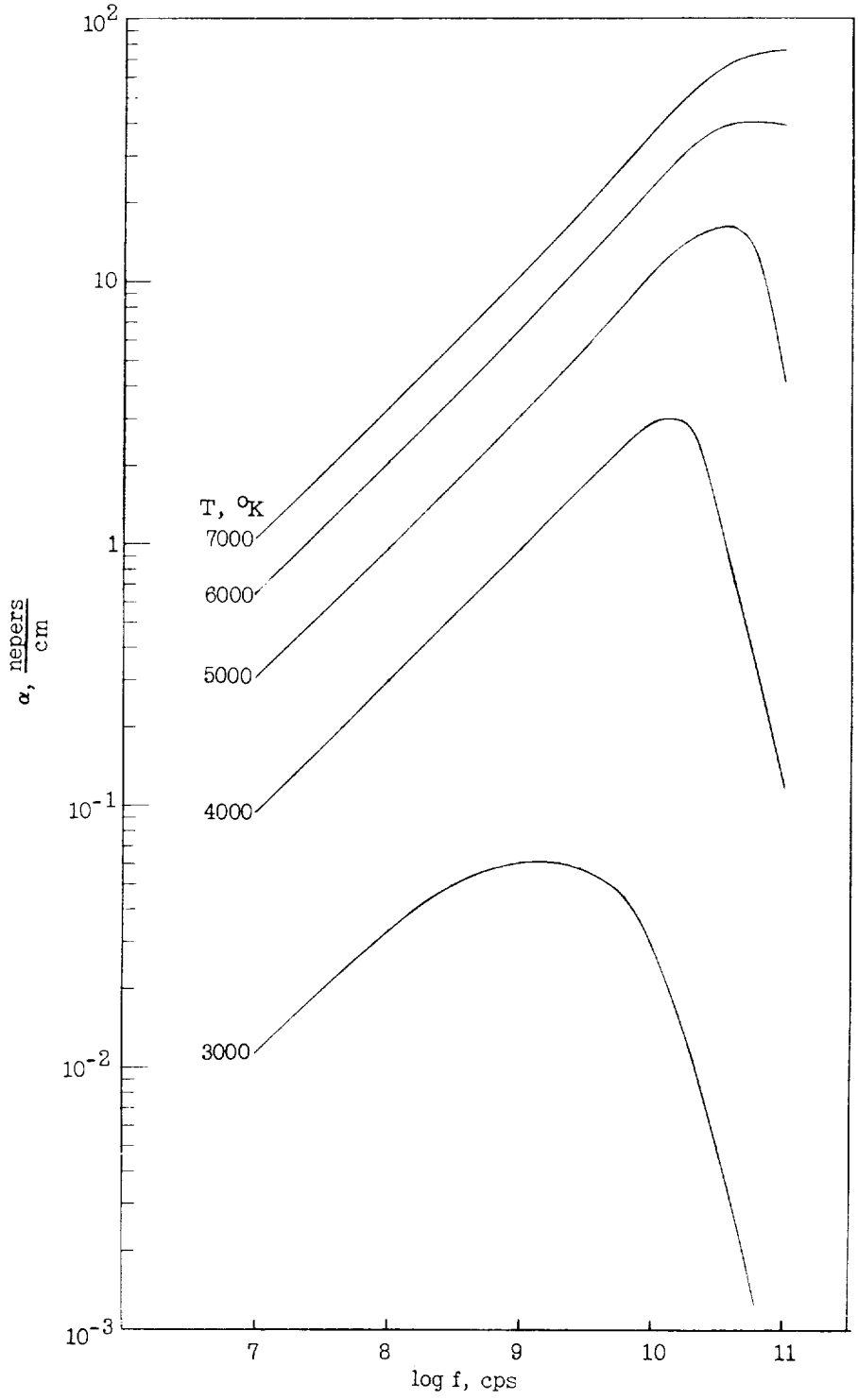

Figure 20.- Variation of attenuation coefficient α with signal frequency for equilibrium air at $\rho/\rho_0 = 10^{-1}$.

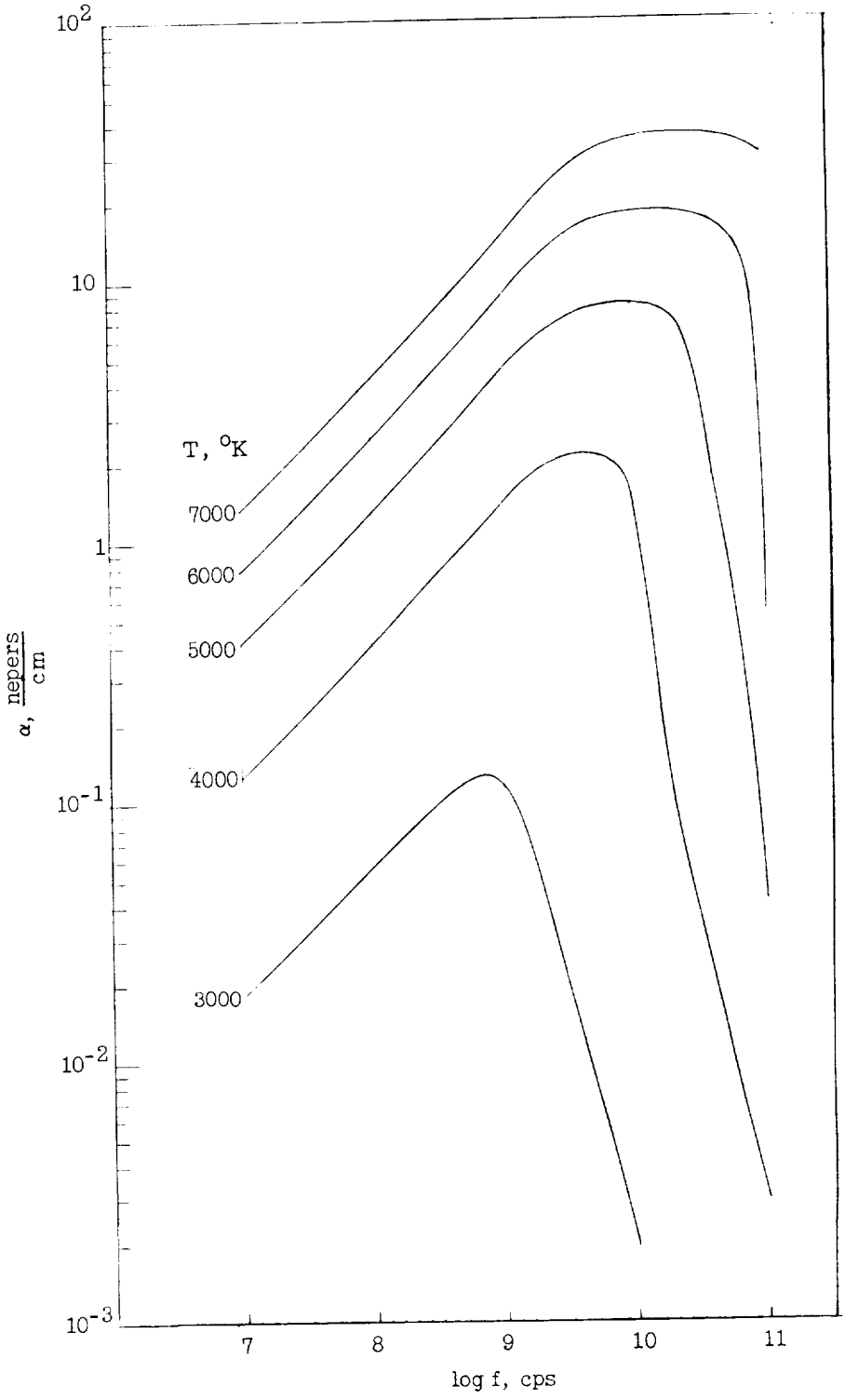

Figure 21.- Variation of attenuation coefficient α with signal frequency for equilibrium air at $\rho/\rho_0 = 10^{-2}$.

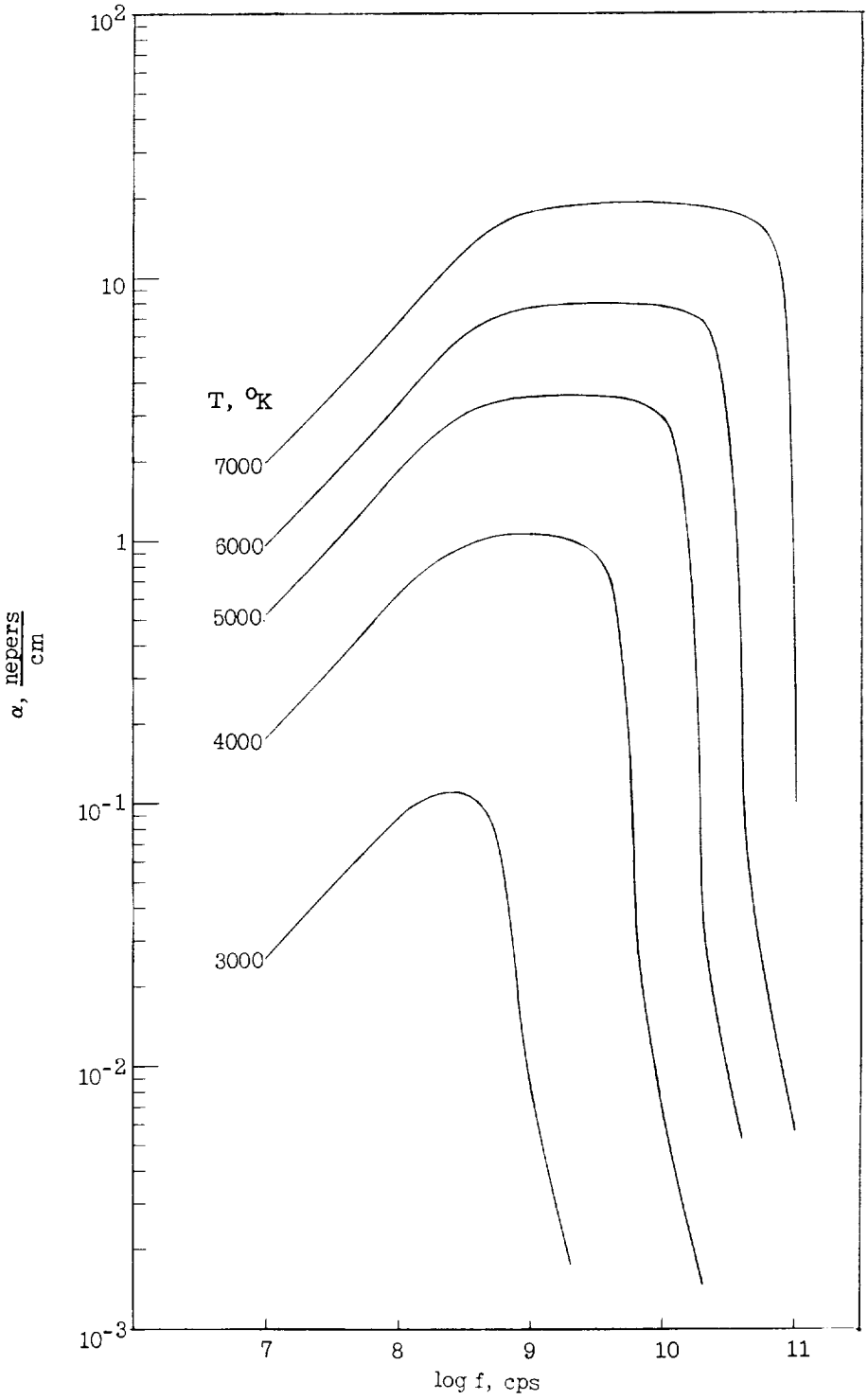

Figure 22.- Variation of attenuation coefficient α with signal frequency for equilibrium air at $\rho/\rho_0 = 10^{-3}$.

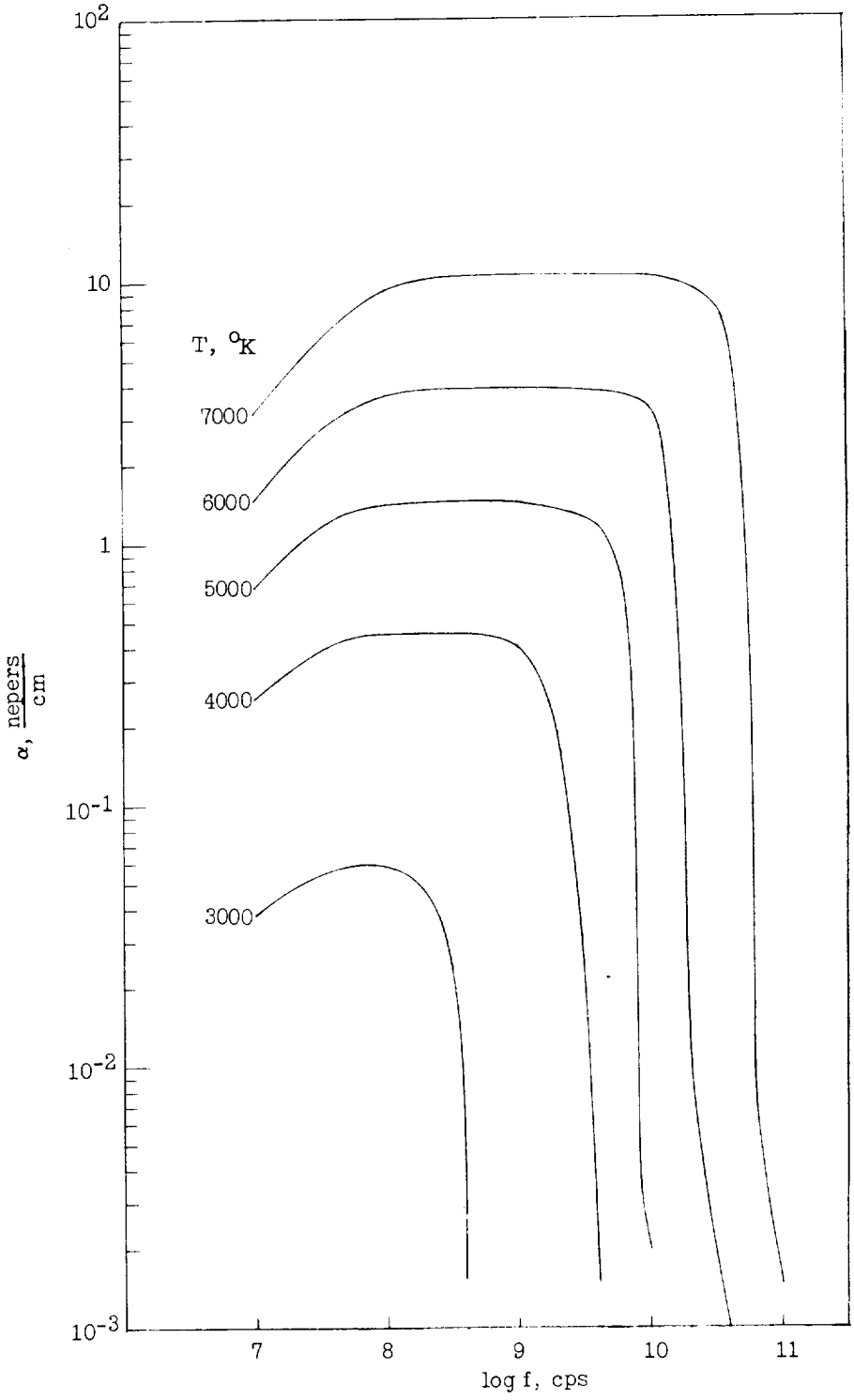

Figure 23.- Variation of attenuation coefficient α with signal frequency for equilibrium air at $\rho/\rho_0 = 10^{-4}$.

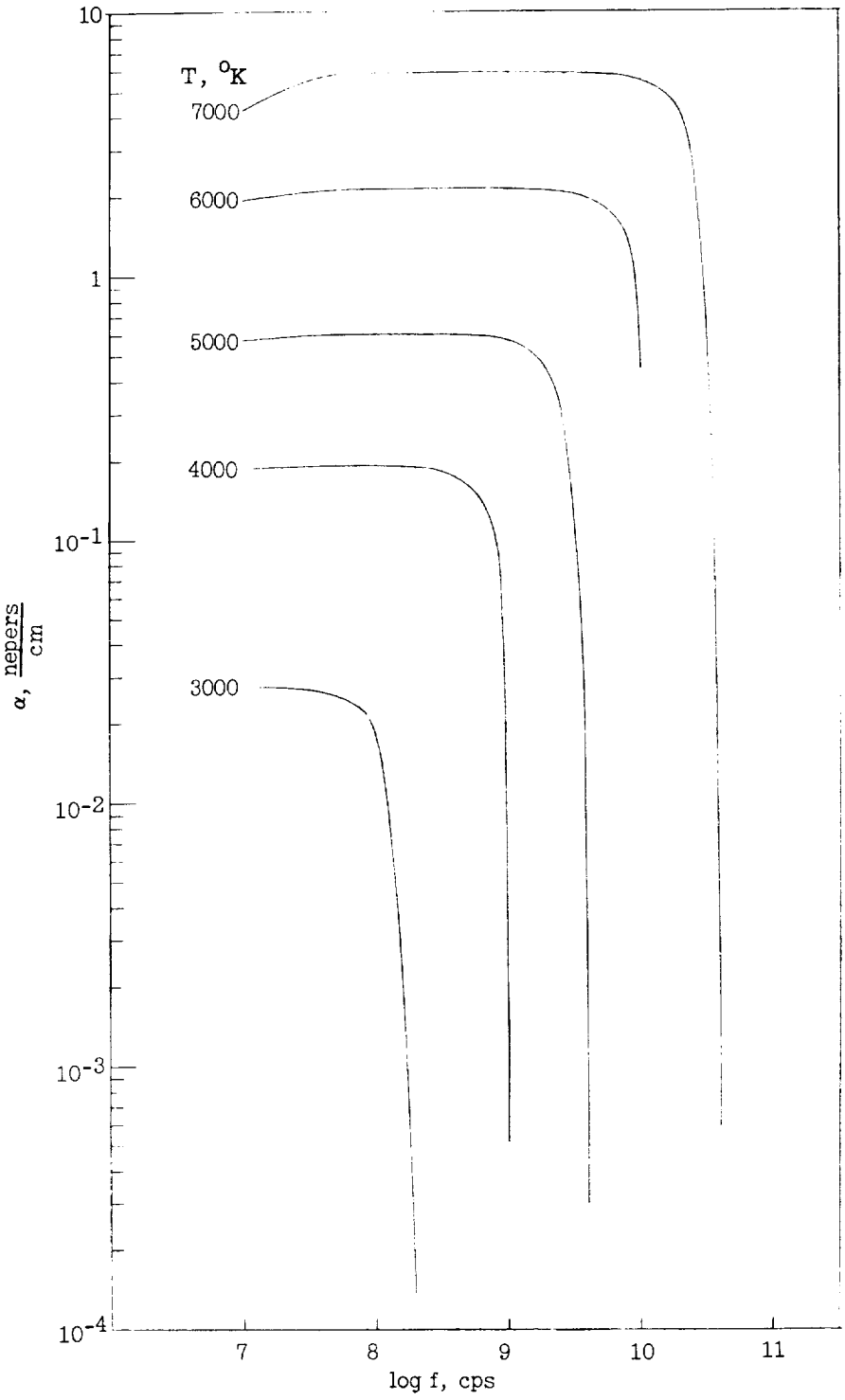

Figure 24.- Variation of attenuation coefficient α with signal frequency for equilibrium air at $\rho/\rho_0 = 10^{-5}$.

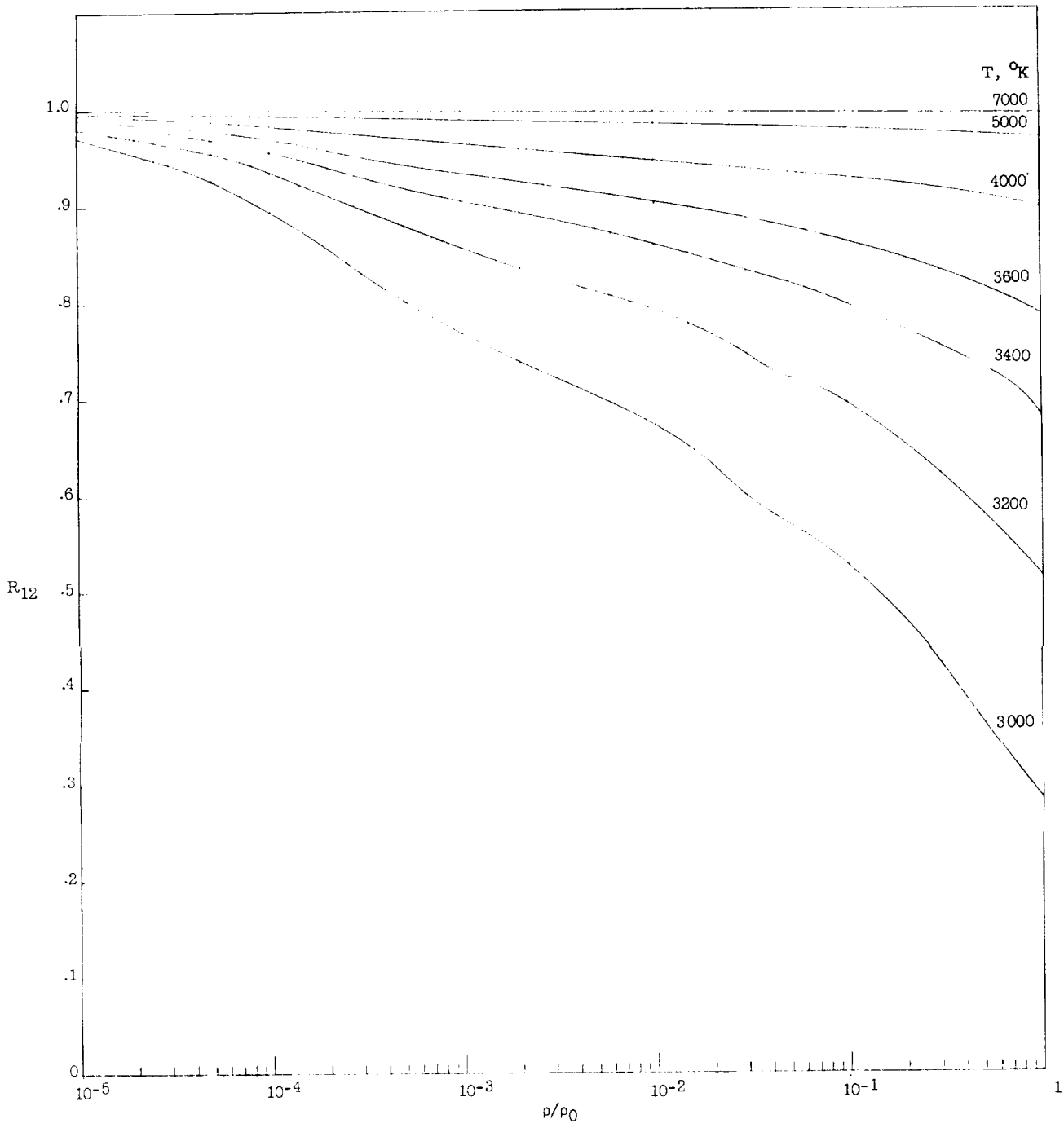

Figure 25.- Variation of reflection coefficient (semi-infinite media) with density for equilibrium air at f = 30 mc.

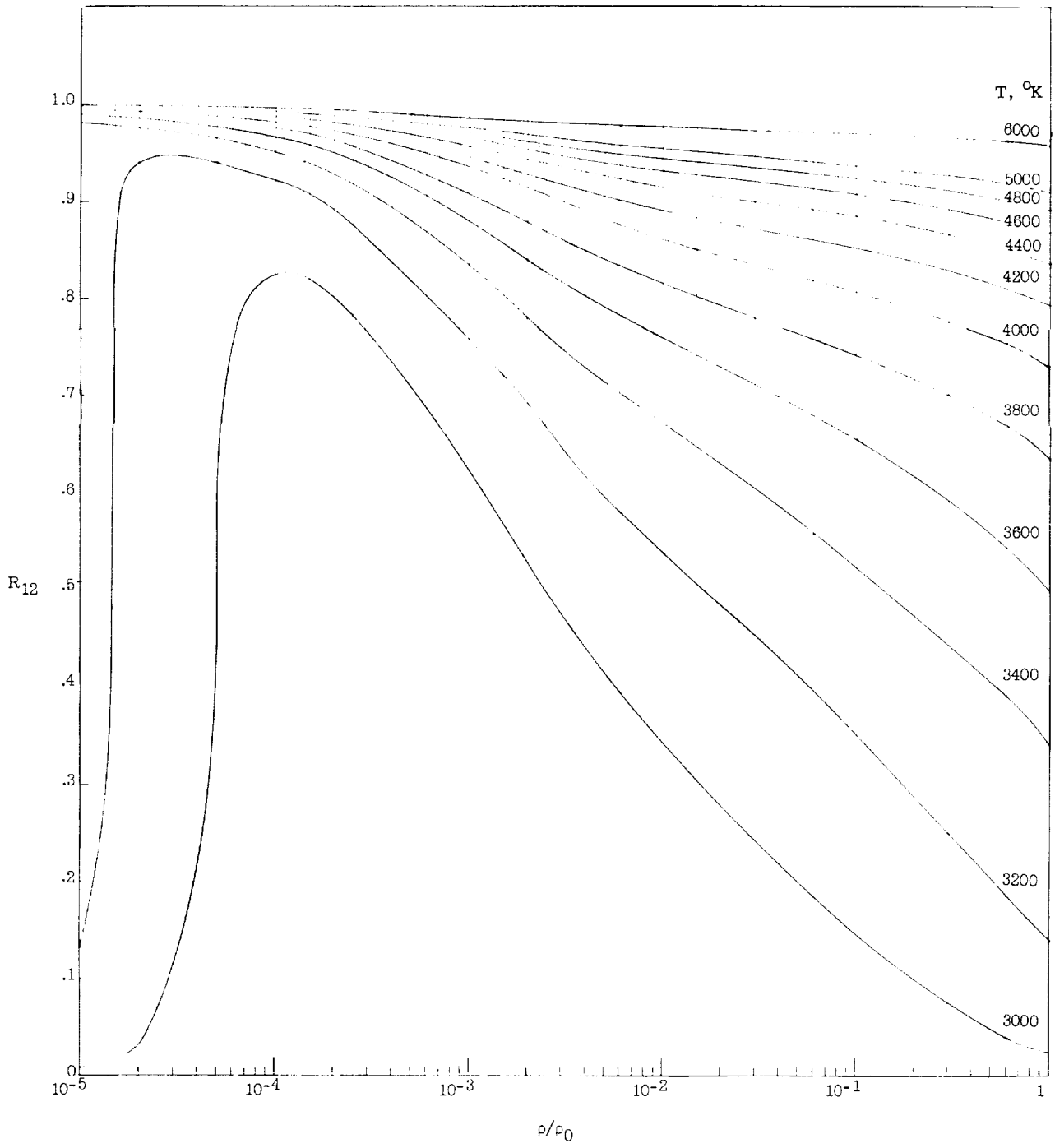

Figure 26.- Variation of reflection coefficient (semi-infinite media) with density for equilibrium air at f = 240 mc.

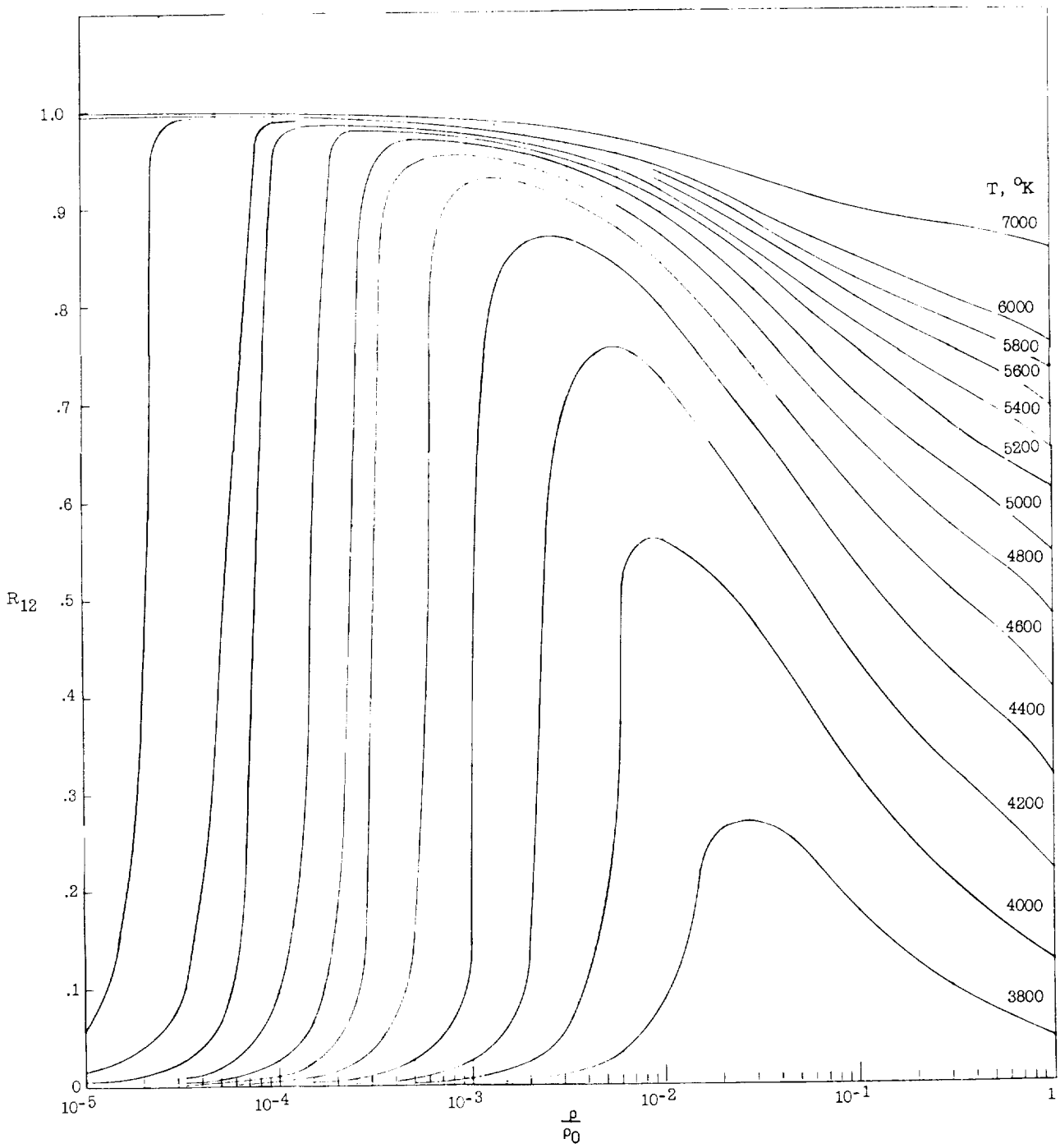

Figure 27.- Variation of reflection coefficient (semi-infinite media) with density for equilibrium air at f = 10,000 mc.

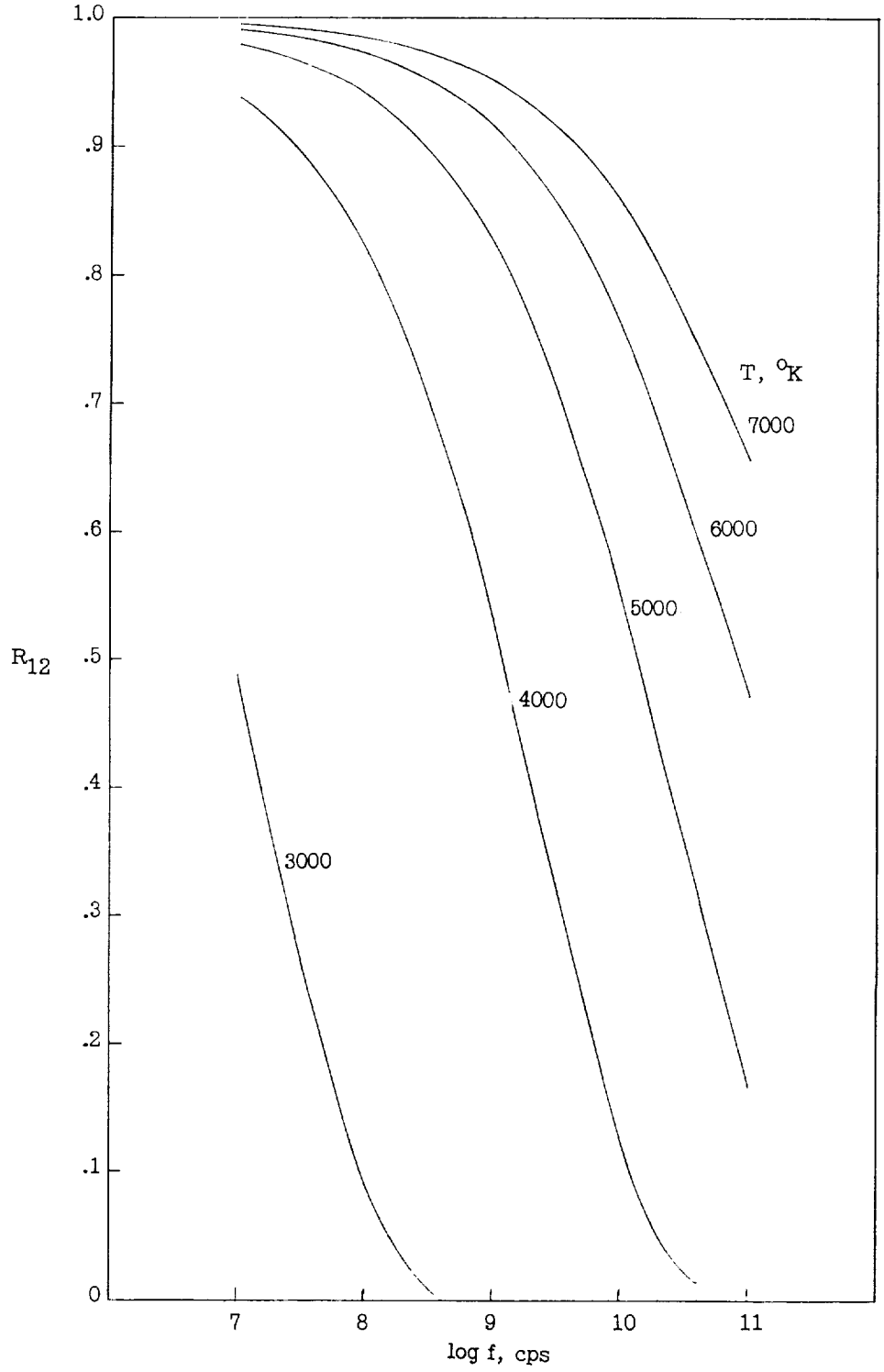

Figure 28.- Variation of reflection coefficient (semi-infinite media) with signal frequency for equilibrium air at $\rho/\rho_0 = 1$.

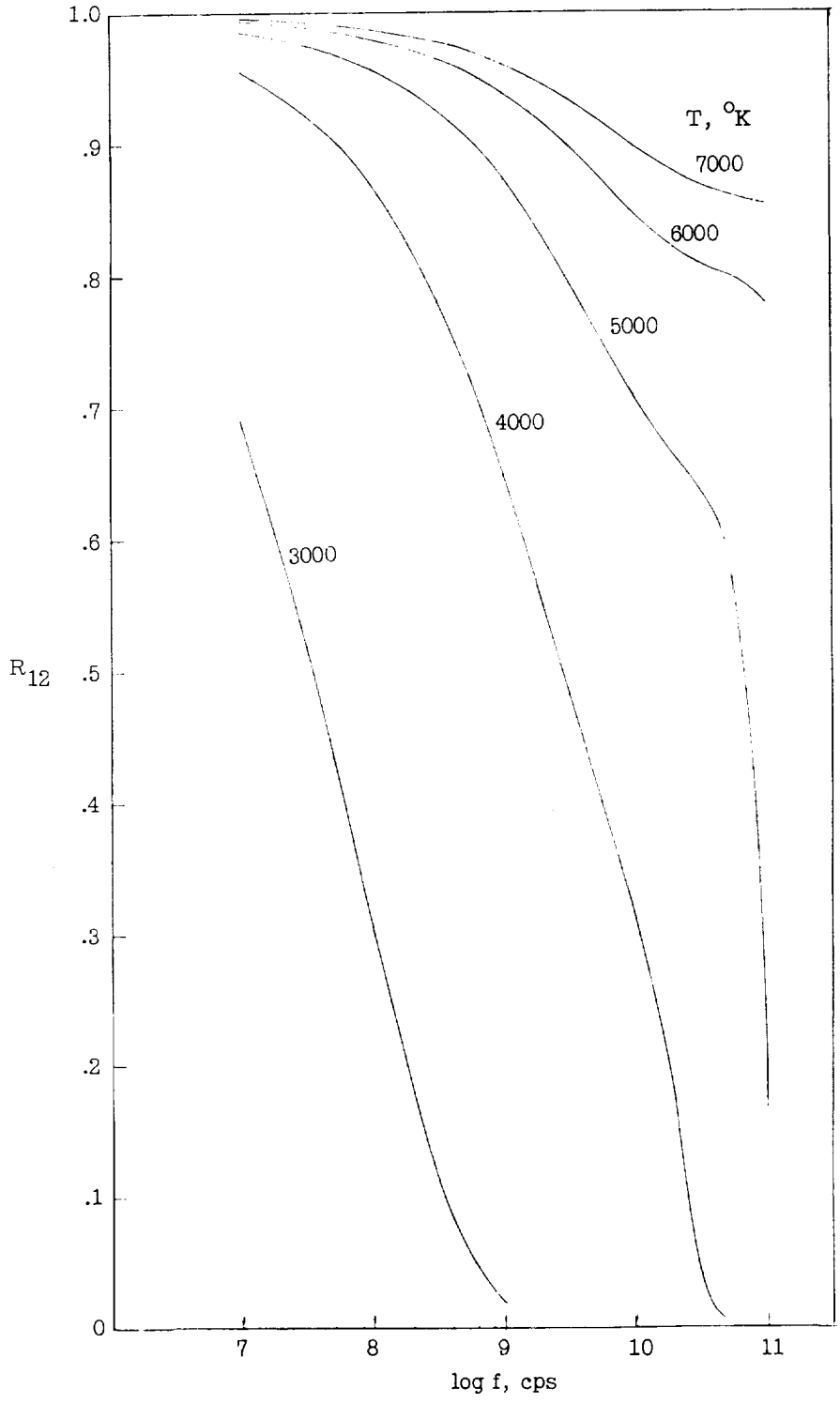

Figure 29.- Variation of reflection coefficient (semi-infinite media) with signal frequency for equilibrium air at $\rho/\rho_0 = 10^{-1}$.

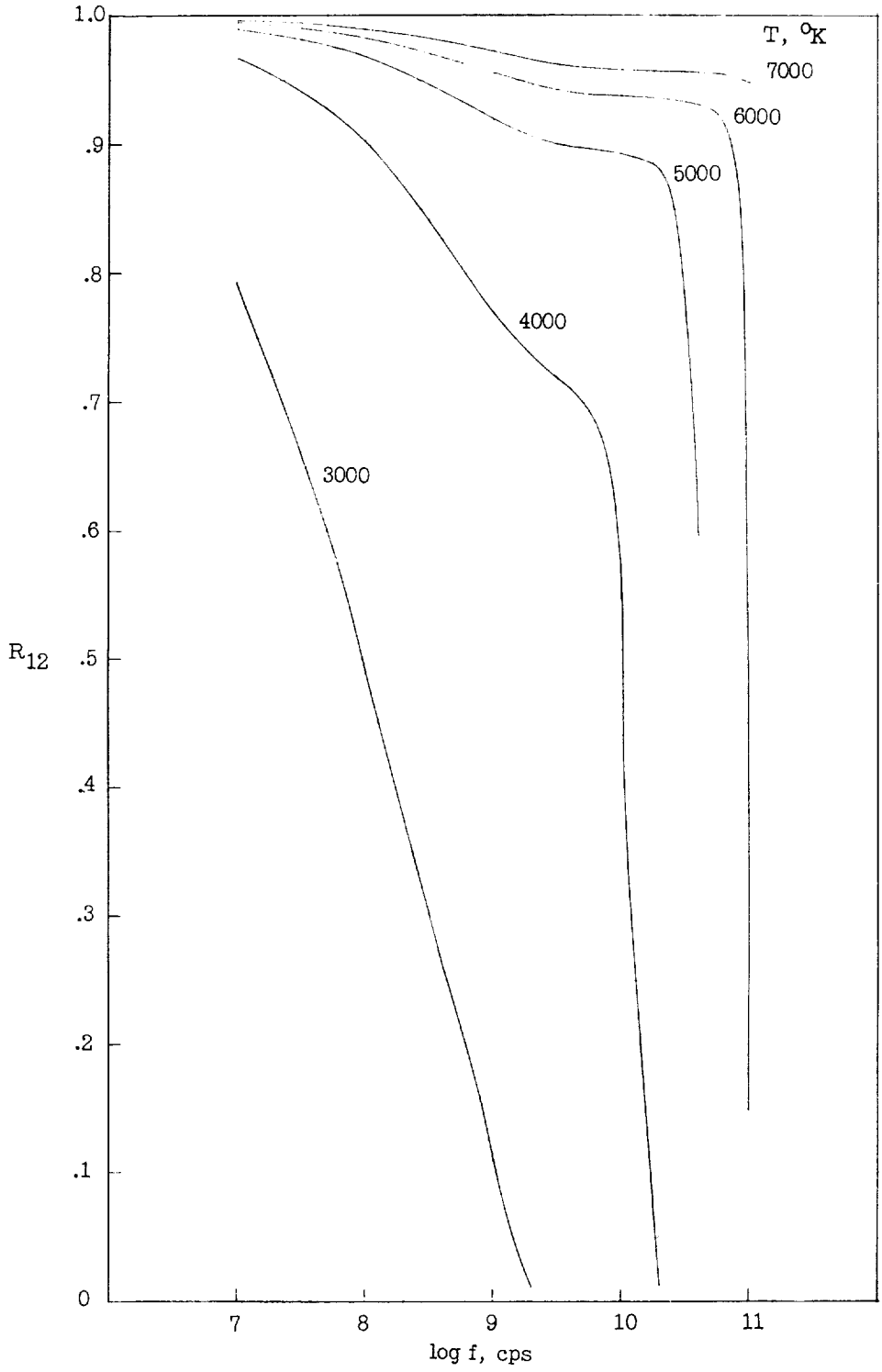

Figure 30.- Variation of reflection coefficient (semi-infinite media) with signal frequency for equilibrium air at $\rho/\rho_0 = 10^{-2}$.

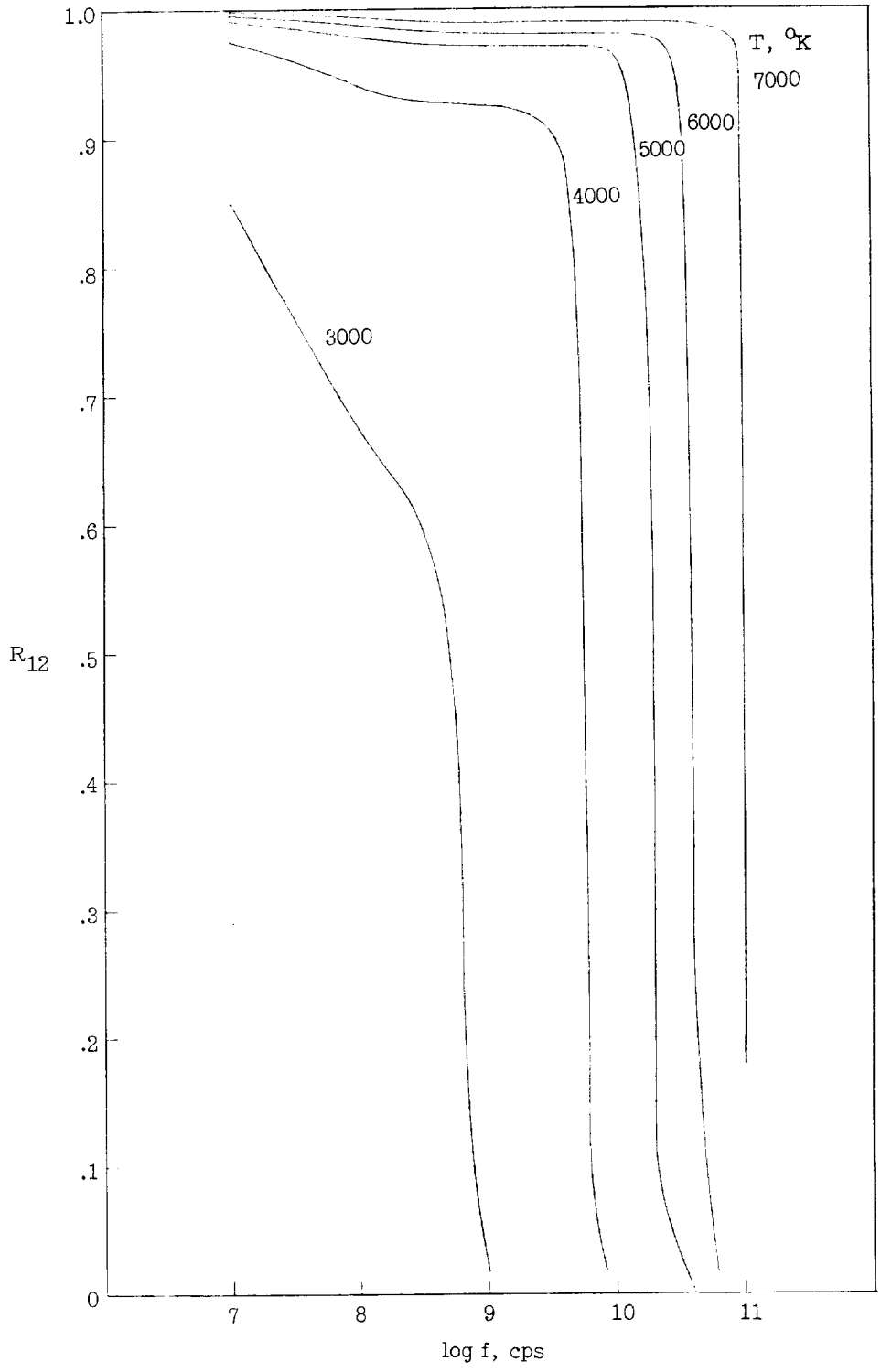

Figure 31.- Variation of reflection coefficient (semi-infinite media) with signal frequency for equilibrium air at $\rho/\rho_0 = 10^{-3}$.

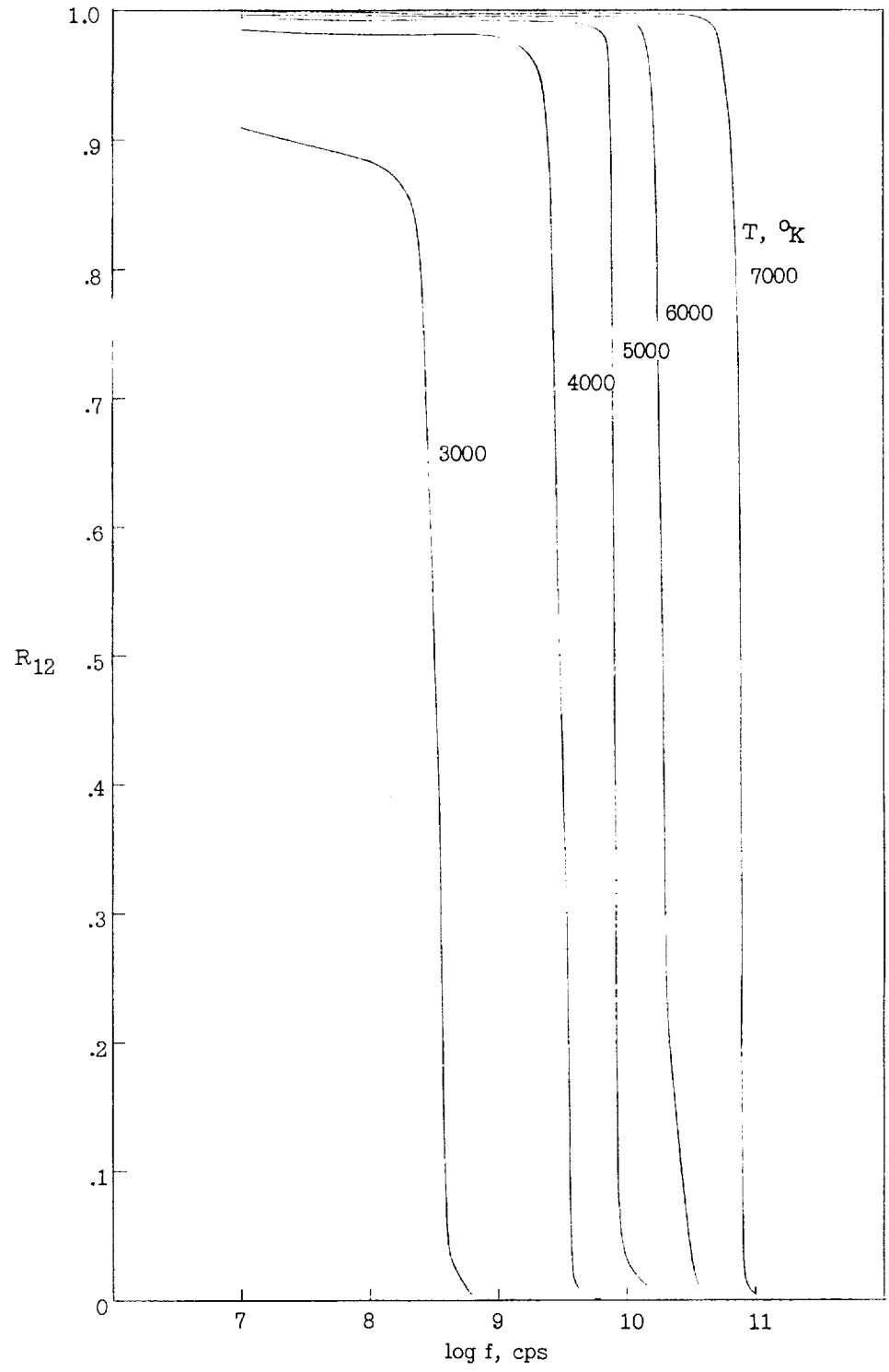

Figure 32.- Variation of reflection coefficient (semi-infinite media) with signal frequency for equilibrium air at $\rho/\rho_0 = 10^{-4}$.

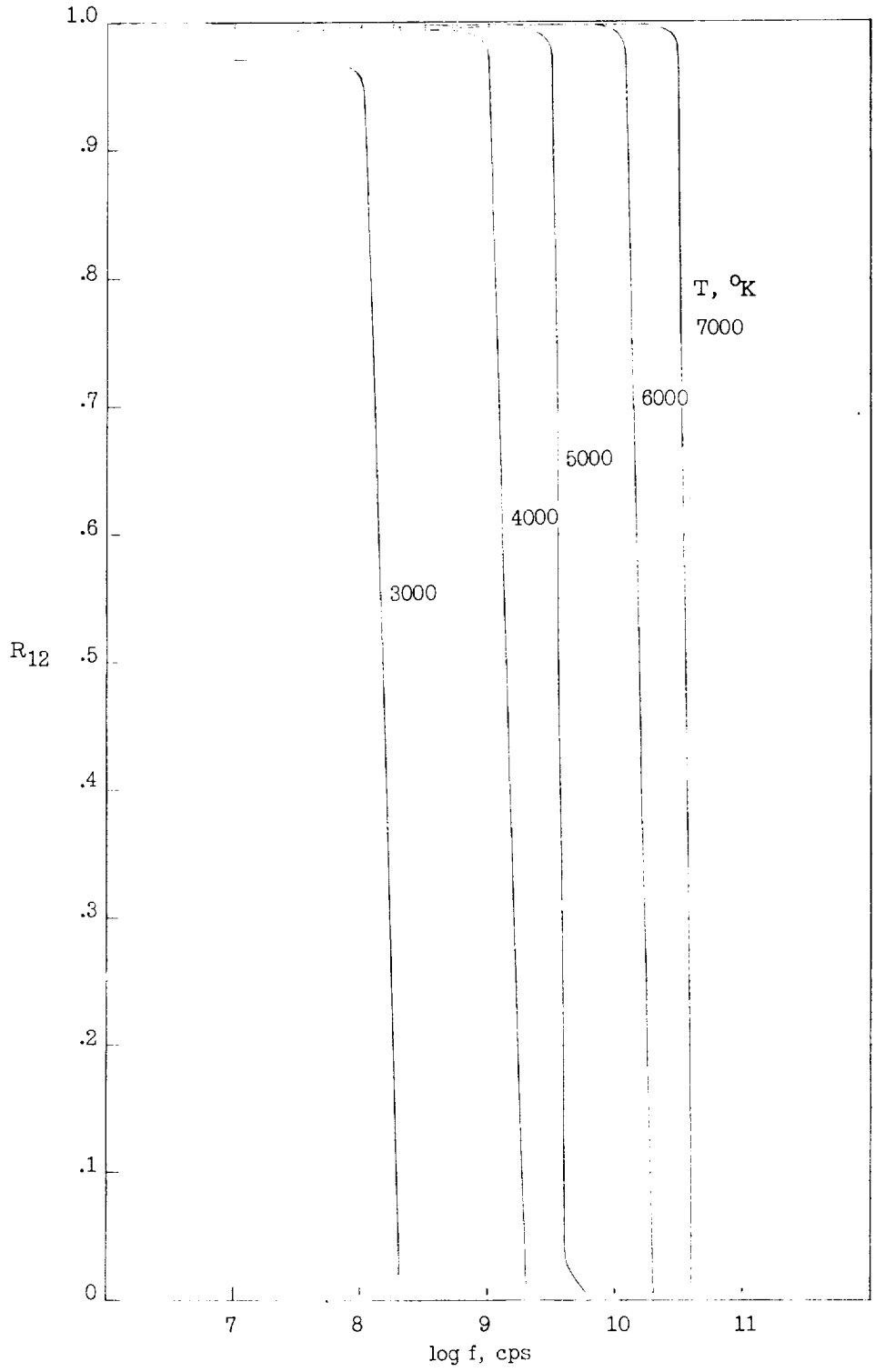

Figure 33.- Variation of reflection coefficient (semi-infinite media) with signal frequency for equilibrium air at $\rho/\rho_0 = 10^{-5}$.

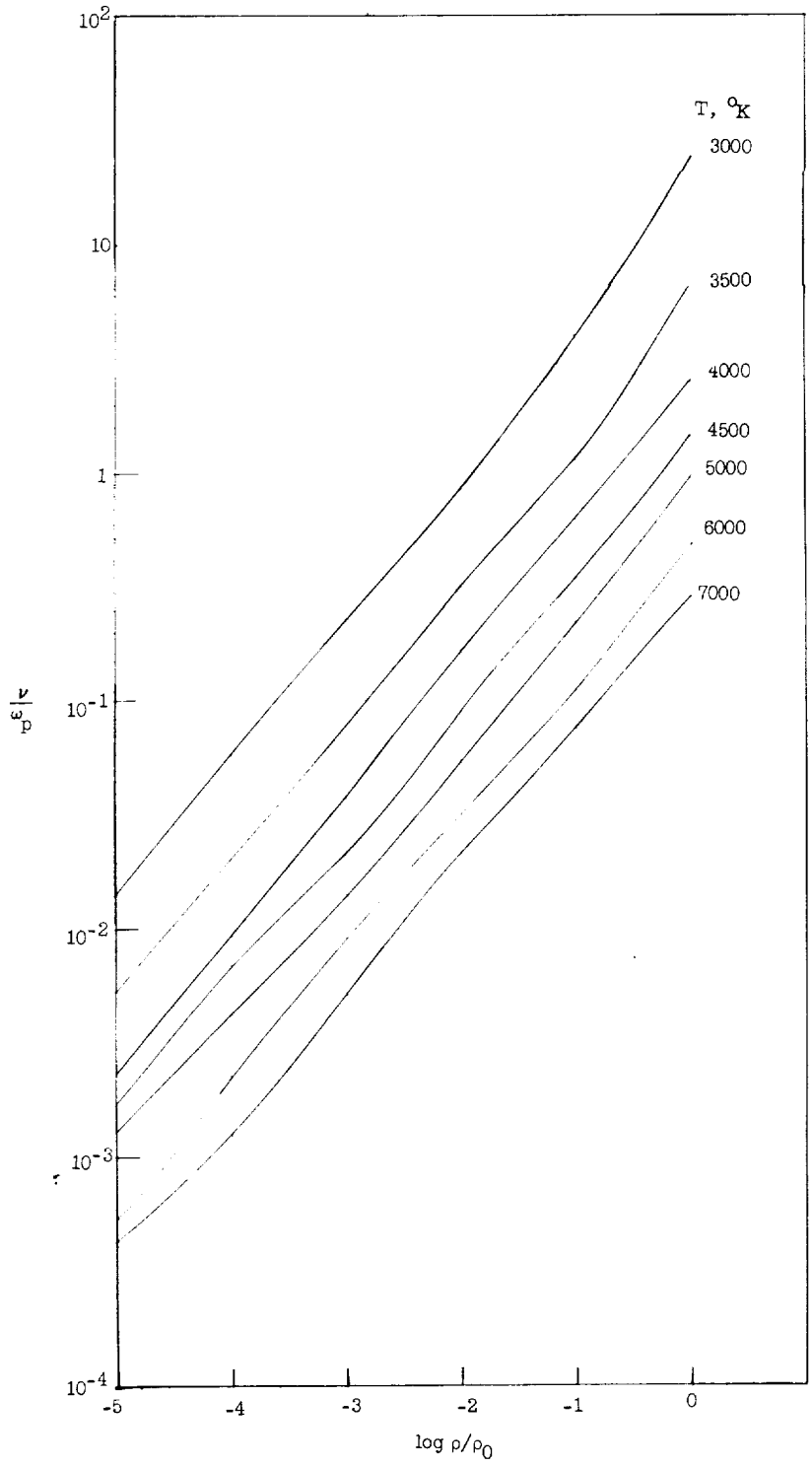

Figure 34.- Normalized electron collision frequency for equilibrium air.

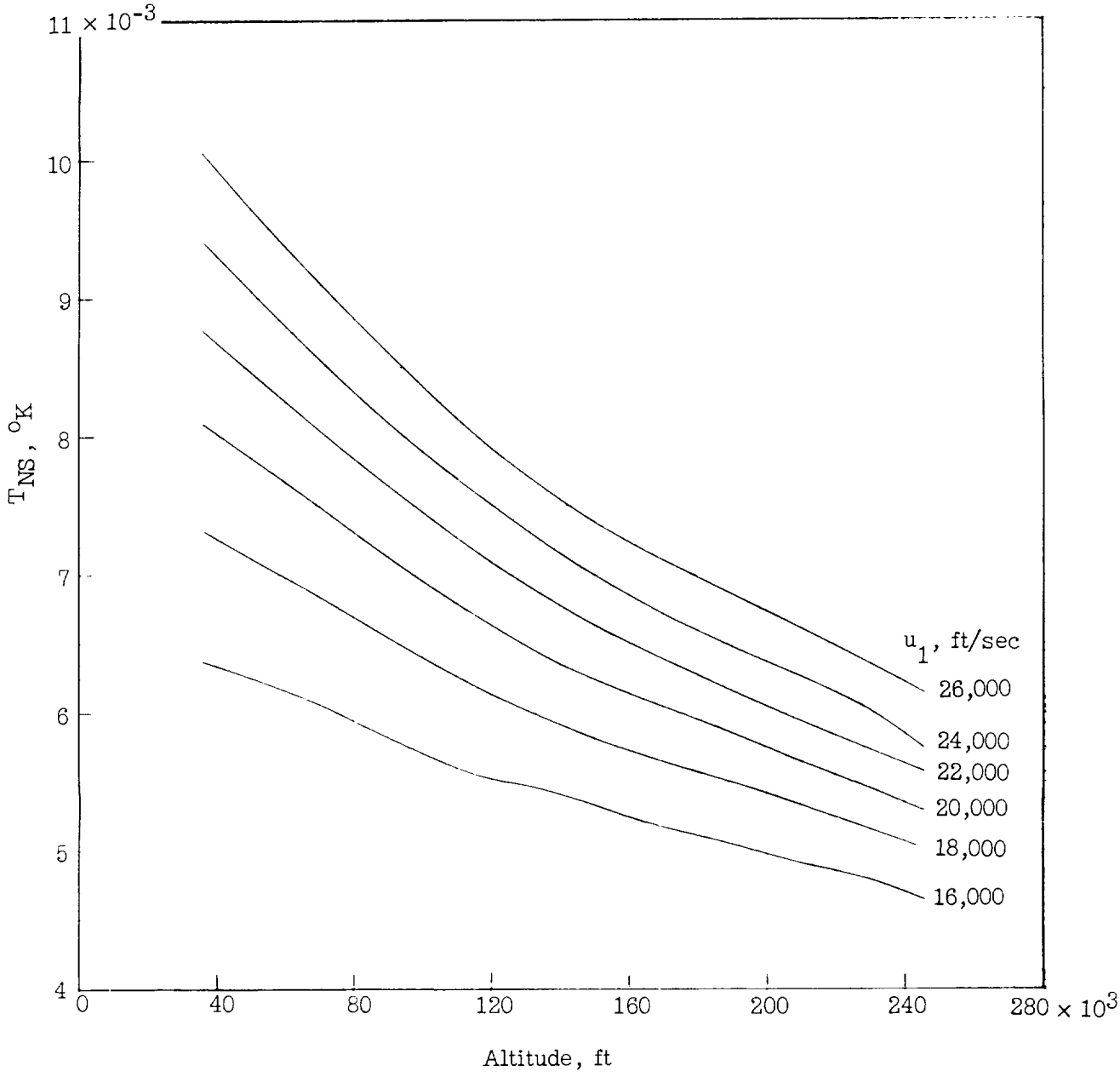

Figure 35.- Normal-shock temperature for equilibrium air.

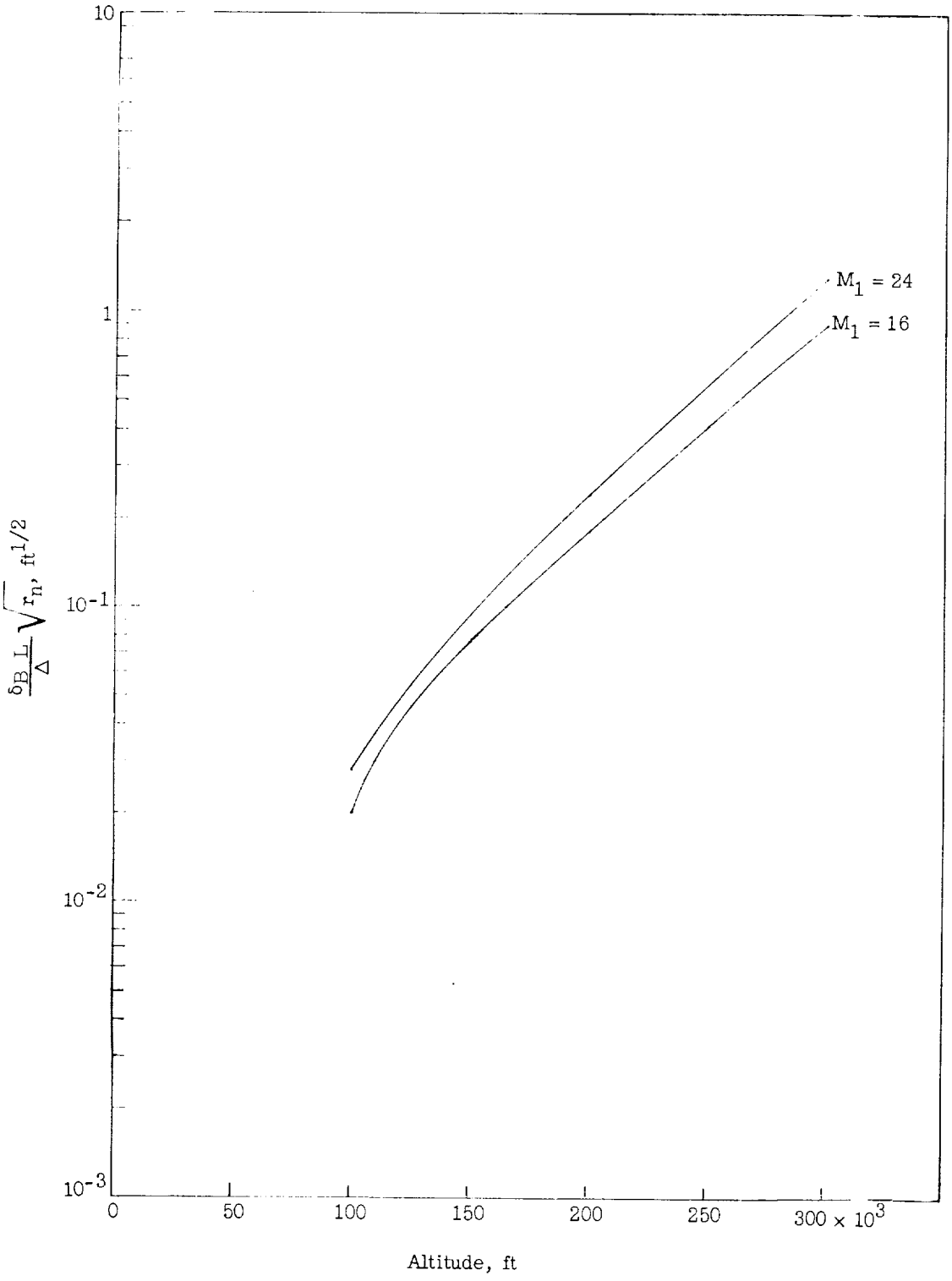

Figure 36.- Stagnation-point viscous flow parameter.

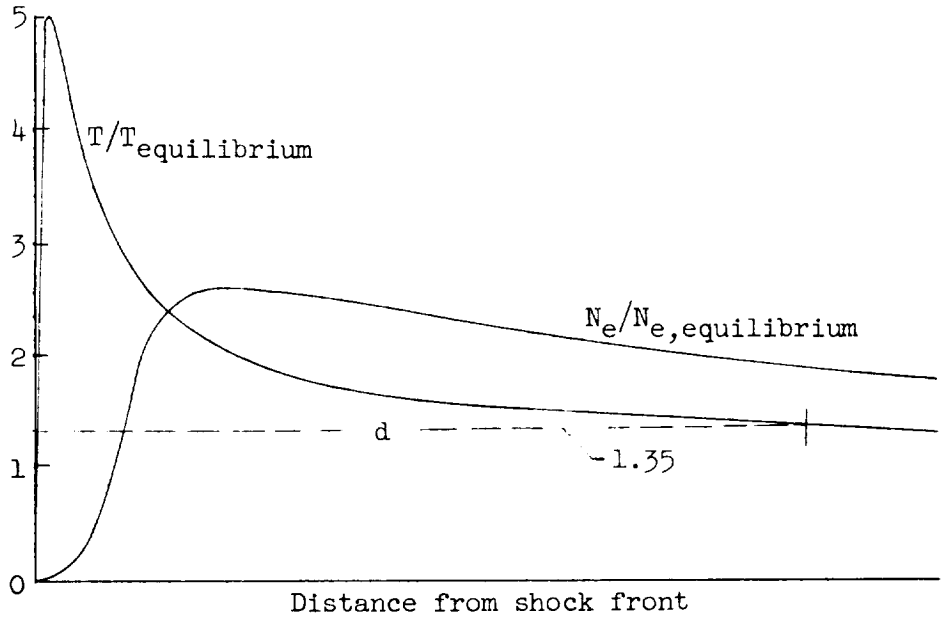

Figure 37.- Typical effects of nonequilibrium flow in the region of the normal shock. (From ref. 16.)

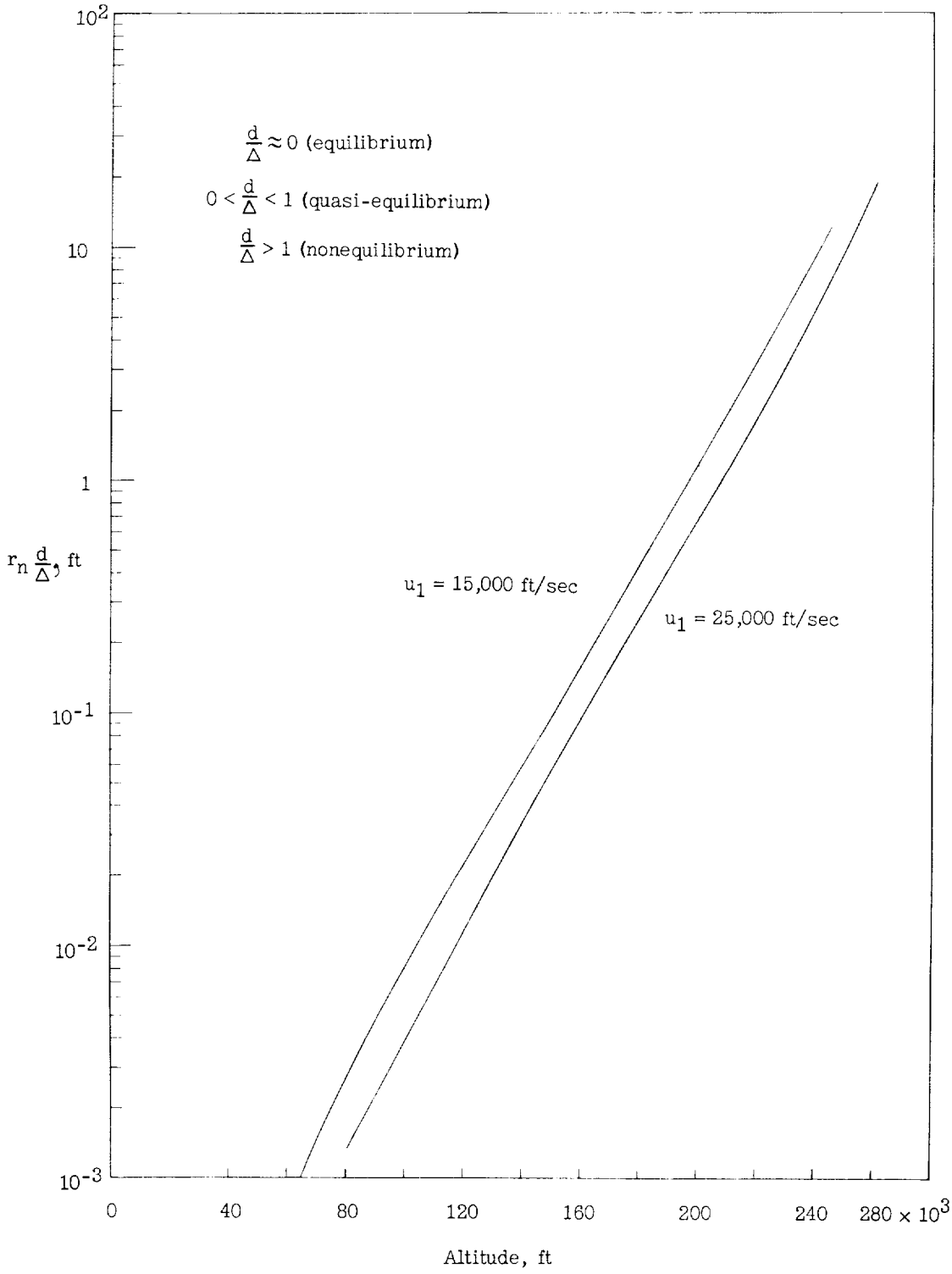

Figure 38.- Nonequilibrium flow parameter.

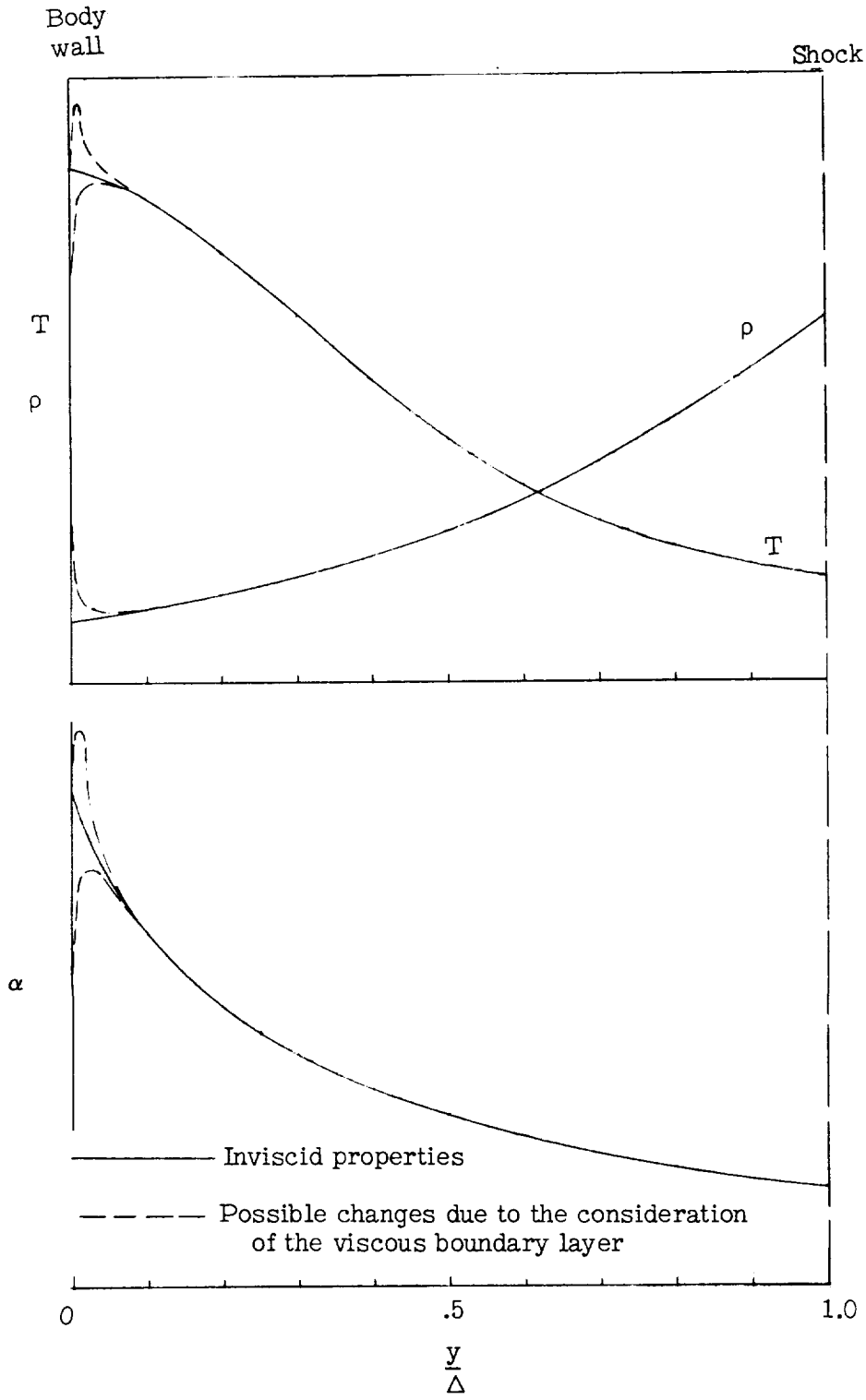

Figure 39.- Typical trends of properties within the shock layer.

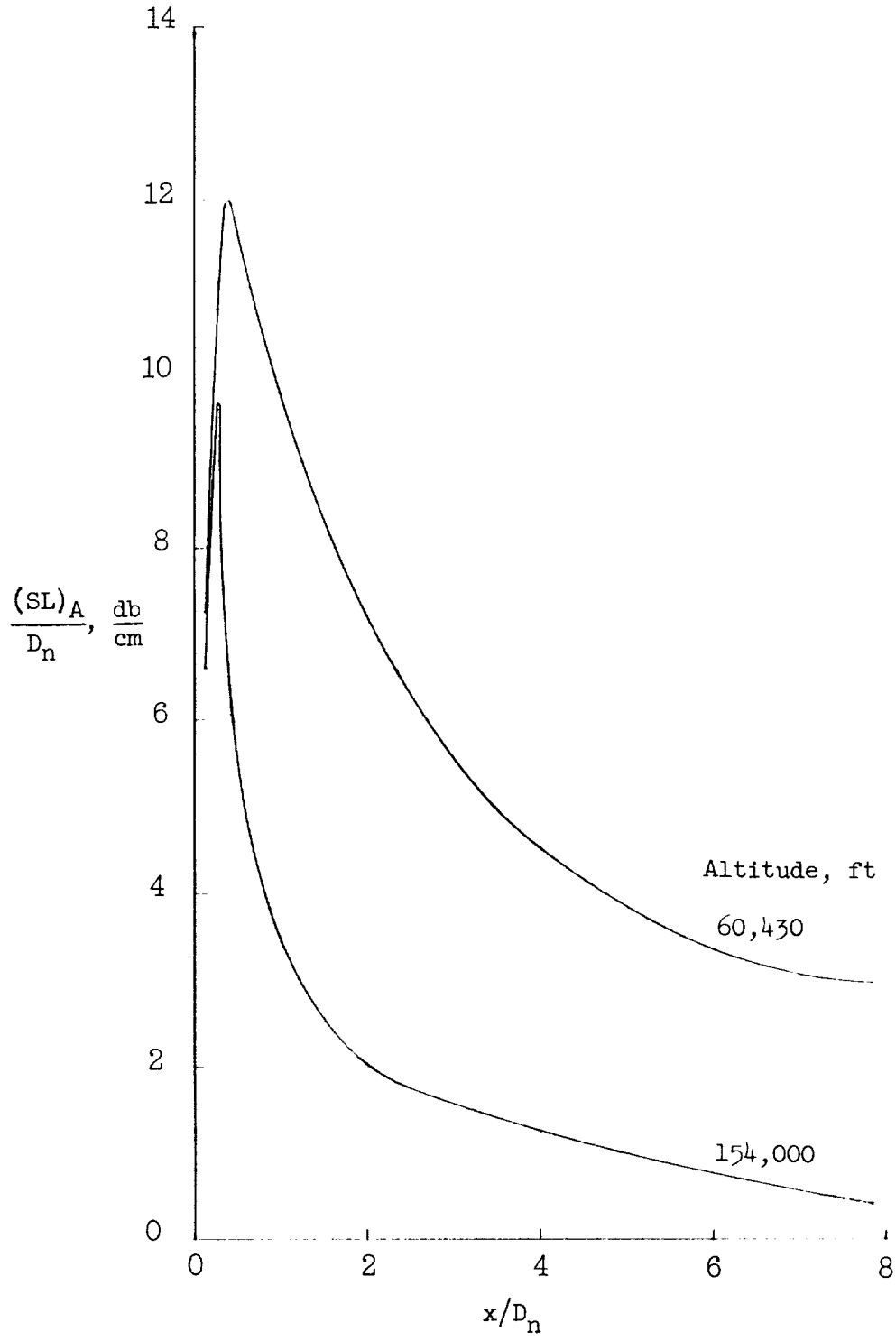

Figure 40.- Typical stationwise attenuation of waves emanating normally from the body. $\theta = 9^o$; M = 20; f = 10,000 mc.

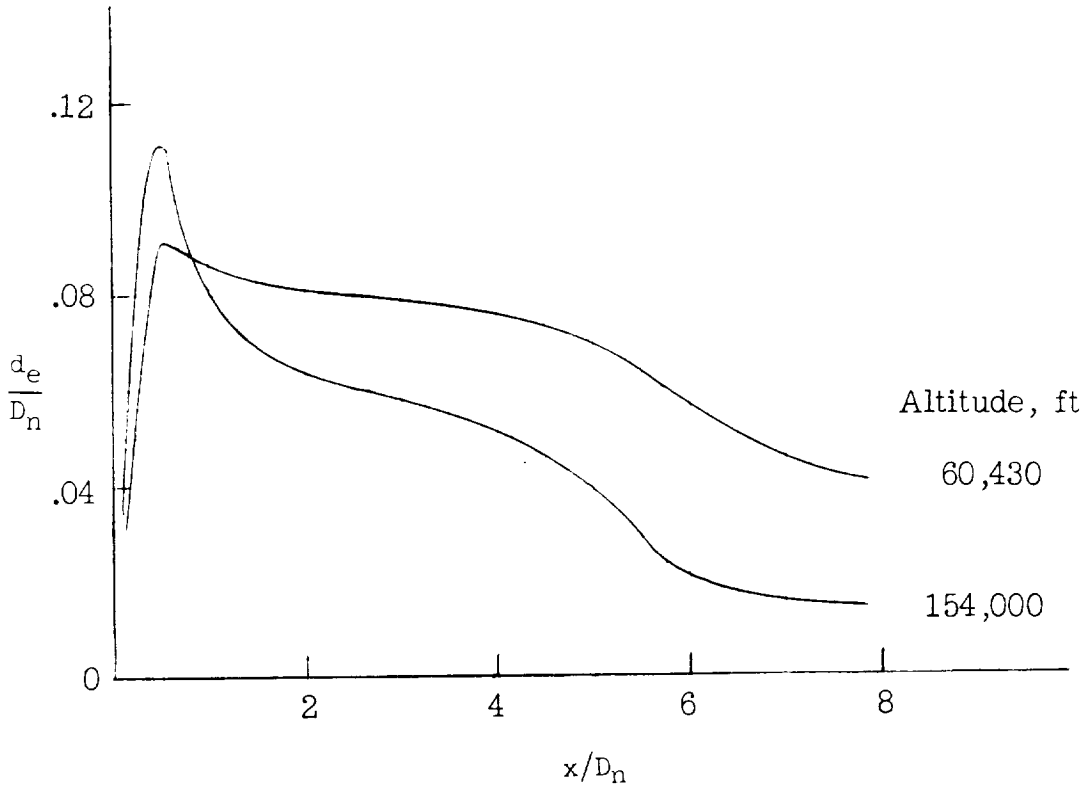

Figure 41.- Typical stationwise variation of the effective plasma thickness. $\theta = 9^\circ$; M = 20; f = 10,000 mc.

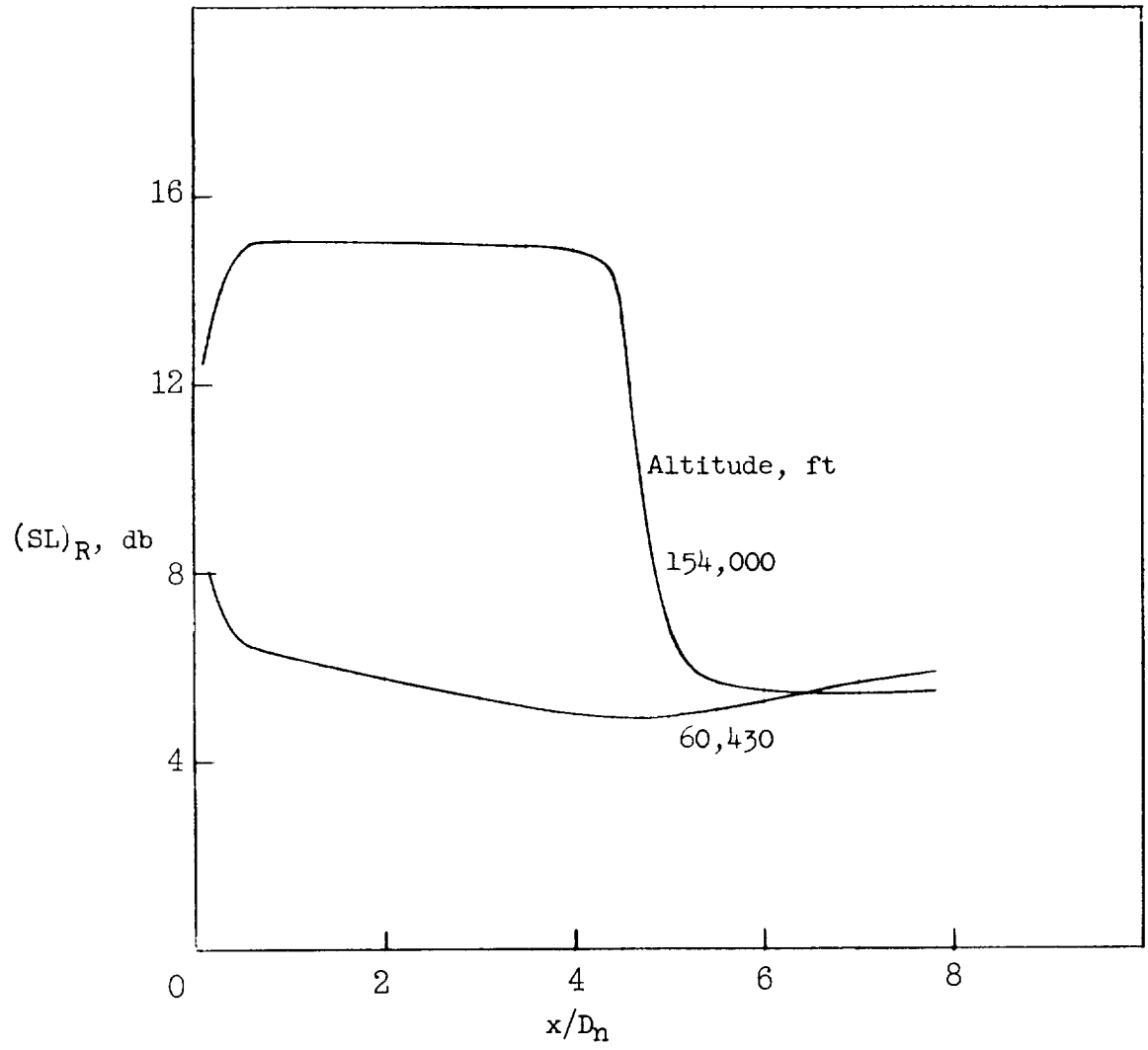

Figure 42.- Example of stationwise variation of the signal loss due to reflection. $\theta = 9^{\circ}$; M = 20; f = 10,000 mc; D_n = 30.48 cm.

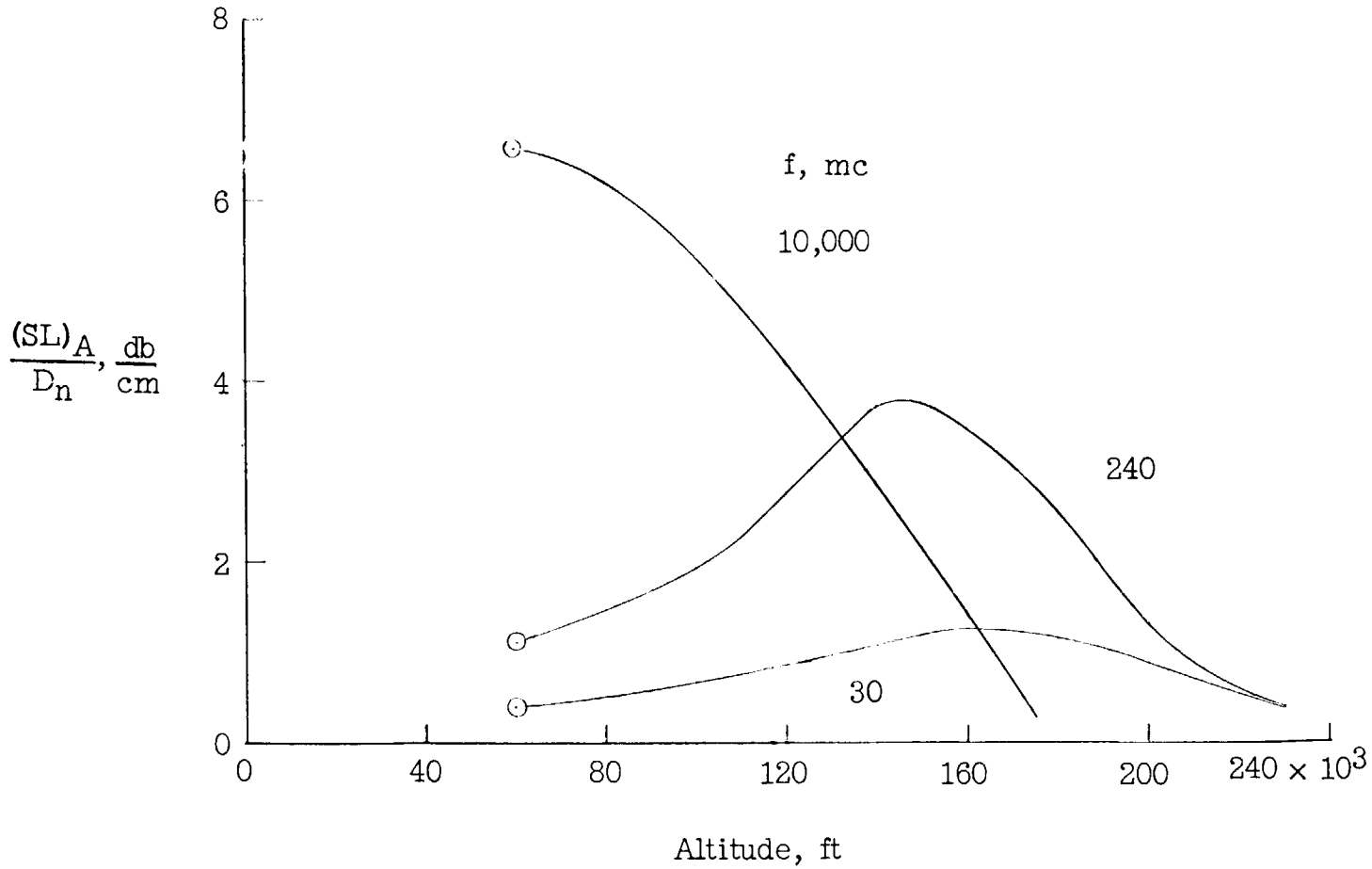

Figure 43.- Example of variation of attenuation with altitude for a constant Mach number trajectory. $\theta = 9^{\circ}$; $M = 20$; $x/D_n = 2.333$.

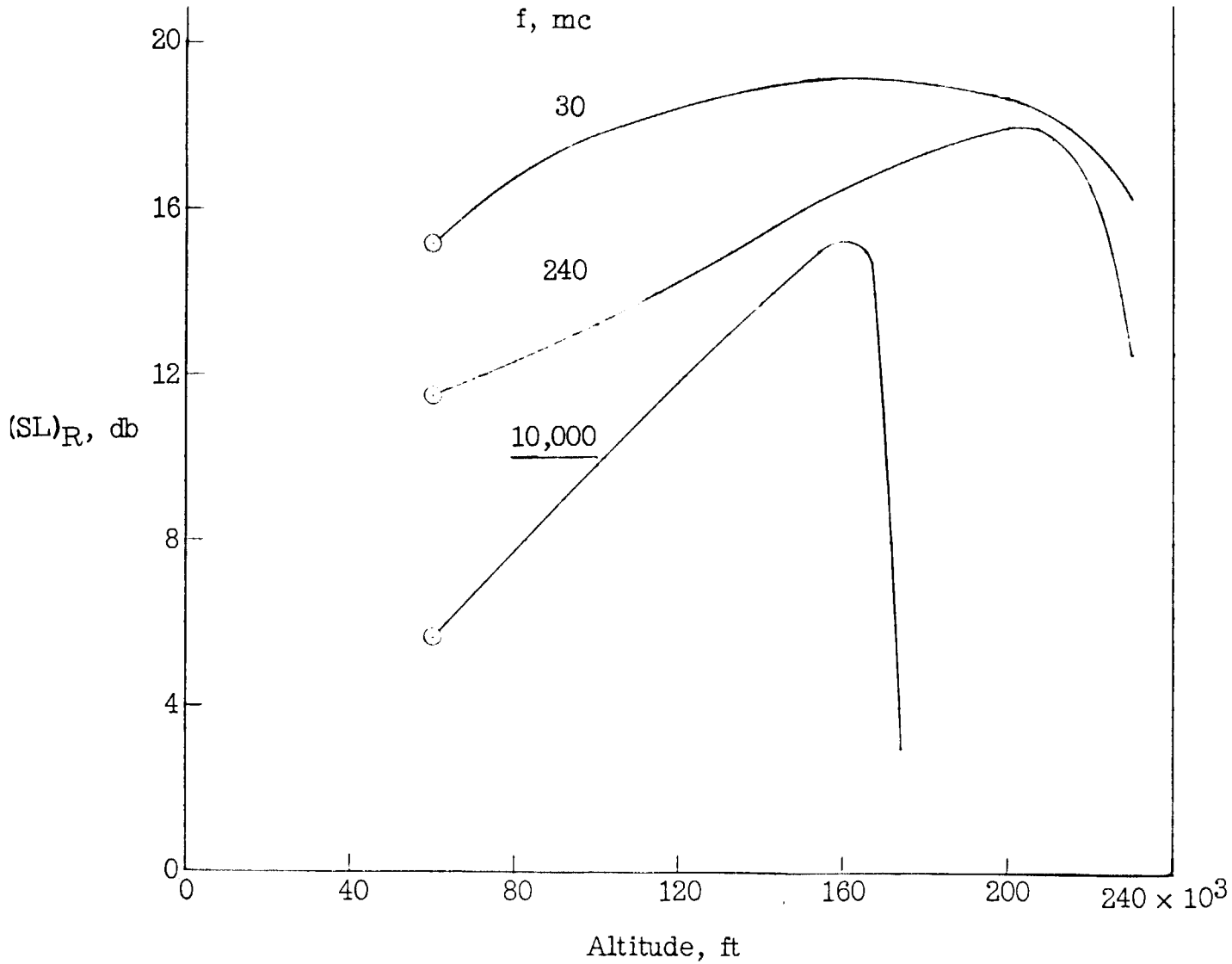

Figure 44.- Example of variation with altitude of signal loss due to reflection (plane sheet theory) for a constant Mach number trajectory. $\theta = 9^\circ$; M = 20; $x/D_n = 2.333$; $D_n = 20.32$ cm.

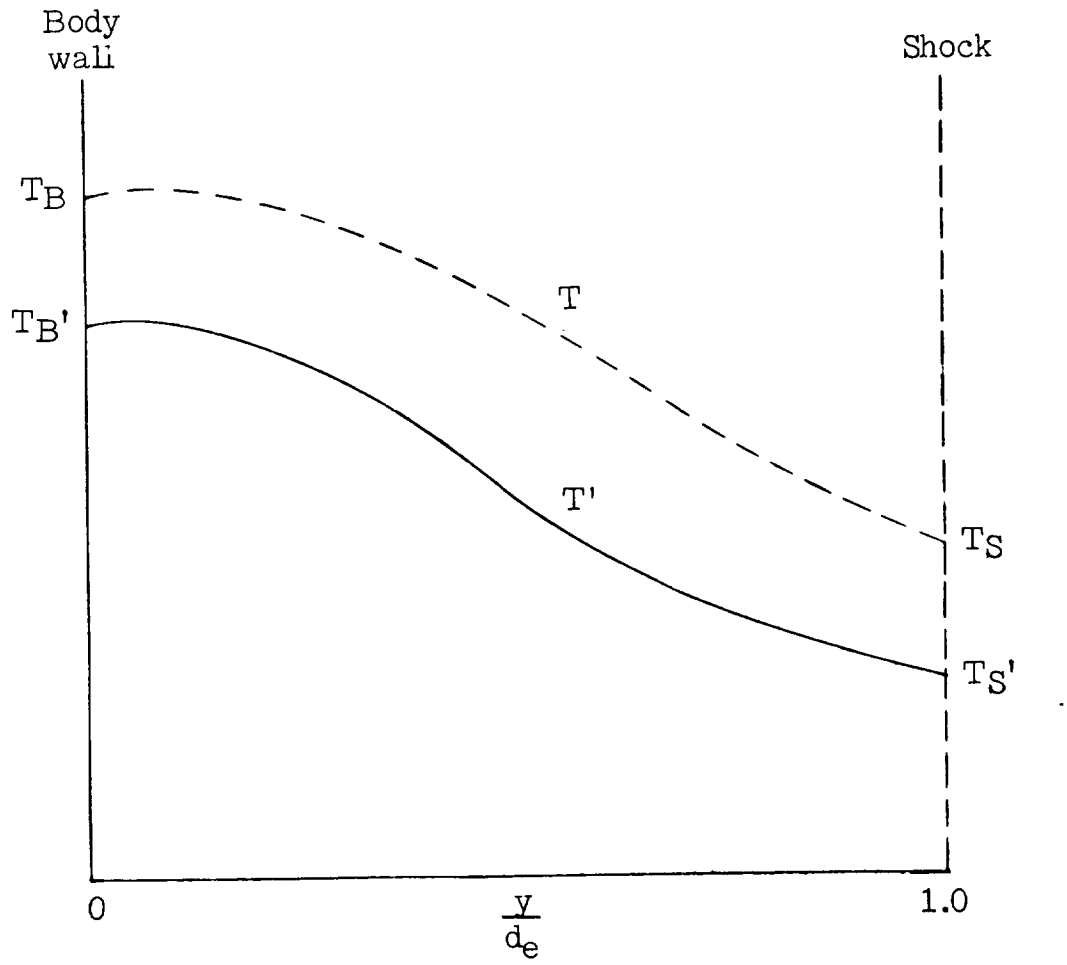

Figure 45.- Modification of temperature distribution for change of altitude at constant Mach number. (T' is given temperature distribution and T is temperature distribution modified for different altitudes.)

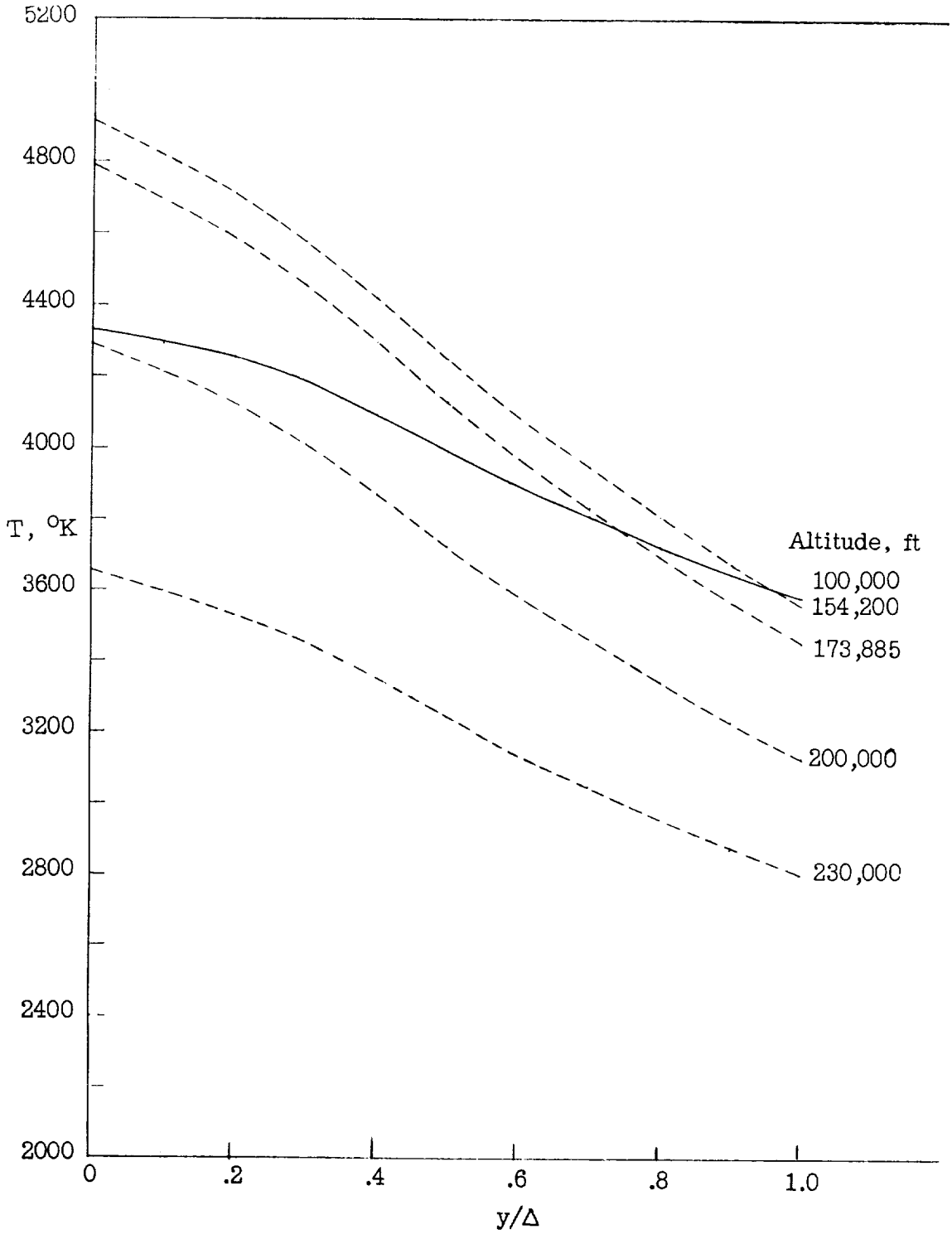

Figure 46.- Modified temperature distributions for the complete altitude range. (θ = 30°; M = 15; x/D_n = 0.17; Δ/D_n = 0.07; base altitude, 100,000 ft.)

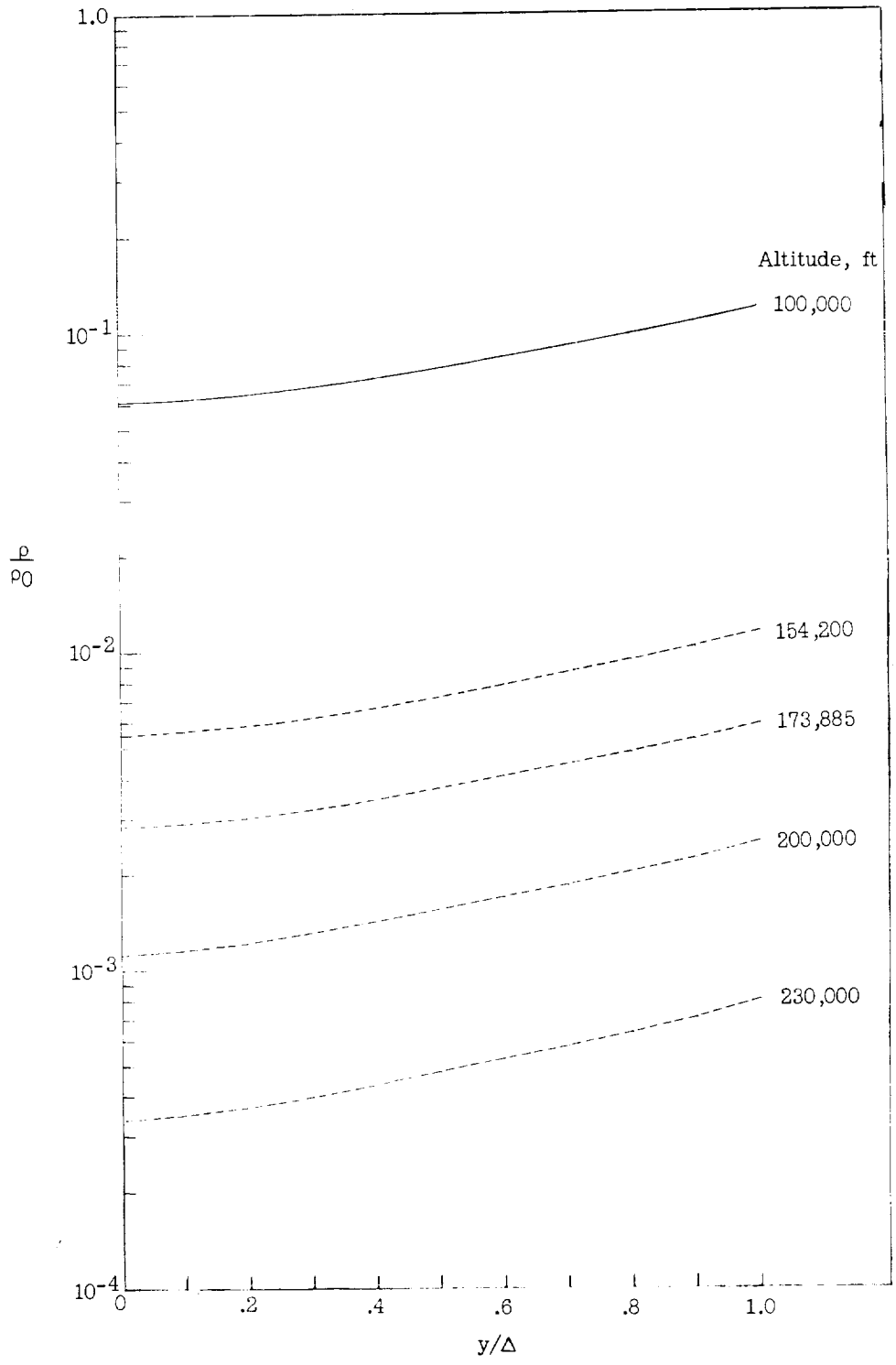

Figure 47.- Example of altitude modification of given flow-field solution. Solid line is original solution. $\theta = 30°$; $M = 15$; $x/D_n = 0.17$; $\Delta/D_n = 0.07$.

NASA-Langley, 1963 L-1901